JOURNAL OF NEUROPHYSIOLOGY
Vol. 46, No. 1, July 1981. *Printed in U.S.A.*

Morphology of Functionally Identified Neurons in Lateral Geniculate Nucleus of the Cat

MICHAEL J. FRIEDLANDER, C.-S. LIN, L. R. STANFORD, AND S. MURRAY SHERMAN

Department of Neurobiology and Behavior, State University of New York, Stony Brook, New York 11794

SUMMARY AND CONCLUSIONS

1. Forty-seven neurons in the dorsal lateral geniculate nucleus of normal adult cats were studied both physiologically and morphologically in order to determine structure/function relationships at the single-cell level. Neurons were initially identified during extracellular recording as W-, X-, or Y-cells. This was followed by intracellular recording of the neuron, revalidation of its classification, iontophoretic filling of the cell with horseradish peroxidase (HRP), histological processing to visualize the HRP-filled cell, and morphological analysis of the physiologically characterized neuron. The sample includes 25 X-cells, 19 Y-cells, 1 W-cell, and 2 physiologically unclassified cells.

2. The 25 X-cells are morphologically different from the 19 Y-cells. All of the X-cells and 14 of the Y-cells were found in laminae A and A1; the other 5 Y-cells, in the C-laminae. Eighteen of the X-cells have morphological features of Guillery's class 2 and/or 3 neurons, and the other seven X-cells could not be placed into one of Guillery's classes. Most of the X-cells with class 3 morphological features are identified geniculocortical relay cells. Class 3 cells were hitherto presumed to be interneurons. The Y-cells have either class 1 or class 2 morphological features. Class 2 X-cells, however, differ morphologically from class 2 Y-cells. The W-cell has class 4 features and was found in the C-laminae, while both of the physiologically unclassified cells are class 1 morphologically and were found in lamina A1.

3. Guillery's morphological classification scheme correlates well but not completely with the physiological W-, X-, and Y-cell classification. Both X- and Y-cells could be class 2, but class 2 X-cells differ morphologically from class 2 Y-cells. The one W-cell has class 4 morphology.

4. Our data permit reasonably confident identification of geniculate neurons as X- or Y-cells based on a battery of the following morphological differences. *a*) X-cell somata are typically smaller than those of Y-cells. *b*) X-cell dendrites are contained completely within the lamina in which the soma is found, while Y-cell dendrites freely cross laminar boundaries. *c*) The dendritic trees of X-cells are asymmetrically elongated along projection lines (i.e., orthogonal to the lamination), whereas those of Y-cells tend to be radially symmetric. *d*) X-cell dendrites tend to be thin, sinuous, and possess many, complex appendages throughout their course. Y-cell dendrites tend to be large, fairly straight, and possess relatively few, simple appendages. *e*) X-cell axons tend to be thinner than those of Y-cells. *f*) Both X- and Y-cell axons issue collaterals occasionally within the lateral geniculate nucleus and more often in the perigeniculate nucleus. Perigeniculate collaterals are more common for Y-cells than for X-cells.

5. For both X- and Y-cells, soma size correlates with the extent of the dendritic arborization. This suggests that factors (e.g., dendritic extent) other than the extent of the cell's axonal projection may relate to soma size.

6. The size distribution of our sample of HRP-filled cells is virtually identical to the size distribution of neighboring cells. Thus,

we found no evidence for electrode sampling biases based on soma size, and we suggest that factors other than soma size (e.g., dendritic extent) might also contribute to electrode sampling biases. Also, this comparison of soma sizes between HRP-filled cells and neighboring neurons permitted us to estimate the relative percentage of X- and Y-cells in the A-laminae. We conclude that roughly one-third of the neurons are relay Y-cells and that the remainder are relay X-cells plus interneurons. If as many as 25% of the neurons are interneurons, then the X- to Y-cell ratio is roughly equal, but if interneurons are rare (as our data suggest), then the ratio is approximately 2 to 1.

7. The observation that geniculate X- and Y-cells differ morphologically suggests that differences in the X- and Y-cell pathways are not determined only in the retinal plexiform layers. Also, since our estimate of the geniculate X- to Y-cell ratio is considerably lower than previous estimates of this ratio in the retina, one consequence of retinogeniculate circuitry may be to expand the Y-cell pathway relative to the X-cell pathway.

INTRODUCTION

During the past decade, a number of laboratories have provided evidence that the mammalian geniculocortical system is comprised of several parallel pathways (for recent reviews, see Refs. 47, 61, 77). This, in turn, has led to a new conceptual framework for the functional organization of mammalian visual systems. Most of this evidence derives from cats and centers on the classification of retinal ganglion and geniculate cells into W-, X-, and Y-cells. This classification is strictly limited to electrophysiological differences in neuronal response properties.

Differences among W-, X-, and Y-cells are similar at both retinal and geniculate levels (for details, see Refs. 8–10, 12, 15, 31, 32, 34, 46, 74, 78, 83). Less is known about W-cells, but compared to X- and Y-cells, they tend to display more sluggish responses and have slower axonal conduction velocities. Much more is known about X- and Y-cells. Compared to Y-cells, X-cells tend to have: *a*) more slowly conducting axons; *b*) more linear spatial summation in their receptive fields; *c*) smaller receptive-field centers; *d*) more heterogeneous fields based on spatiotemporal maps; *e*) slightly greater sensitivity to visual stimuli consisting of higher spatial frequencies, but much less to lower ones; *f*) slightly poorer sensitivity to visual stimuli of higher temporal frequencies or speeds of movement; and *g*) more sustained responses to visual stimuli of appropriate standing contrast.

These cell groups appear to be links in three parallel, relatively independent neural chains from retina through the lateral geniculate nucleus to visual cortex, and even cortical neurons may be identified as part of one or another of these chains (5–7, 33, 34, 51). It has been suggested that each of these chains analyzes somewhat different features of the visual scene, and that these analyses are integrated at some as yet undefined central structure. Presumably, the different functional roles played by these W-, X-, and Y-cell chains relate to the above-mentioned physiological differences among the component cell types (37, 38, 46, 47, 67, 69, 77).

W-, X-, and Y-cells have been confidently identified only with electrophysiological criteria. Our knowledge of them is consequently unidimensional, since it is based only on electrophysiological data. It thus would be useful to develop identification criteria for these cell classes along other dimensions, such as morphological, chemical, etc. Several laboratories have suggested specific structure/function relationships at the single-cell level for W-, X-, and Y-cells both in retina (4, 12, 52, 81) and the lateral geniculate nucleus (48, 83), but these suggestions are based on evidence that, although impressive, is nonetheless indirect.

Prior suggestions of structure/function relationships for geniculate neurons usually can be traced to the morphological classification scheme proposed by Guillery (25) and based on Golgi impregnations. Guillery described four broad morphological groups, but he emphasized that the plurality of neurons (roughly 40% of his sample) could not be placed into any one of these groups (see also Refs. 16, 80). Three of these groups were described for the A-laminae (see Fig. 1). Class 1 cells have the largest somata (25–40 μm in diameter) with thick, fairly straight and cruciate dendrites that often cross lam-

inar boundaries. These dendrites tend to have sparse, simple spinelike appendages. Class 2 cells have intermediate-sized somata (15–30 μm in diameter) with thinner, curved dendrites that only occasionally cross laminar boundaries. A striking feature of these cells are grapelike clusters appended in or near dendritic branch points. Class 3 cells have the smallest somata (10–20 μm in diameter) with very fine, sinuous dendrites. A heterogeneous assortment of appendages, many quite complicated in appearance and often connected to dendrites by long stalks, can be found all along the dendrites. Class 4 cells were briefly described and were found only in the C-laminae.[1] These have medium-sized somata, fine dendrites, and a dendritic tree oriented in a plane parallel to the lamination.

LeVay and Ferster (48) offered several converging lines of indirect evidence to support the notion that Guillery's classes 1, 2, and 3, respectively, represent relay Y-cells, relay X-cells, and interneurons. The concentration of W-cells in the C-laminae led others to suggest that these are morphologically class 4 (83). While these specific structure/function relationships for geniculate neurons in the cat are widely accepted (cf. Refs. 47, 61, 77, 83, and many others), it nonetheless seems logical to question such relationships, since they are based on indirect evidence. Also, retinal ganglion X- and Y-cell properties are already distinguishably provided by the retinal plexiform layers; and nearly all geniculate X- or Y-cells, respectively, receive their excitatory optic tract input exclusively from retinal X- or Y-cells (8). If additional differential processing in the lateral geniculate nucleus specifically related to X- and Y-cells were lacking, there might be no further structural correlates to X- and Y-cells central to the optic tract.

We wished to test with a direct approach whether or not geniculate X- and Y-cells differ morphologically and, if so, to what extent the LeVay and Ferster (48) hypothesis is correct. Consequently, we adapted a technique used successfully in other mammalian neural pathways (39, 44). That is, we intracellularly injected horseradish peroxidase (HRP) into single geniculate neurons after each was studied with electrophysiological techniques and identified as a W-, X-, or Y-cell. The HRP yields a Golgi-like filling that permits a detailed morphological assessment of the neuron.

Indeed, we found many different structural features among geniculate W-, X-, and Y-cells. We have confirmed parts of the LeVay and Ferster (48) hypothesis, but suggest changes in others. Based on Guillery's (25) classification scheme, we find class 1 cells to be Y-cells, but class 2 cells include both X- and Y-cells. Also, many neurons with class 3 morphological characteristics are X-cell relay neurons. Many X-cells could not be placed into one of Guillery's (25) classes. Nonetheless, apart from this morphological classification scheme, many different structural features are seen between X- and Y-cells, and these are described below. Limited data from the C-laminae are consistent with the notion that W-cells have class 4 morphology. Preliminary reports of these findings have appeared elsewhere (20, 73).

MATERIALS AND METHODS

General preparation

Adult cats (2.0–4.0 kg) were used in these experiments. Most of the methods have been described in detail elsewhere (20, 34, 45, 46) and will be briefly outlined here. The cats were initially given 0.4 mg atropine sulfate subcutaneously to prevent excessive respiratory secretions. Initial anesthesia was induced with 3% halothane delivered in a 1:1 N_2O:O_2 mixture, and both the femoral vein and trachea were cannulated. The animals were then transferred to a stereotaxic apparatus. The anesthesia level was changed to 1% halothane in a 70:30 N_2O:O_2 mixture for further surgical procedures. Paralysis was initially induced with 40 mg of Flaxedil and maintained throughout the experiment by an intravenous infusion of a mixture of 3.6 mg/h of Flaxedil and 0.7 mg/h of *d*-tubocurarine in a 5% lactated Ringer solution given at 6.0 ml/h. The cats were artificially ventilated. End-tidal CO_2 was continuously monitored and maintained near 4%. After completion of all surgical procedures, including craniotomies, the wounds and pressure points were infiltrated with 1% lidocaine and the cat was removed from the halothane. Additional lidocaine

[1] The other major cell group of the cat's dorsal lateral geniculate nucleus, beside the A- and C-laminae, is the medial interlaminar nucleus. No detailed studies of Golgi-impregnated neurons from this region have, to our knowledge, yet been published. The medial interlaminar nucleus contains practically only Y-cells, although occasional W- and X-cells have been found there (13, 45, 55).

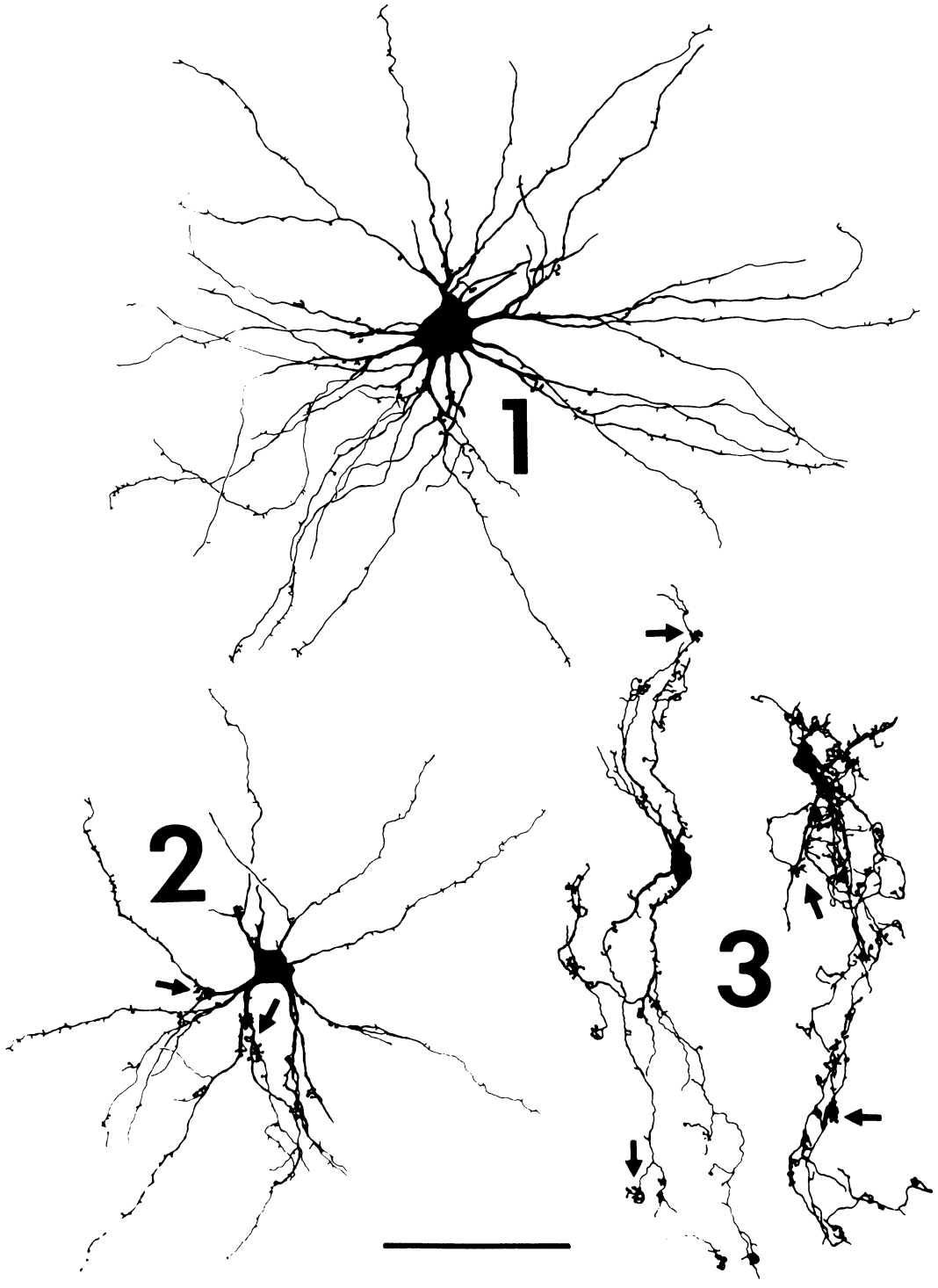

FIG. 1. Tracings of geniculate neurons impregnated by the Golgi-Kopsch method. These cells are all from laminae A and A1 of adult cats and represent the three major morphological classes described by Guillery (25) for these laminae. The class 1 cell has a large soma and thick, cruciate dendrites with occasional, simple spinelike appendages. The class 2 cell has an intermediate-sized soma and dendrites of medium thickness with clusters of grapelike appendages near dendritic branch points (arrows). Two examples of class 3 cells are shown. They have small somata and thin sinuous dendrites with complex, stalked appendages (arrows). Scale: 100 μm.

was applied at intervals of approximately 6 h. The animal was maintained for recording during the rest of the experiment (16–36 h) on a 70:30 N_2O:O_2 mixture. Body temperature was maintained at 38.0°C with a blanket-control unit.

Visual stimulation

Neo-Synephrine and atropine were applied topically to the cat's eyes to retract the nictitating membranes and dilate the pupils, and the corneas were covered with zero-power contact lenses. We then performed retinoscopy to ensure that each retina was conjugate with the visual stimuli on a plotting screen or cathode-ray tube. To do this, spectacle lenses were occasionally placed in front of the cat's eyes. Retinal landmarks, including the optic disk, were then projected onto the plotting screen by the method of Fernald and Chase (18). Receptive-field positions could thus be measured with respect to the optic disk which, in turn, places the field with respect to the area centralis (41, 65). In each case in which a geniculate cell was intracellularly injected with HRP, retinal landmarks were replotted immediately after withdrawal of the electrode from the cell.

Visual stimulation was accomplished either by means of bright or dark targets presented on a plotting screen or by patterns generated on a cathode-ray tube (for details, see Ref. 46). The patterns on the cathode-ray tube were vertically oriented, counterphased, sine-wave gratings. We could continuously vary the spatial frequency, the temporal frequency (counterphase rate), and the position (spatial phase angle) of the gratings. Overall mean illumination was 38 cd/m^2, and contrast (defined as $(L_{max} - L_{min})/(L_{max} + L_{min})$ where L_{max} and L_{min} are, respectively, the maximum and minimum luminances across the grating) could be varied between 0 and 0.6.

Electrophysiology

ELECTRODES. Recording micropipettes were made from glass tubing (1.2 mm OD, 0.6 mm ID) with internal glass filaments. Each tube was then drawn to a fine tapered tip with a pipette puller and backfilled with a solution consisting of 0.2 M KCl, 0.05 M Tris, and 2–5% HRP (Sigma VI). The solution was buffered at pH 7.6 and filtered through a 0.05-μm pore diameter "nucleopore" system. Each micropipette was then beveled to a final outer diameter of 0.2–0.4 μm, as estimated from scanning electron micrographs of several examples. The final impedance range was 80–120 MΩ measured at 200 Hz. The micropipette was stored in a hydrated chamber for up to 36 h before use.

A pair of bipolar stimulating electrodes (insulated tungsten wires; exposed tip lengths $\simeq$ 0.5 mm) was lowered into the brain to straddle the optic chiasm. Five similar electrodes were placed into cortical gray matter for bipolar stimulation of areas 17 and 18. Orthodromic activation of geniculate neurons was achieved by placing current pulses (10–100 μs; 1.0–3.0 mA) across the chiasm electrodes. Transynaptic activation was ascertained by variability in response latency to the shocks and by the cell's inability to follow high frequencies (>200 Hz) of stimulation. Both transynaptic and antidromic activation of geniculate cells were seen from applying similar currents across various pairs of cortical electrodes. When present, antidromic activation was identified by: little or no variability in evoked spike latency (<0.1 ms), the ability of the cell to respond to high-frequency (>300 Hz) stimulation, and most important, by the ability of an orthodromically traveling spike to block the antidromic spike (i.e., spike "collision").

ELECTROPHYSIOLOGICAL RECORDINGS. Single-cell recordings were made with a DC amplifier having internal bridge and current injection circuitry. The micropipette was advanced through a hydraulically sealed craniotomy and durotomy to the lateral geniculate nucleus. A hydraulic seal was created by cementing a Plexiglas cylinder (10 mm high, 12 mm diameter) to the bone around the craniotomy and filling it first with a layer of agar solution followed, after the agar hardened, with melted wax. We found it necessary to insert the micropipette tip 1–2 mm into the brain before the agar was applied to prevent clogging of the tip. We also found that traverses through overlying tissue to the thalamus often clogged or broke the tips, so we employed the procedure of aspirating a portion of the overyling tissue roughly 5 mm in diameter and 4–8 mm deep before electrode penetrations (cf. Ref. 56). However, this ablation somehow interfered with our ability to activate geniculate neurons antidromically from cortex, although we had thought the ablation would be too anterior and dorsal to interrupt the optic radiations (cf. Ref. 20). After the first few experiments, we abandoned this ablation procedure, at the expense of occasionally ruining recording micropipettes, in order to permit antidromic activation of geniculate neurons.

The response properties of geniculate neurons were first studied during extracellular recording with methodology described in detail elsewhere (8, 15, 31, 32, 34, 46, 71). Each neuron's response latency to electrical stimulation of optic chiasm and visual cortex was measured, and in the case of cortical stimulation, the antidromic or transynaptic nature of the response was determined. We also assessed the following receptive-field properties: ocular dominance, receptive-field position, center and surround type (i.e., on or off), center size, responsiveness to fast-moving targets, and the tonic or phasic nature of responses to pro-

longed stimulation of the center. Finally, we partially assessed each cell's spatial summation properties from the responses to the counterphased, sine-wave gratings. That is, a cell was "linear" if it responded at the fundamental temporal frequency of the stimulus and if a grating position of phase angle could be found at which responsiveness practically ceased; this is the "null position." A cell was "nonlinear" if its response pattern was distorted by higher (even) harmonics of the stimulus temporal frequency and if no null position could be found. We identified geniculate neurons in the A-laminae as X-cells or Y-cells by relying chiefly on response latency to optic chiasm stimulation, linearity of spatial summation, and responsiveness to fast-moving targets. Only if all three of these properties led to the same X- or Y-cell identification was the cell classified; otherwise, it was considered physiologically unclassified. Unclassified cells were rarely (<5%) sampled (see RESULTS). Occasional electrode penetrations entered the C-laminae in which W-cells were encountered. These were identified by sluggish responses to visual stimuli and long latencies to optic chiasm stimulation (9, 10, 11, 83).

Neurons were initially studied and classified during extracellular recording. The electrode was then advanced in 1-μm steps until electrical effects of mechanical contact with the cell's membrane were evident. These included fluctuations in the DC level, increased spike amplitude, and small, slow-wave activity. Brief (100 ms) depolarizing current pulses (1.0–3.0 nA) were applied to penetrate the neuron. Intracellular recording was indicated by a rapid, 30- to 65-mV drop in the DC level, the appearance of 30- to 70-mV monophasic, positive action potentials (with up to 5-mV overshoot), and the appearance of depolarizing and hyperpolarizing synaptic potentials.

The cell's electrophysiological properties (i.e., responses to chiasm stimulation, receptive-field plot, linearity of spatial summation) were quickly revalidated to ensure that the penetrated neuron was the same cell from which extracellular data were obtained. Then HRP was ejected through the tip into the neuron with 200-ms depolarizing pulses of 2.5–10.0 nA at 3 Hz for 1–10 min. Brief pauses in the injection procedure permitted us to monitor the neuron's electrical activity and ascertain that the micropipette tip remained within the same neuron for the entire iontophoretic period.

The HRP iontophoresis ended the electrode penetration. The micropipette was withdrawn and a new penetration started at least 500 μm distant. Since we attempted to inject each physiologically defined geniculate neuron and since such an injection terminated a penetration, the C-laminae were rarely reached. We injected no more than two neurons per lamina, and these were widely spaced. The histological location of each injected cell could readily be matched to the appropriate receptive-field location and ocular dominance based on Sanderson's (63) retinotopic maps of the lateral geniculate nucleus.

Histology

The cats were sacrificed 12–36 h after the first neuron was injected and at least 1 h after the final injection. This was accomplished by a large, intravenous dose of barbiturate, followed by transcardial perfusion with Karnovsky's fixative. The lateral geniculate nucleus was stereotaxically blocked, removed, postfixed for 4–12 h, and washed overnight in phosphate buffer. Sections were subsequently cut in the coronal plane at 100 μm on a vibratome and reacted with diaminobenzidine. Many of the sections were then counterstained for Nissl substance with cresyl fast violet.

Microscopic examination and tracing of filled cells was done with a Kodak Wratten 48A or 49B (deep blue) filter. The filter was chosen on the basis of its spectral transmission being complementary to that of the HRP-diaminobenzidine reaction product. Cells were traced by means of a drawing attachment on a microscope with a 100×, oil-immersion objective (numerical aperture (NA), 1.32).

For comparison, Nissl-stained geniculate cells were measured from 11 cats. These included six cats from which HRP-filled geniculate neurons were recovered plus five other cats from which no HRP-filled cells were obtained. However, the brains were processed identically in each of the 11 cases. Somata were traced with the same microscope optics. Cell samples were selected from the middle of the A-laminae (mediolaterally and anteroposteriorly). To avoid sampling errors, only cells with visible nucleoli were sampled, and every such neuron in the field of view was included. The samples included the entire dorsoventral extent of the A-laminae, so that neurons near the interlaminar zones were included. Roughly equal numbers of neurons in laminae A and A1 were measured. Most of the measurements involved cross-sectional area (A) of the soma. This was accomplished by means of a planimeter used with the drawings. From the area measurement, we estimated soma diameter (D) and volume (V) by assuming that the soma approximated a sphere. That is, $A = \pi r^2$, $V = {}^4/_3\ \pi r^3$, and $D = 2r$.

RESULTS

We obtained successful intracellular recordings from over 150 physiologically identified geniculate neurons. Both extracellular and intracellular recording were used to

TABLE 1. *Morphological and physiological classes of geniculate neurons*

Morphological Class	Physiological Class				
	W	X	Y	Unclassified	Total
1	0	0	12*	2	14
2	0	9	7	0	16
2-3	0	4	0	0	4
3	0	5*	0	0	5
4	1	0	0	0	1
Unclassified	0	7	0	0	7
Total	1	25	19	2	47

* All cells are confirmed relay cells except one of the class 1 Y-cells and three of the class 3 X-cells.

identify these neurons as W-, X-, or Y-cells based on the criteria listed in MATERIALS AND METHODS. Forty-seven of these neurons were injected with HRP and successfully recovered after histological processing. That is, complete and detailed physiology and morphology were available for each of these 47 geniculate cells. Geniculate neurons were considered to be relay cells either if they were antidromically activated from cortex or if they possess an HRP-filled axon that can be followed into the optic radiations. Thus, either electrophysiological or morphological criteria were employed.

The recovered cells to date include 25 X-cells (22 of which are confirmed relay cells), 19 Y-cells (18 of which are confirmed relay cells), one W-cell relay neuron, and two physiologically unclassified relay cells (see Table 1).[2] Therefore, of the 47 neurons, only 3 X-cells and 1 Y-cell could not be positively identified as relay cells. Each of the three X-cells that could not be identified as relay cells was obtained from early preparations in which antidromic stimulation was not possible (see MATERIALS AND METHODS). Also, it must be emphasized that failure either to activate a cell antidromically from cortex or to demonstrate an axon projecting from it and entering the optic radiation does not necessarily identify the cell as an interneuron (see DISCUSSION).

We found the morphology of X-cells to be quite different from that of Y-cells, but considerable variability occurs within each group. Based on Guillery's (25) classification scheme, most X-cells have structural features that are generally characteristic of class 2 cells, class 3 cells, or intermediate between these. Some X-cells cannot be classified structurally. Y-cells tend to be class 1 or class 2 in structure (see INTRODUCTION and Fig. 1). The two physiologically unclassified cells have class 1 morphology. Table 1 summarizes these relationships. Of particular interest is the identification of several class 3 cells and all cells intermediate between classes 2 and 3 as relay X-cells. Other structural differences between X- and Y-cells, including details of the above observations, are described below.

Electrophysiology

The records in Fig. 2 illustrate several examples of electrophysiological recordings taken from cells that were ultimately filled with HRP. Figure 2*A–C* shows intracellular records taken from the Y-cell illustrated in Figs. 12*B* and 13*C*. Figure 2*A* and *B* shows responses to electrical activation of the optic chiasm at two sweep speeds. The latency from chiasm stimulation was 1.1 ms, and the action potential had a 60-mV amplitude with a 1.5 ms duration and a 100 V/s rise time. The resting potential of this neuron was −64 mV, and thus no overshoot of the action potential was seen. When the micropipette was finally withdrawn, the resting potential had shifted by only 7 to −57 mV. Figure 2*C* illustrates intracellular responses from the same neuron as a visual target is moved through its receptive field. Note that the individual action potentials ride on slow depolarizing potentials of 4–5 ms duration which, in turn, ride on larger, slower depolarizing waves.

Figure 2*D–G* shows records from the X-cell illustrated in Fig. 19*H*. Figure 2*D* shows impalement of the cell with the micropipette. The trace begins with extracellular recording of 5-mV action potentials. The large os-

[2] Of the X-cells, 12 were identified as relay cells only by virtue of an axon traced into the optic radiations; 3, only by the collision test; and 7, by both criteria. Of the Y-cells, 8 were identified as relay cells by the morphological criterion alone; one, by the electrophysiological criteria alone; and 9, by both criteria. The W-cell was identified as a relay cell by both criteria. Finally, one of the two physiologically unclassified cells was identified as a relay cell by the morphological criterion alone; and the other cell, by both criteria.

cillation (arrow 1) represents an unsuccessful attempt to penetrate the cell by applying a large negative capacitance to the electrode. Then, a 2-nA depolarizing pulse was delivered (arrow 2) and penetration ensued. This was indicated by a 10-mV initial drop in the DC level followed by a second, rapid drop of 45 mV (arrow 3). This saturated the FM tape recorder, and the oscilloscope beam had to be repositioned (arrow 4). Figure 2*E–G* shows intracellular recording from this neuron as a counterphasing, sine-wave grating covered its receptive field. The three traces include a null position of the grating (Fig. 2*F*) plus spatial phase shifts of the grating by 90° to either side of the null position (Fig. 2*E*, *G*). These responses helped to characterize the neuron as an X-cell (see MATERIALS AND METHODS). The traces from Fig. 2*E*, *F* were taken before and the trace from Fig. 2*G* was taken 3 min after HRP iontophoresis. Between the time Fig. 2*E* and *F* and *G* was recorded, the resting potential had dropped by 8 mV. A rapid positive 45-mV return to base line DC level accompanied withdrawal of the micropipette from the cell.

Another X-cell's records are shown in Fig. 2*H–L*. These illustrate antidromic activation from cortical stimulation, as inferred from the collision test. Figure 2*H* shows an orthodromic, spontaneously occurring action potential (closed arrow) used to trigger the cortical stimulation unit; the shock artifact (asterisk) and evoked action potential (open arrow) are also shown. As the interval between the orthodromic action potential and cortical stimulation was reduced (Fig. 2*I–L*), the evoked action potential was blocked (Fig. 2*K*, *L*). This indicates antidromic activation of the neuron from cortex which, in turn, identified this X-cell as a relay neuron. Of particular interest is the subsequent morphological characterization of this neuron, shown in Figs. 3*A* and 4*A* and *B*, as a class 3 cell.

Qualitative Morphological Features

Somadendritic properties

As mentioned above, X- and Y-cells represent heterogeneous morphological classes that are, nonetheless, distinct from one another. X-cells tend to possess class 2 and/or 3 morphology, and Y-cells, class 1 or 2 morphology. X-cells have smaller somata. These X-cells display a wide variety of complex, often stalked, dendritic appendages and tend to have thin, sinuous dendrites arranged in a tree oriented perpendicular to the geniculate laminae (i.e., along "projection lines"; cf. Ref. 63). Y-cells generally have larger somata, thicker and straighter dendrites, with few, simple appendages, and a radially symmetric dendritic tree. Dendrites of X-cells never leave the lamina of origin, whereas such extralaminar dendrites are common among the Y-cells. Although examples of both X- and Y-cells are found with class 2 morphology, class 2 X-cells nonetheless differ morphologically from class 2 Y-cells. The class 2 X-cells are smaller and none have translaminar dendrites; each of the larger class 2 Y-cells displays translaminar dendrites.

All of our X-cell sample is located in laminae A and A1. Of the 19 Y-cells, 14 are from the A-laminae, and the others are from the C-laminae. The W-cell example is located in the C-laminae, and the physiologically unclassified neurons are both in lamina A1. Except as noted below, no obvious interlaminar differences in qualitative morphological features exist either for X-cells or for Y-cells.

X-CELLS. *Class 3 X-cells.* Figures 3 and 4 illustrate two X-cells that are morphologically class 3. The class 3 X-cell shown in Fig. 3*A* is a confirmed relay cell as demonstrated both by its antidromic activation from cortical stimulation (see Fig. 2*H–L*) as well as by the course of its axon into the optic radiations. Note the relatively small soma, the complex, stalked structures appended to the dendrites, and the fine sinuous dendrites. Figure 4*A*, *B* illustrates these dendritic characteristics with photomicrographs of the same field at two different focal planes. All of these features signify class 3 morphology (25). This cell also has axon collaterals within lamina A, and all of its dendrites are confined to that lamina. For this X-cell, as well as for every other X- and Y-cell individually illustrated in Figs. 3–18, Table 2 provides a summary of its receptive-field type (X- or Y-cell, on- or off-center), field-center size, eccentricity of the receptive field from the area centralis, latency of re-

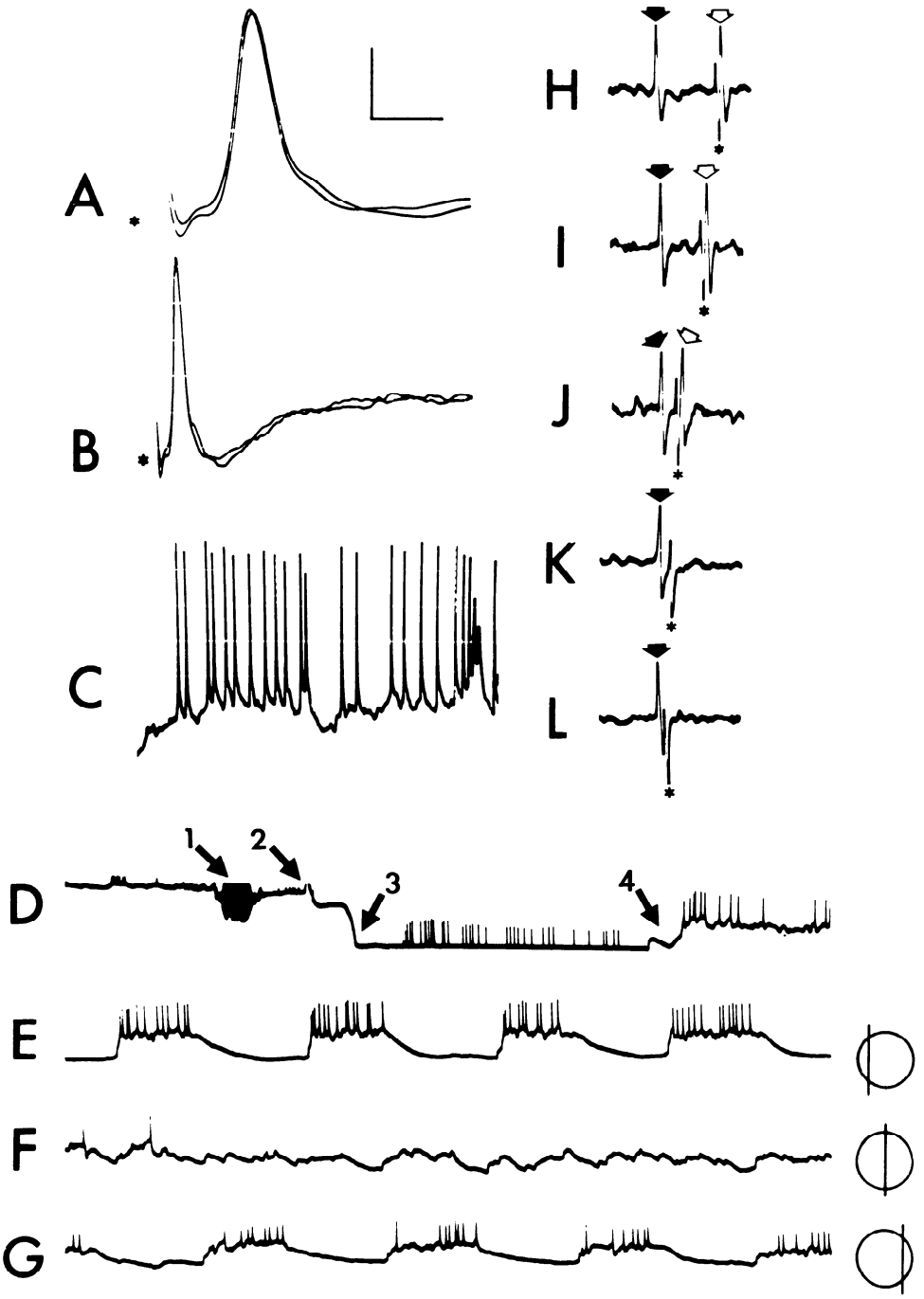

FIG. 2. Electrophysiological records from geniculate neurons that were subsequently stained with HRP and morphologically analyzed. *A–C*: intracellular records from the Y-cell shown in Figs. 12*B* and 13*C*. *A* and *B* each show two superimposed responses to stimulation of the optic chiasm, and the asterisks indicate the stimulus artifact. *A* represents a faster sweep speed than does *B*. This cell's resting potential was −64 mV, its action potential had an amplitude of 60 mV, and its latency to stimulation of the optic chiasm was 1.1 ms. *C* shows the response to movement of a visual stimulus through the neuron's receptive field. Note that bursts of action potentials ride on slow, depolarizing waves. *D–G*: extra- and intracellular records from the X-cell shown in Fig. 19*H*. *D* shows the transition from extra- to intracellular recording. We overcompensated the negative capacitance arm of the amplifier (arrow 1) in an unsuccessful attempt to penetrate the cell, then we passed a depolarizing pulse of 2 nA for 200

sponse to electrical stimulation of the optic chiasm, the eye that provided excitatory input, the lamina in which the soma was located, and the figure(s) in which it is illustrated.

Another example of a class 3 X-cell is found in Fig. 3*B*. This neuron could not be confirmed as a relay cell due to failure to identify an axon entering the optic radiation. This cell, unfortunately, was obtained from an early experiment in which cortical stimulating electrodes were not used due to extirpation of cortex (see MATERIALS AND METHODS). The extremely thin and sinuous dendrites as well as the delicate, complex dendritic appendages can be appreciated in the two photomicrographs of Fig. 4*C*, *D*, which also are from two different focal planes of the same field of view. The appendages vary from single-headed spines to complicated, multiheaded structures. Three other features of the cell are noteworthy: the soma is quite small, the dendritic tree has an orientation dramatically orthogonal to the lamination, and the dendrites end abruptly at the laminar boundaries (cf. Fig. 19*B*).

Class 2/3 X-cells. The X-cells illustrated in Fig. 5 are both confirmed relay cells and they have morphological features that incorporate characteristics of both class 2 and class 3 cells. These include grapelike appendages at some dendritic branch points (class 2; filled arrows in Fig. 5) in addition to complex stalked appendages along fine, sinuous dendrites (class 3; open arrows in Fig. 5). Thus, we have identified these as morphologically intermediate cell types. The photomicrographs of Fig. 6 are of the cell illustrated in Fig. 5*A*. These photomicrographs illustrate the limitation of the dendritic tree to lamina A (Fig. 6*A*, *B*), the orientation of the dendrites orthogonal to the lamination (Fig. 6*A–C*), a class 2 characteristic of grapelike clusters at dendritic branch points (Fig. 6*D*, filled arrow), and class 3 characteristics of complex appendages on thin, sinuous dendrites (Fig. 6*E*, *F*, filled arrows signify such appendages). The soma and several other dendrites are found in the adjacent coronal sections and are included in the drawing of Fig. 5*A*. The soma occupies the region indicated by the open arrow in Fig. 6*C*. Of particular interest with respect to this cell is the beaded or varicose appearance of the terminal section of dendrites (Fig. 6*D*). This has been seen on other X- and Y-cells, as discussed below.

Class 2 X-cells. Several X-cells display class 2 morphology. They are characterized both by intermediate soma sizes and dendrite diameters as well as by grapelike clusters at branch points of dendrites. Three such examples, all relay cells, are shown in Fig. 7. All of these cells possess dendrites confined to one lamina.

Figures 7*A* and *B* and 8*A* illustrate a class 2 X-cell located in lamina A1. This cell responded to cortical stimulation in a fashion indicative of transynaptic activation.[3] That is, the evoked spike could not be abolished by collision with orthodromic spikes, and it occurred with variable latency after stimu-

[3] We use the term transynaptic instead of orthodromic, because we cannot be certain that the action potential has traveled down a corticogeniculate axon. For example, as we have shown elsewhere in this paper, geniculocortical relay axons occasionally have intrageniculate axonal branches. The possibility thus exists that the action potentials could travel antidromically down the geniculocortical axon, invade the intrageniculate branch, and excite the neurons from which we have recorded. Since we cannot distinguish this form of activation from orthodromic activation, we use the term transynaptic, a term that describes both possibilities.

ms (arrow 2), which resulted in a large drop in the DC level (arrow 3) and subsequent penetration. This DC-level drop saturated the amplifier of our recorder, and the beam was repositioned (arrow 4). *E–G* shows intracellularly recorded responses to a counterphased, sine-wave grating (0.5 contrast, 2 cycles/deg spatial frequency, and 2 cycle/s temporal frequency) at three spatial phase angles (see diagrams at end of traces). *F* is at the null position, while *E* and *G* are phase shifted by 90° left and right, respectively, from the null position. *G* was taken after 3 min of HRP injection. By this time the cell had depolarized by 8 mV. *H–L*: extracellularly recorded responses from the class 3 X-cell illustrated in Figs. 3*A* and 4*A* and *B*. These records show collision of an antidromically activated spike (open arrow) with a spontaneously generated, orthodromic spike (filled arrow). The latter spike triggered the cortical stimulator (the stimulus artifact is shown by the asterisk) at decreasing delays in *H–L*. Note the disappearance of the antidromic spike in *K* and *L*. The scale near the record in *A* applies to all traces as follows: 20 mV and 1 ms for *A*; 20 mV and 4 ms for *B*; 20 mV and 40 ms for *C*; 120 mV and 1 s for *D–G*; and 5 mV and 4 ms for *H–L*.

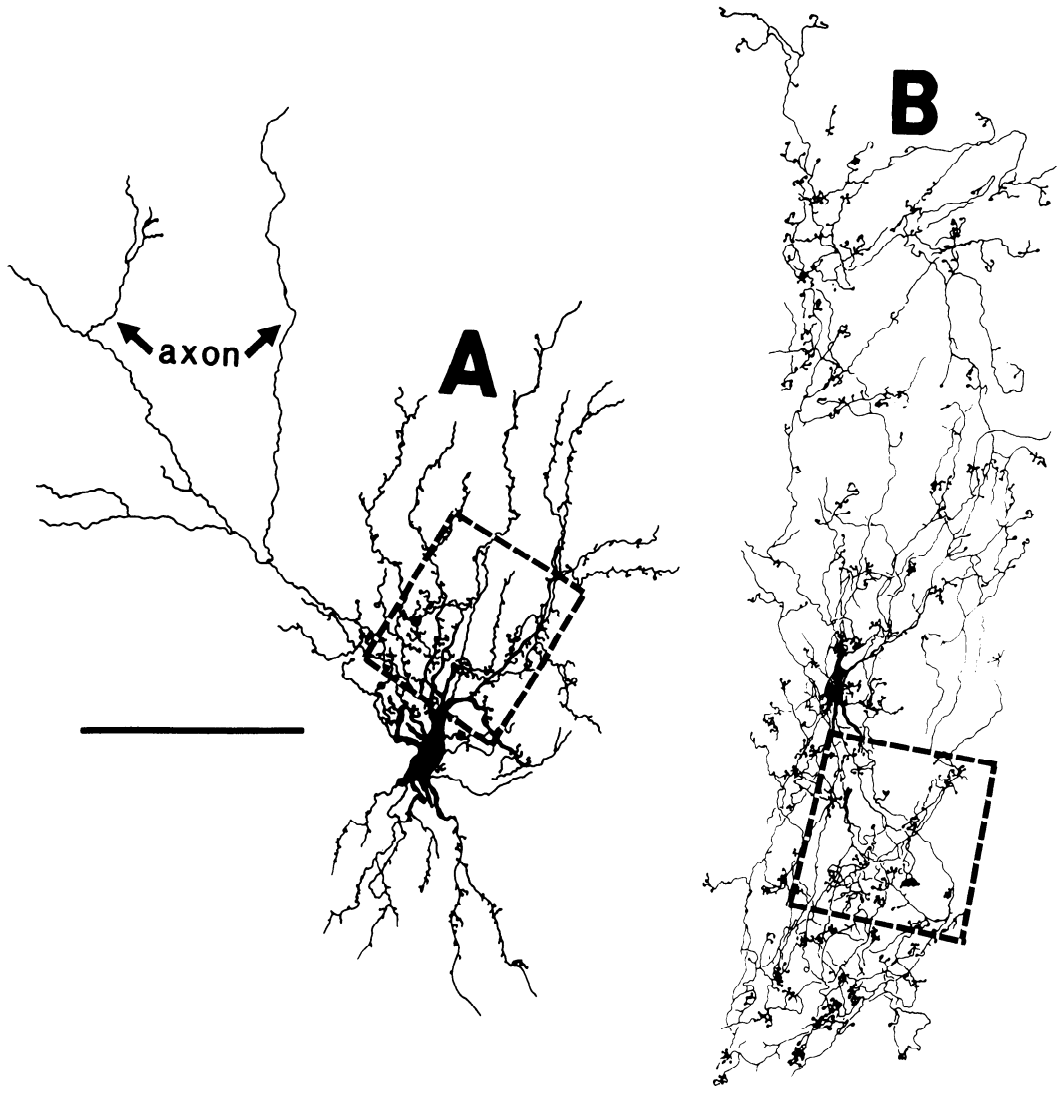

FIG. 3. Drawings of two morphological class 3 X-cells. Both cells have thin, sinuous dendrites that are limited to one lamina, are perpendicular to the lamination, and have numerous, complex appendages. *A*: lamina A relay cell with intrageniculate axon collaterals. In this and most subsequent drawings, only part of the axon is drawn. The outlined area is further illustrated in Fig. 4*A*, *B*. *B*: lamina A1 cell that could not be identified as a relay cell (however, see text). Note the extensive dendritic tree, which nearly fills the dorsoventral extent of but stays entirely within lamina A1 (see also Fig. 19*B*). The outlined area is further illustrated in Fig. 4*C*, *D*. Scale: 100 μm.

lation. Dubin and Cleland (14) adopted such criteria of transynaptic activation from cortex as a means of positively identifying an interneuron. Yet, Fig. 7*B* clearly shows that this is a relay cell by virtue of its axon entering the optic radiations. Although Fig. 7*B* shows the axon just entering the optic radiations, we were able to trace the axon nearly 1 mm further into the optic radiations. Apparently, this axon either could not be electrically excited from cortex with our array of stimulating electrodes or it failed to conduct antidromic impluses at some point (i.e., perhaps at a branch point). This illustrates some of the difficulty in applying these electrophysiological criteria to the positive identification of interneurons.

The X-cell shown in Figs. 7*C* and 8*B* and *C* has the largest soma among X-cells (410 μm^2), but this is well within the range reported for class 2 cells (25). Also, the cell possesses the class 2 signature of clusters

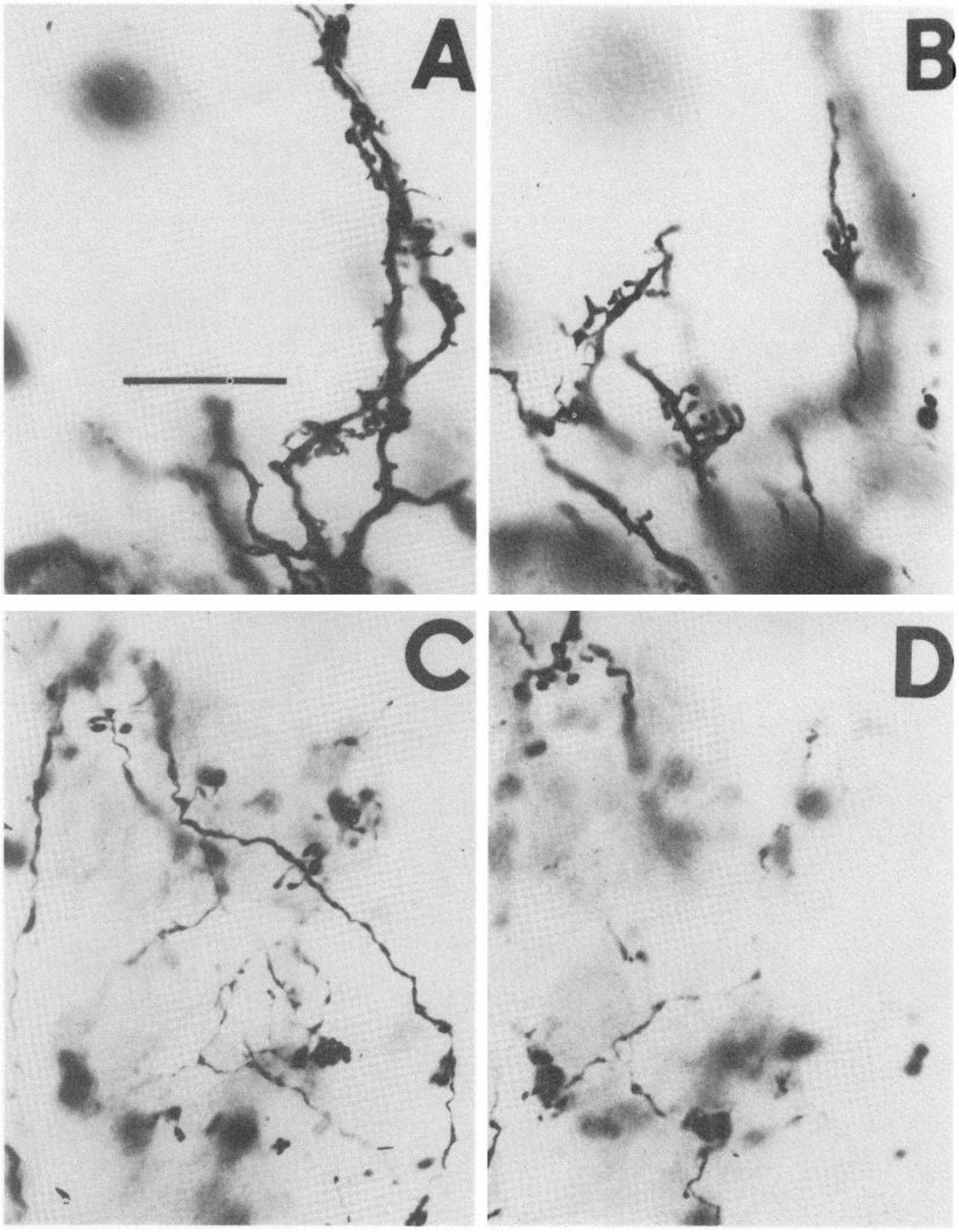

FIG. 4. Photomicrographs of dendritic regions from class 3 X-cells drawn in Fig. 3. Note the thin, sinuous dendrites and complex, stalked appendages. *A*, *B*: same field of view at two focal planes from region of cell indicated in Fig. 3*A*. *C*, *D*: same field of view at two focal planes from region of cell indicated in Fig. 3*B*. Scale in *A*: 20 μm and applies as well to *B*–*D*.

appended at dendritic branch points (Figs. 7*C*, 8*B*). A curious feature seen on the terminal segment of its dendrites are delicate, sinuous hairlike appendages (Fig. 8*C*). As described below, this feature is also seen on one Y-cell.

The neuron shown in Fig. 7*D* is morphologically atypical for an X-cell because its

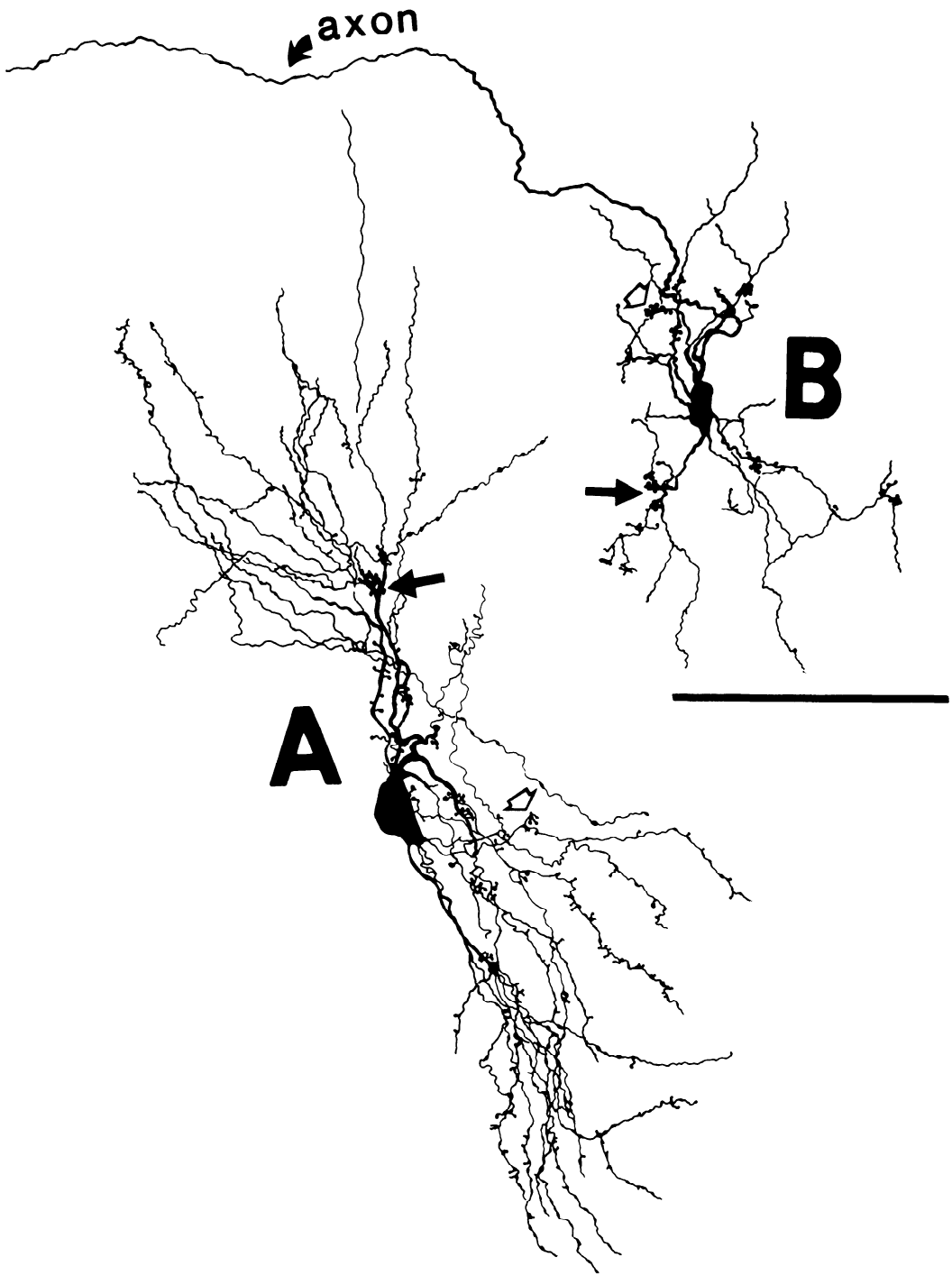

FIG. 5. Tracings of two X-cells with morphological features intermediate between classes 2 and 3. Both X-cells have the class 2 feature of grapelike clusters appended near dendritic branch points (e.g., filled arrows) as well as the class 3 feature of complex, stalked appendages distant from such branch points (e.g., open arrows). Also, both neurons have thin, sinuous dendrites oriented perpendicular to but contained entirely within a single lamina, and both are confirmed relay cells. *A*: lamina A neuron also illustrated in Fig. 6. *B*: lamina A neuron. Scale: 100 μm.

dendritic tree is relatively uniformly distributed. However, the soma is placed close to a blood vessel (shaded area in Fig. 7*D*) around which many of the dendrites wrap. This could possibly distort the dendritic tree from the more typical X-cell geometry that is orthogonal to the lamination. It should also be noted that some other X-cells do not exhibit a dramatic orientation of the dendritic tree along projection lines.

Morphologically unclassified X-cells. Finally, some X-cells display morphological features not clearly identified with the classes of Guillery's (25) schema. Figure 9 illustrates three examples, all of which are relay cells. They are too small to be class 1 cells, do not have the grapelike clusters at dendritic branch points or other characteristics of class 2 cells, and their dendrites lack the complex appendages found on class 3 cells. However, they do exhibit morphological features common to other X-cells, including relatively small somata, fine dendrites, and a dendritic tree that is both oriented orthogonal to the lamination and wholly contained within a single lamina. The cells shown in Fig. 9*A*, *D* are the only cell in our entire sample nearly totally free of dendritic appendages. A curious feature of the two cells in Fig. 9*A*, *D* is the extensively beaded or varicose appearance of dendrites beyond the first branch point, and this is further demonstrated with photomicrographs in Figs. 10 and 11. Cells with beaded dendrites have been described previously from Golgi-impregnated material, and it has been suggested that they constitute a separate morphological class (16, 80). However, it is clearly possible that such beads or varicosities could be pathological (e.g., an early response to cell injury due to the intracellular recording).

Y-CELLS. *Class 1 Y-cells.* The most common morphological type for the Y-cells in our sample is class 1 (Table 1). Figures 12 and 13 illustrate two Y-cells with typical class 1 somadendritic morphology. Their somata are large, and their dendrites are thick and fairly straight. Dendritic appendages are rare, and when they occur, they tend to be simple, spinelike structures (Fig. 13*B*). The dendrites occupy a fairly circular zone and readily cross laminar boundaries, from the C-laminae into lamina A1 in one case and from lamina A1 to lamina A in the other. Note that some dendritic branch points can be found outside the lamina in which the soma is located.

Figures 14 and 15 represent an unusual class 1 Y-cell. The large soma and fairly straight, thick dendrites of this cell are typical features for a class 1 cell. This cell's dendrites are covered with filamentous, hairlike processes (Figs. 14 and 15*F*), which seems to set the cell apart morphologically. However, Fig. 1 of Guillery's paper (25) represents a similar class 1 cell with dendrites that appear to be covered with filamentous appendages. Note also that our example has translaminar dendrites, since it projects a substantial fraction of its ventral dendrites from lamina A into lamina A1 (Figs. 14, 15). Perhaps the most interesting feature of this cell is the ocular dominance of its receptive field. Although the soma and majority of dendrites are in lamina A, the cell could be excited by visual stimulation only through the ipsilateral eye. Since retinal terminals from one eye are found strictly within geniculate laminae dominated by that eye (30), this neuron must have been powerfully influenced via synapses located fairly peripherally on relatively few dendrites. That is, the translaminar dendrites in lamina A1 seem to determine the cell's functional ocular dominance. However, this is the only example of 47 geniculate cells of a soma located in an inappropriate lamina according to the eye through which it can be stimulated. It is thus not yet possible to estimate the precise frequency of such cells, but they seem to be rare.

The class 1 cells in our sample, with few exceptions, are fairly homogeneous in morphological properties. These cells have roughly radially symmetric dendritic trees, and all but one have dendrites that cross laminar boundaries. The one exception is a faintly labeled cell with dendrites that can be traced only a relatively short distance from the soma. The failure to trace any of these dendrites across a laminar border may have been an artifact of poor filling, although this point must remain in doubt. Of particular interest is that this is the only Y-cell not identified as a relay cell and is the smallest Y-cell in our sample. Perhaps the light HRP filling failed to penetrate the relay axon as well as translaminar dendrites or

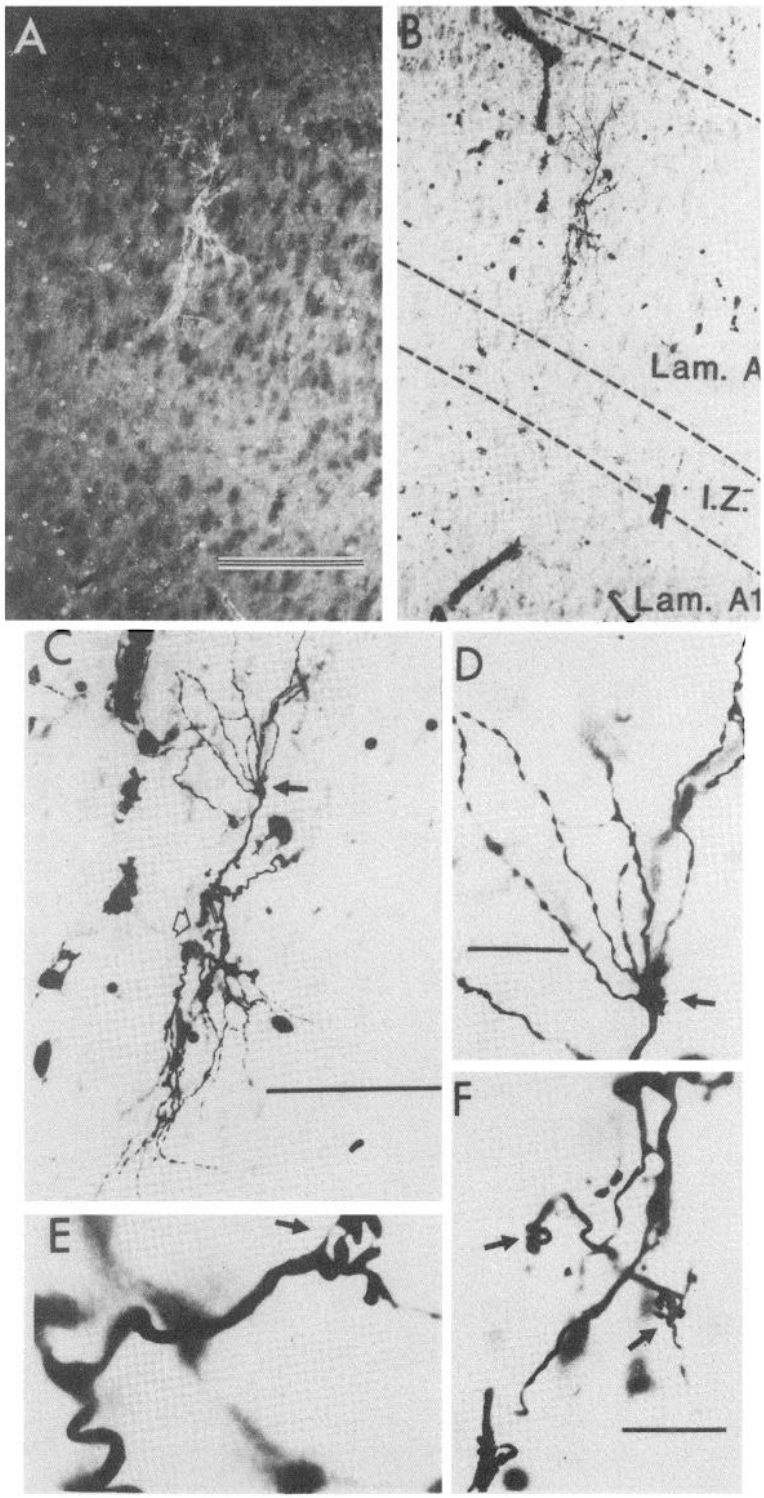

FIG. 6. Photomicrographs of the X-cell shown in Fig. 5*A* with morphological features intermediate between classes 2 and 3. *A, B*: low-power darkfield (*A*) and brightfield (*B*) views of the same area. The section was lightly counterstained with cresyl fast violet, and the lamination, which is more evident in *A*, is indicated in *B* (I.Z., interlaminar zone). Note the vertical orientation of dendrites, which are completely confined to lamina A. Scale

perhaps interneurons do not possess such dendrites. In any case, every identified relay Y-cell in our sample has dendrites that cross laminar boundaries.

Class 2 Y-cells. Figure 16 illustrates three Y-cells in our sample with class 2 morphology and all were relay cells. Each of these somata are located in lamina A1. Among the characteristic class 2 features seen in these cells are the grapelike clusters at dendritic branch points. Figure 17*A* is a photomicrograph of the cell drawn in Fig. 16*A*, and it illustrates modest appendages at dendritic branch points. Figure 18*A*, *B* are photomicrographs of the cell drawn in Fig. 16*B* and illustrates large, globular appendages.

Class 2 morphological features, then, can be shared by X- and Y-cells. However, there are two main differences in our sample between the class 2 X-cells and the class 2 Y-cells. First, the Y-cell somata are larger than are those of X-cells (mean ± SD, 410 ± 86 μm^2 for the class 2 Y-cells; 257 ± 63 μm^2 for the class 2 X-cells), and this difference is statistically significant ($P < 0.001$ on a Mann-Whitney *U* test). Second, none of the class 2 X-cell dendrites cross laminar borders, but each of the class 2 Y-cells has dendrites that do so. It is noteworthy that all of the grapelike clusters at dendritic branch points of the class 2 Y-cells are found in the same lamina as the soma. Guillery (25) noted similar patterns for the class 2 cells whose dendrites cross laminar boundaries.

The class 2 Y-cell illustrated in Figs. 16*B* and 18 possesses some unusual morphological features. Many secondary dendrites flare out into a spray of varicose processes as they leave the large grapelike clusters (Fig. 18*C*). Also, this is the only Y-cell with a strongly oriented dendritic tree and the orientation is orthogonal to the lamination, as is typical for X-cells.

SUMMARY OF SOMADENDRITIC MORPHOLOGY OF X- AND Y-CELLS. Clearly, geniculate X- and Y-cell morphological features are qualitatively different from one another. This, in turn, suggests that differences between X- and Y-cell pathways are not completely limited to the retina and, consequently, that these differences are not simply relayed to the cortex through an otherwise homogeneous population of geniculate neurons.

We can summarize these morphological differences in two ways. First, Table 1 shows how X- and Y-cells are distributed in the Guillery (25) classification scheme. X-cells occupy the class 2–3 portion, and Y-cells, the class 1–2 portion. Despite overlap in the class 2 category, the morphological distributions of X- and Y-cells within this classification scheme are quite different ($P < 0.001$ on a χ^2 test).

A second, related way to summarize X- and Y-cell differences in somadendritic morphology can be appreciated from Figs. 19 and 20. Figure 19 shows tracings of 11 typical X-cells for direct comparison to 10 typical Y-cells selected for Fig. 20. The following morphological differences should be evident from a comparison of these figures: *a*) X-cells have smaller somata than do Y-cells; *b*) X-cell dendrites are finer and more sinuous than are those of Y-cells; *c*) X-cell dendrites always remain within a single lamina, whereas all relay Y-cells have dendrites that cross laminar boundaries; *d*) X-cell dendritic trees tend to be oriented perpendicular to the lamination, while those of Y-cells occupy a fairly circular zone, although exceptions to this generalization are seen; and *e*) dendritic appendages tend to be more numerous and complex on X-cells than they are on Y-cells.

GENICULATE NEURONS OTHER THAN X- AND Y-CELLS. *W-cells.* One W-cell from the C-laminae was recovered in this study, and it could be antidromically activated from cortex. This cell had an on-center receptive field located 6° from the area centralis, sluggish responses to visual stimuli, a field center diameter of 0.25°, a response latency of 4.0 ms to electrical stimulation of the optic

in *A*: 200 μm and applies as well to *B*. *C*: medium-power brightfield view. The soma and other dendrites are found in an adjacent section, and the relative location of the soma is indicated by the open arrow. The filled arrow refers to the class 2 characteristic of a grapelike cluster appended near a dendritic branch point, and this is shown in higher power in *D*. Scale: 100 μm. *D*: high-power brightfield view of the grapelike cluster (arrow). Note the many varicose dendrites that branch from this cluster. Scale: 25 μm. *E*, *F*: high-power brightfield views of the class 3 feature of complex, stalked dendritic appendages (arrows). The arrow in *E* shows the appendage indicated by the open arrow in Fig. 5*A*. Scale: scale in *C* represents 10 μm in *E*; the scale in *F* is 20 μm.

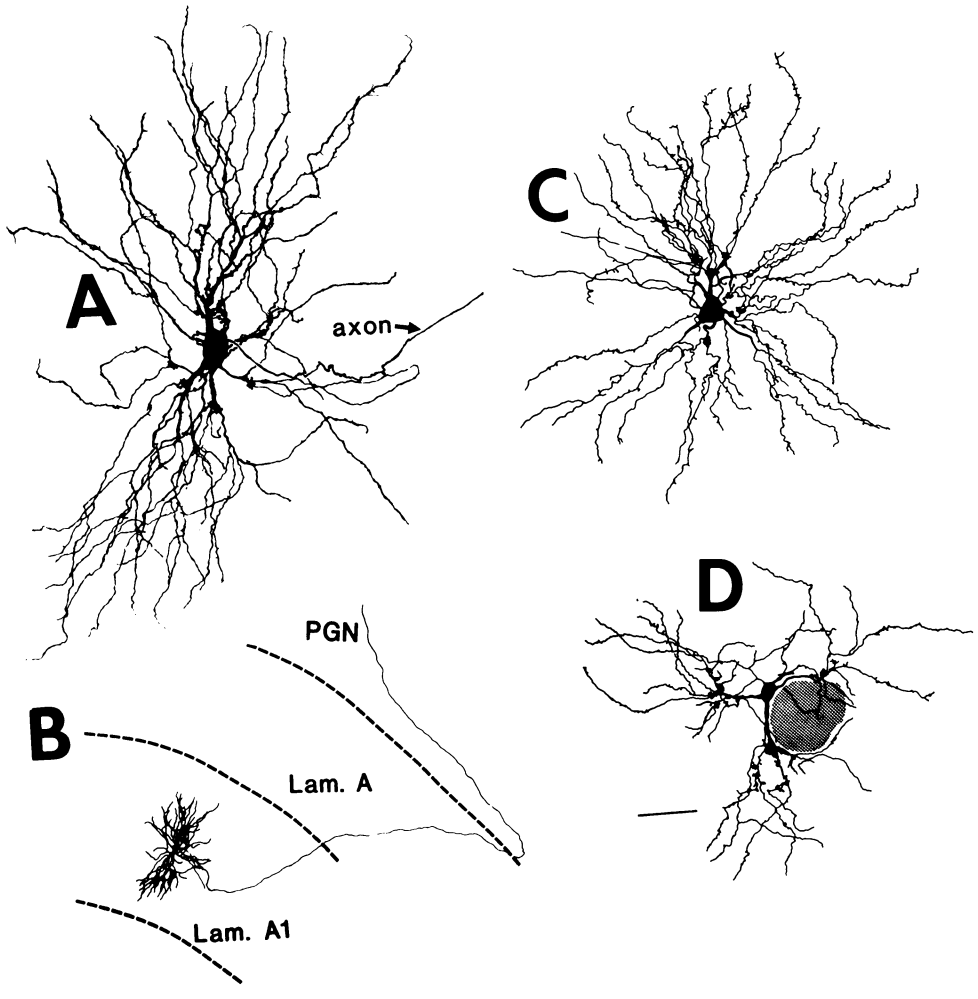

FIG. 7. Drawings of three examples of class 2 X-cells with numerous grapelike clusters appended at dendritic branch points. Each is a confirmed relay cell. *A*, *B*: high- and low-power drawings, respectively, of lamina A1 neuron. This cell is further illustrated in Fig. 8*A*. Despite the fact that this neuron could be activated transynaptically but not antidromically from cortical stimulation, it possesses an axon that courses through the perigeniculate nucleus (PGN) and well into optic radiations. The axon could be traced nearly 1 mm beyond the point shown in *B*, and this identified the neuron as a relay cell despite its transynaptic activation from cortical stimulation. Note the circuitous course of the axon in *B*. *C*: lamina A1 neuron further illustrated in Fig. 8*B*, *C*. A curious feature of this cell is the filamentous appendages along the terminal dendritic segments (see Fig. 8*C*). *D*: lamina A1 neuron without a vertical orientation to the dendritic tree. However, the dendrites wrap around a nearby blood vessel (shaded area) a factor that might distort the geometry of the dendritic tree (see text). Scale: 50 μm for *A*, *C*, *D*, and 200 μm for *B*.

chiasm, and a receptive field only for the contralateral eye. Figures 21 and 22 illustrate this cell. Because we have not used special techniques to elucidate the separate C-laminae (30), we cannot be certain how to relate the soma or dendritic ramifications to individual C-laminae.

This cell has a small soma (156 μm^2 in cross-sectional area), very fine dendrites, and a dendritic tree oriented moderately parallel to the lamination. These morphological features are consistent with the description of class 4 neurons (25). However, note the grapelike structures appended at dendritic branch points (Figs. 21 and 22), as occurs in class 2 cells.

Physiologically unclassified cells. Two recovered neurons in our sample of 47 could

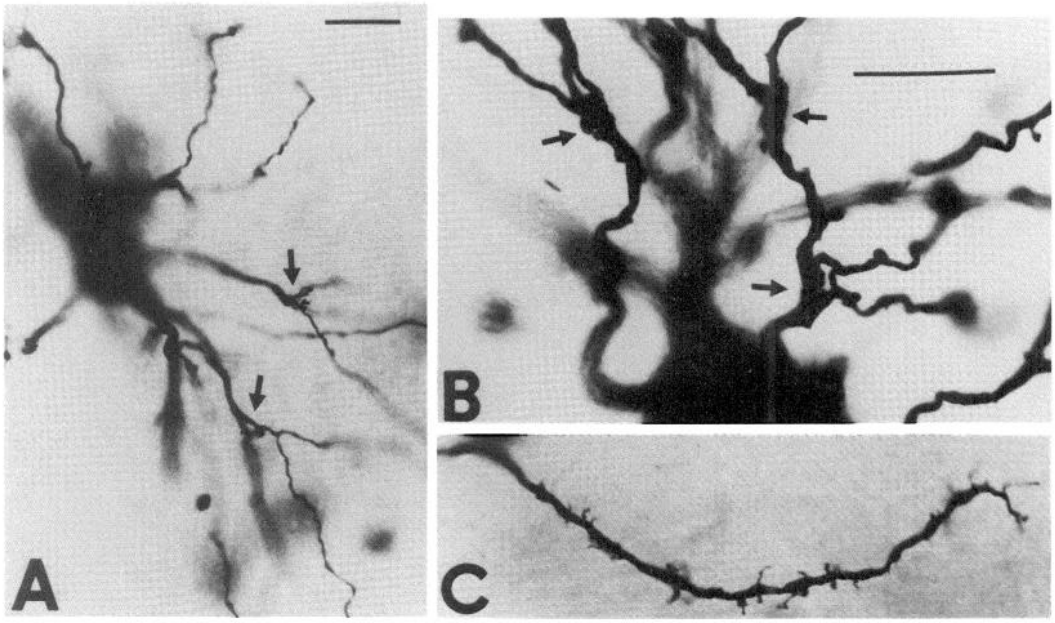

FIG. 8. Photomicrographs of class 2 X-cells. *A*: cell drawn in Fig. 7*A*, *B*. Note the soma, out of the plane of focus, and several appendages at dendritic branch points (arrows). Scale: 20 μm. *B*: cell drawn in Fig. 7*C*. As in *A*, this shows a soma out of the plane of focus and appendages near dendritic branch points (arrows). Scale: 20 μm, and applies as well to *C*. *C*: terminal section of dendrite of cell shown in *B*. Note the filamentous appendages that occur on all of the terminal dendrites.

not be confidently classified as W-, X-, or Y-cells. This is roughly the percentage of unclassified cells reported previously (34, 83). These two cells could not be classified because, on the battery of tests used for this purpose (see MATERIALS AND METHODS), the cells responded like an X-cell on some tests and like a Y-cell on others. Both cells are in lamina A1 and both have class 1 morphology indistinguishable from class 1 Y-cells except for somewhat small somata for class 1 cells (see also below).

OTHER STRUCTURE/FUNCTION RELATIONSHIPS. In the above sections, we have shown in a general way some morphological differences among identified physiological types, particularly X- and Y-cells. Another functional manner in which to divide geniculate cells is on the basis of center type. We found no obvious morphological differences between on- and off-center cells, and an inspection of Figs. 3–18 and Table 2 will document this point. It also seems clear that, despite obvious morphological differences between X- and Y-cells, there is considerable heterogeneity in structural features within each group (cf. Figs. 19 and 20). We found no variation in electrophysiological data among X- or Y-cells that could provide a clear correlation for much of this structural heterogeneity, although some subtle correlations are described in a subsequent section.

X- and Y-cell axons

Filled axons could be traced from 20 of the 25 X-cells and 17 of the 19 Y-cells. Nearly always the axon emerges from the soma, but occasionally it issues from a primary dendrite. The axon trajectories vary from a fairly direct course vertically through the laminae and the perigeniculate nucleus (located just dorsal to lamina A) into the optic radiations to oddly circuitous routes. Figures 9*B*, 14, and 16*A* and *B* illustrate axons that take a fairly direct route; tortuous routes are shown in Figs. 7*B*, 9*D*, and 12A.

Axon collaterals within the geniculate laminae are rare in our sample (see also Ref. 60). However, such collaterals are seen for five X-cells and one Y-cell, all relay neurons (see Figs. 3*A* and 16*B*). These collaterals are much finer (<0.5 μm in diameter) than the

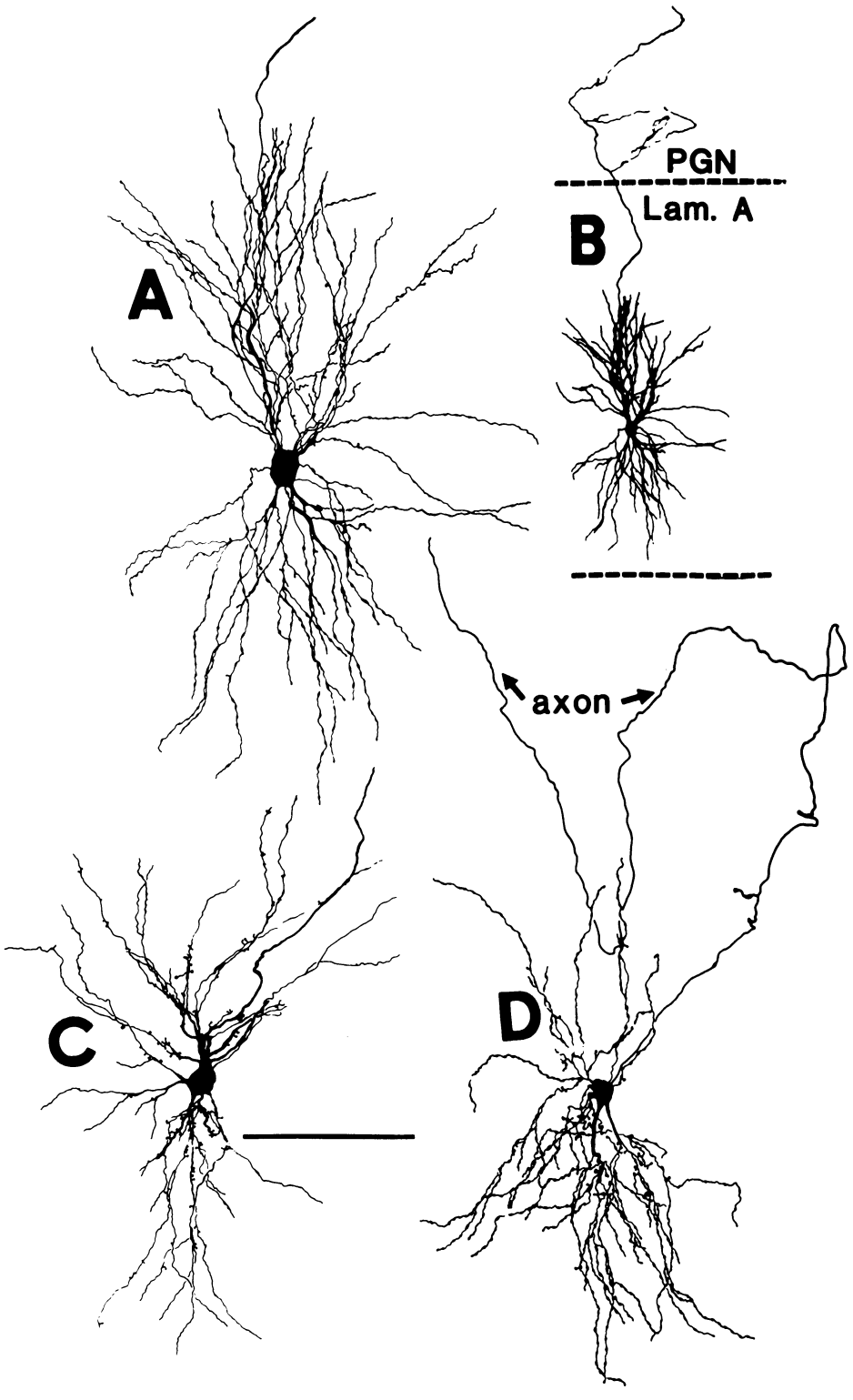

FIG. 9. Drawings of three examples of X-cells that could not be placed into one of Guillery's morphological classes (see text and Ref. 25). Each is an identified relay cell, and shares with other X-cells a small soma, fine dendrites oriented perpendicular to the lamination, and a dendritic tree limited to one lamina. *A*, *B*: high- and

parent axon and tend to be fairly simple structures. They are often a single branch, and they travel for a fairly short distance (<200 μm) from the parent axon. Swellings often occur along or at the end of these collaterals. These swellings are likely to be presynaptic terminals, although ultrastructural analysis is, of course, needed to verify this suggestion. In each of the five X-cells, the intrageniculate collaterals remain within the lamina occupied by the cell's soma. The Y-cell has several intrageniculate collaterals (Fig. 16*B*); its soma is in lamina A1, and the collaterals occur near the interlaminar zone between the A-laminae.

Axon collaterals are much more common in the perigeniculate nucleus. Each of the cells with intrageniculate axon collaterals also have axon collaterals in the perigeniculate nucleus, but many cells with perigeniculate axon collaterals display no intrageniculate collaterals. All of the cells with perigeniculate collaterals are confirmed relay cells. The perigeniculate collaterals, like the intrageniculate collaterals, are quite fine (<0.5 μm in diameter). For some cells, these collaterals occupy a wide extent, while in others, they are more restricted (Figs. 9*B*, 14, and 16*A*). They range in mediolateral extent from 52 to 375 μm. Many geniculate axons take a circuitous route and do not follow lines of projection (63) through the nucleus. However, perigeniculate collaterals from such axons are directed in such a way that they occupy the same line of projection as does the soma of origin. These collaterals thus seem to relate to the same region of visual field as does the parent soma. Figure 17*B* is a photomicrograph that illustrates the swellings that occur along and at the end of these perigeniculate collaterals. Preliminary observations suggest that these indeed are presynaptic terminals (82). The large extent of these collateral branches is consistent with the large receptive fields reported for perigeniculate neurons (14), since these neurons can evidently pool inputs from many geniculate neurons.

Both X- and Y-cells have perigeniculate collaterals. However, only 7 of 19 X-cells with a visibly stained axon that could be followed through the perigeniculate nucleus issue collateral branches there, while 15 of 17 Y-cells do. This difference is statistically significant ($P < 0.001$ on a χ^2 test), but such data are difficult to interpret. For instance, it is possible that most X- and Y-cells issue perigeniculate collaterals from their axons, but that these collaterals are less likely to be filled with HRP from the thinner parent axons of X-cells (see below).

Quantitative Morphological Features

Soma size

From a casual inspection of our recovered neurons, it seems clear that Y-cell somata are larger than those of X-cells. We have pooled our cell size data across receptive-field eccentricity for two reasons. First, although soma measurements from Nissl-stained preparations show that somata located more medially in the nucleus tend to be slightly larger than the more laterally distributed somata, this tendency is barely discernible. Second, most of our data were obtained from a portion of the lateral geniculate limited to the middle third of the nucleus in the mediolateral and anteroposterior dimensions and, as Fig. 23 shows, we found no evidence of any variation in soma size with receptive-field eccentricity for either X-cells ($r = -0.28$, $P > 0.2$) or Y-cells ($r = +0.18$, $P > 0.2$).

Figure 24*A* shows, for all of the pooled data, that little overlap in soma size occurs between X- and Y-cells, and Fig. 24*C*, upper histogram, shows a similar difference for the subpopulation of our sample in the A-laminae. In the A-laminae, X-cells average 219 μm^2 in soma cross-sectional area, and the mean for Y-cells is 493 μm^2. This difference in soma size between X- and Y-cells is statistically significant ($P < 0.001$ on a Mann-Whitney *U* test). Interestingly, the two physiologically unclassified neurons have an in-

low-power drawings, respectively, of lamina A neuron that is further illustrated in Fig. 10. This neuron has very few dendritic appendages, but dendrites become distinctly varicose after the first branch point. As shown in *B*, the cell's axon emits collateral branches as it passes through the perigeniculate nucleus (PGN). *C*: lamina A1 neuron. The fine dendrites have occasional spinelike appendages. *D*: lamina A1 neuron also illustrated in Fig. 11. Occasional appendages exist on dendrites, but most remarkable is the beaded appearance of dendrites (see Fig. 11). Also note the circuitous route of the axon. Scale: 100 μm for *A*, *C*, *D*, and 250 μm for *B*.

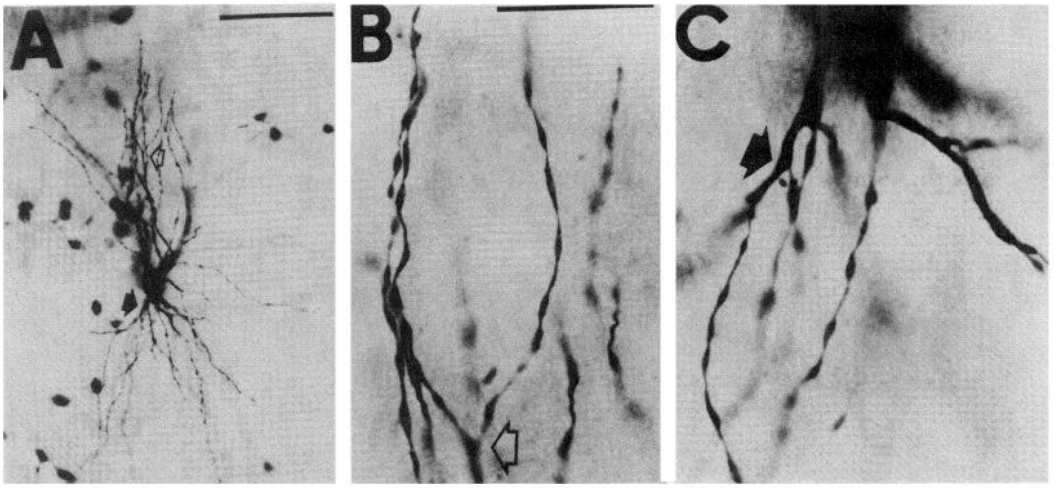

FIG. 10. Photomicrographs of the morphologically unclassified X-cell shown in Fig. 9*A*, *B*. *A*: lower power view of cell showing dendritic geometry elongated in a direction orthogonal to the lamination. The open arrow points to the same region as does the open arrow in *B*, and likewise for the filled arrows in *A* and *C*. Scale: 100 μm. *B*, *C*: higher power views of dendrites showing extensive varicosity. The arrow in *C* points to one of the rare appendages, a bulbous structure attached to a fine stalk (the stalk is out of focus). Scale in *B* is 20 μm and refers as well to *C*.

termediate soma size (Fig. 24*A*, *C*). Figure 24*A* also shows the three X-cells and one Y-cell not identified as relay neurons (indicated by stars), plus the W-cell.

For comparison, Fig. 24*C*, lower histogram, shows the sizes of A-laminae somata from Nissl-stained sections. These sections are from tissue treated identically to the tissue in which HRP-filled cells are found (see MATERIALS AND METHODS), and included the lateral geniculate nuclei from which the largest injected X-cell and smallest injected Y-cell are found, plus nine other nuclei randomly selected. Somata (n = 1,246) were measured from the middle third (mediolaterally and anteroposteriorly) of laminae A and A1. Relatively little interanimal variability in soma size is evident, and Fig. 24*C* shows the standard errors of the mean geniculate soma sizes for these 11 cats. That is, the mean from each cat was treated as a single datum. The distributions in Fig. 24*C* for HRP-filled and Nissl-stained somata are surprisingly close ($P > 0.2$ on a χ^2 test) and suggest that our sample of cells includes a fair representation of what is actually available based on soma size.

Figure 24*B* shows a further breakdown between laminae A and A1 in the size of HRP-filled somata. X-cells in lamina A1 are significantly larger than are their counterparts in lamina A (272 versus 175 μm^2; $P < 0.001$ on a Mann-Whitney U test). A smaller difference is seen for Y-cell somata, but the difference is not statistically significant, perhaps due to our small sample size (439 μm^2 for lamina A versus 467 μm^2 for lamina A1; $P > 0.2$ on a Mann-Whitney U test).

The relationships in Fig. 24*C* permit an estimate of the actual relative frequency and soma size distribution of X- and Y-cells in the A-laminae. This is shown in Fig. 24*D* and is derived in the following manner. The two unclassified cells are not considered. All somata below 250 μm^2 are considered to be X-cells and above 450 μm^2, Y-cells. For somata-between 250 and 450 μm^2, the relative percentage of X- and Y-cells in each bin of Fig. 24*C*, upper histogram, is calculated. The relative percentage in each bin is then multiplied by that in Fig. 24*C*, bottom histogram, to derive the separate distributions for X- and Y-cells in Fig. 24*D*. From this, we estimate that Y-cells represent slightly more than one-third (35%) of A-laminae neurons.

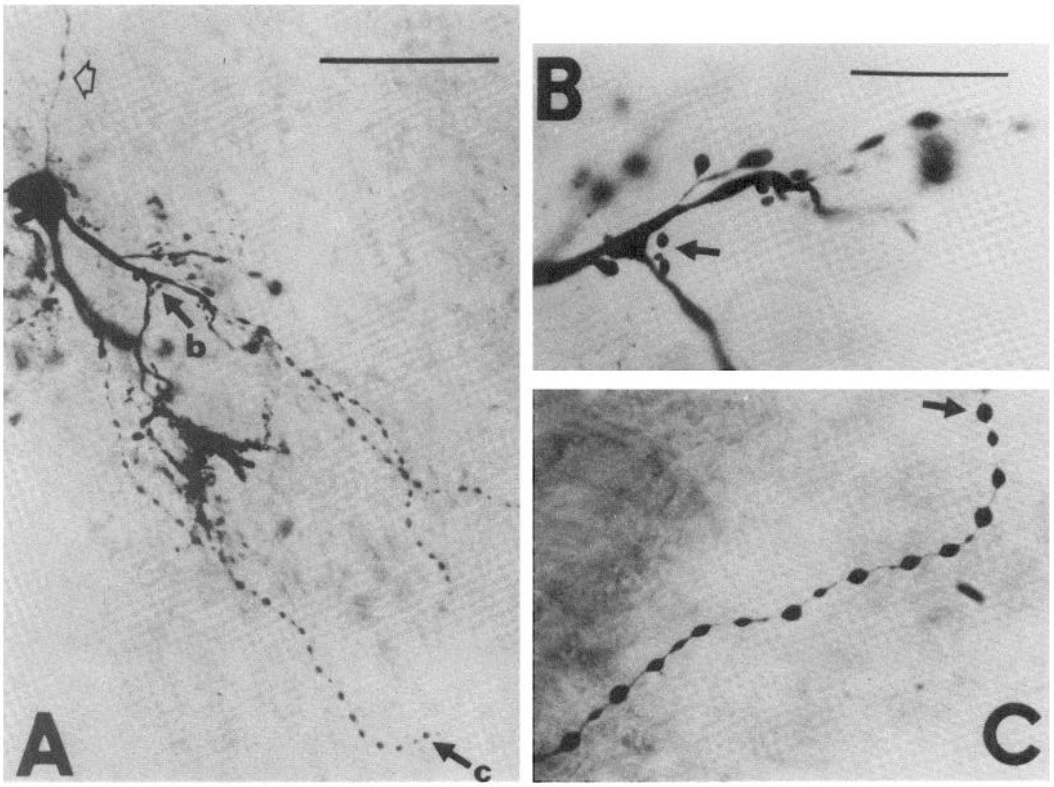

FIG. 11. Photomicrographs of the morphologically unclassified X-cell shown in Fig. 9*D*. *A*: lower power view showing soma and some of the ventral dendrites. The other dendrites drawn in Fig. 9*D* are from adjacent sections. The open arrow shows the axon. Filled arrows b and c refer, respectively, to structures shown in *B* and *C*. Scale: 50 μm. *B*: higher power view of dendritic branch point showing the only dendritic appendages found on this neuron. Scale: 20 μm and applies as well to *C*. *C*: higher power view of one of dendrites. Note the extensively beaded appearance of this dendrite, an appearance characteristic of the neuron's other dendrites.

Dendritic geometry

From Figs. 19 and 20, it is clear that the dendritic geometry of X-cells is generally different from that of Y-cells. Among other differences, X-cell dendrites tend to be elongated perpendicular to the laminae, whereas Y-cell dendrites tend to show no obvious orientation bias. We attempted to quantify this observation in the following manner. A series of five concentric rings at 50-μm intervals was centered on a drawing of the soma (cf. Ref. 70). The outermost ring, with a diameter of 500 μm, was large enough to include practically all dendrites of each cell. The rings were then divided into quadrants by two lines passing through the center at right angles to one another. Each line was oriented 45° to the left or right of the axis perpendicular to the lamination. This creates two vertical and two horizontal quadrants (see inset in Fig. 25*A*). By "vertical" and "horizontal," we now mean perpendicular and parallel, respectively, to the laminae. For a given cell, we then simply counted the number of intersections made by the dendrites with these rings, and the counts were made separately for each of the quandrants.

Figure 25*A* plots the number of intersections in vertical versus horizontal quandrants for each cell. The line of slope 1 is drawn simply to illustrate the loci of points expected for radially symmetric dendritic trees. The number of vertical versus horizontal intersections correlates for both X- and Y-cells (for X-cells: $r = +0.57$, $P < 0.001$; for Y-cells: $r = +0.57$, $P < 0.01$). However, note that most X-cell points fall well above the

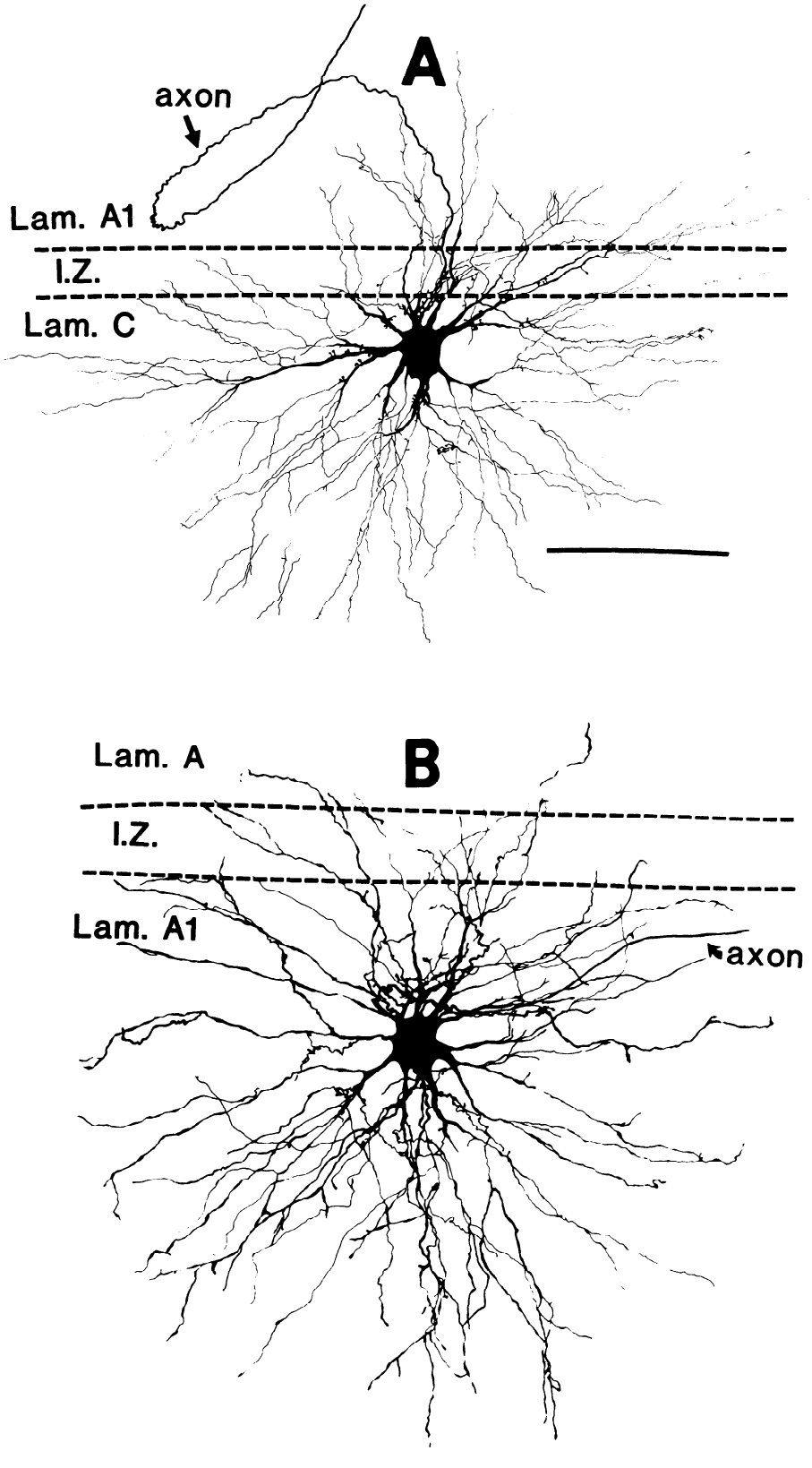
A
axon
Lam. A1
I.Z.
Lam. C
B
Lam. A
I.Z.
Lam. A1
axon

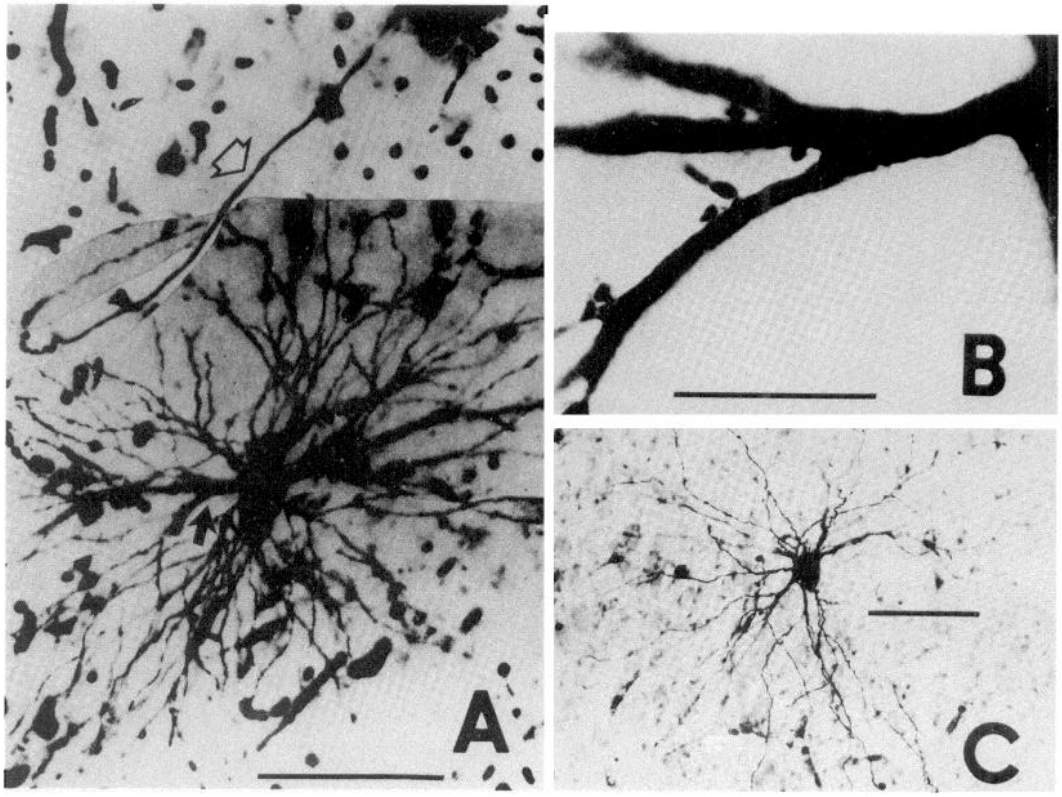

FIG. 13. Photomicrographs of class 1 Y-cells drawn in Fig. 12. *A*: low-power montage of neuron drawn in Fig. 12*A*. Note looping axon (open arrow). The filled arrow points to the dendritic branch point shown in *B*. Scale: 100 μm. *B*: high-power view of dendritic branch point of neuron shown in *A*. Several simple, spinelike appendages can be seen. Scale: 15 μm. *C*: low-power view of neuron drawn in Fig. 12*B*. Scale: 100 μm.

line of slope 1, as expected for their vertically oriented dendritic arbors, while most Y-cell points fall near the line. Indeed, the average ratio of vertical to horizontal intersections is 2.5 for X-cells and is 1.0 for Y-cells, and this difference between cell types is statistically significant ($P < 0.001$ on a Mann-Whitney U test). Thus, the vertical orientation of X-cell dendritic trees is quite different from the radially symmetric trees of Y-cells. One Y-cell point falls well above the line of slope 1 (this is the cell shown in Figs. 16*B* and 18). Without this point, the Y-cell correlation for vertical versus horizontal dendritic intersections becomes much better ($r = +0.93$, $P < 0.001$). Finally, note that the one W-cell point falls slightly below the line of slope 1. This is expected since this W-cell appears to be class 4 morphologically, and such cells have dendritic trees oriented parallel to the laminae (25).

Figure 25*B* shows, for X- and Y-cells, the frequency histograms of the total number of intersections in all quadrants, in just the vertical quadrants, and in just the horizontal quadrants. Generally X- and Y-cells have equal numbers of total intersections ($P > 0.2$ on a Mann-Whitney U test). The number of total intersections can be taken as a measure of dendritic density. Compared to Y-

FIG. 12. Drawings of two Y-cells with morphological class 1 features. Each has a large soma and thick, cruciate dendrites oriented in a radially symmetric fashion with few spinelike appendages. Each is a confirmed relay cell. *A*: lamina C neuron with some dendrites that cross the interlaminar zone (I.Z.) into lamina A1. Note the looping path taken by the axon. This cell is also shown in Fig. 13*A*, *B*. *B*: lamina A1 neuron with some dendrites that cross the interlaminar zone into lamina A. This cell is further illustrated in Fig. 13*C*. Scale: 100 μm.

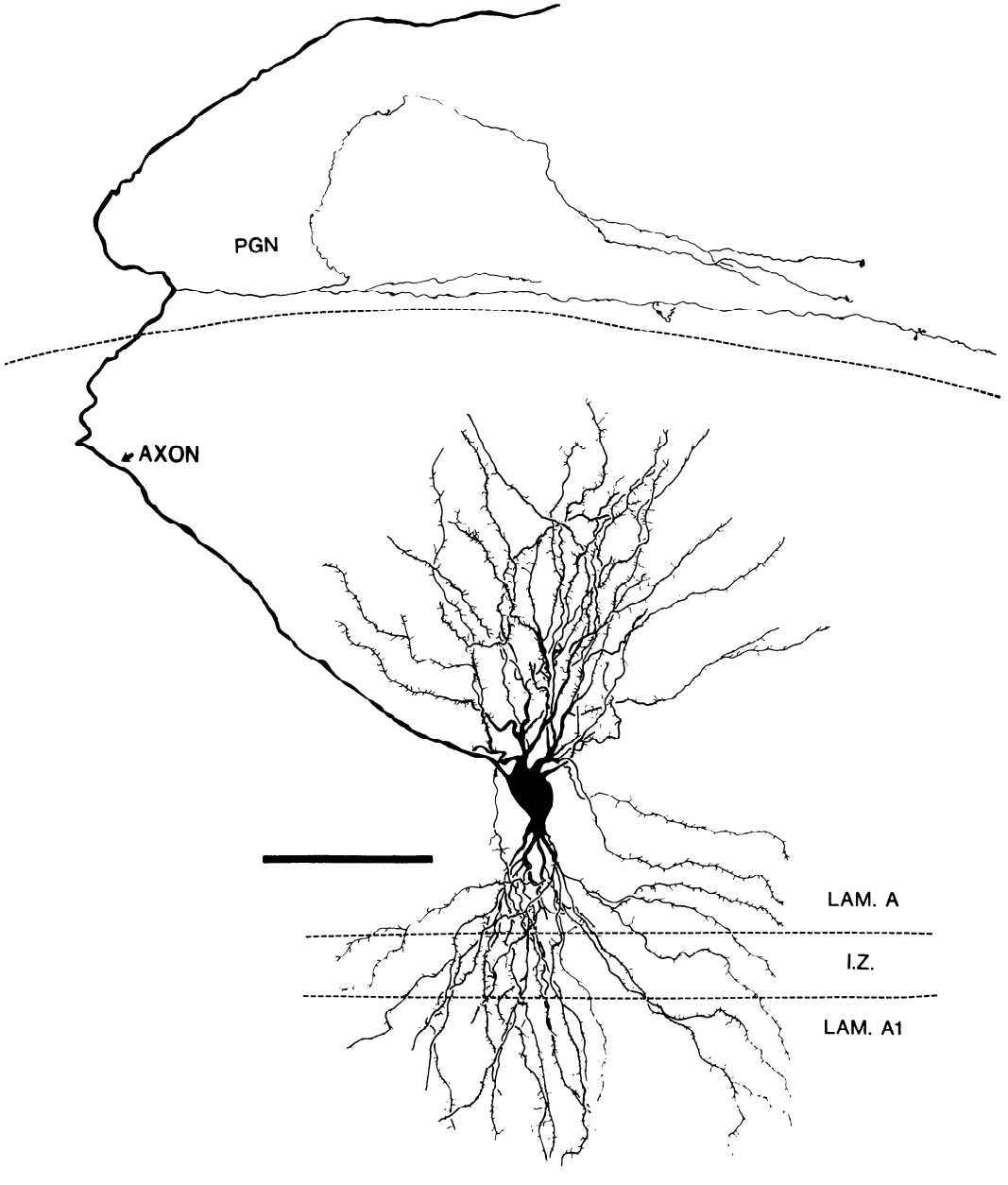

FIG. 14. Drawing of a relay Y-cell with class 1 morphological features. The axon passes through the perigeniculate nucleus (PGN) where an extensive collateralization occurs. These collaterals have numerous swellings that are probably presynaptic terminals. The perigeniculate nucleus is found just dorsal to lamina A (i.e., just above the upper dashed line). The soma and most dendrites are in lamina A, but some dendrites pass through the interlaminar zone (I.Z.) into lamina A1. The neuron had an excitatory receptive field only for the ipsilateral eye. Note the numerous filamentous appendages all along dendrites. The cell is further illustrated in Fig. 15. Scale: 100 μm.

cell dendritic trees, those of X-cells are less dense within the horizontal and more dense within the vertical quadrants ($P < 0.001$ for horizontal and $P < 0.01$ for vertical on a Mann-Whitney U test).

It should be emphasized that the data il-

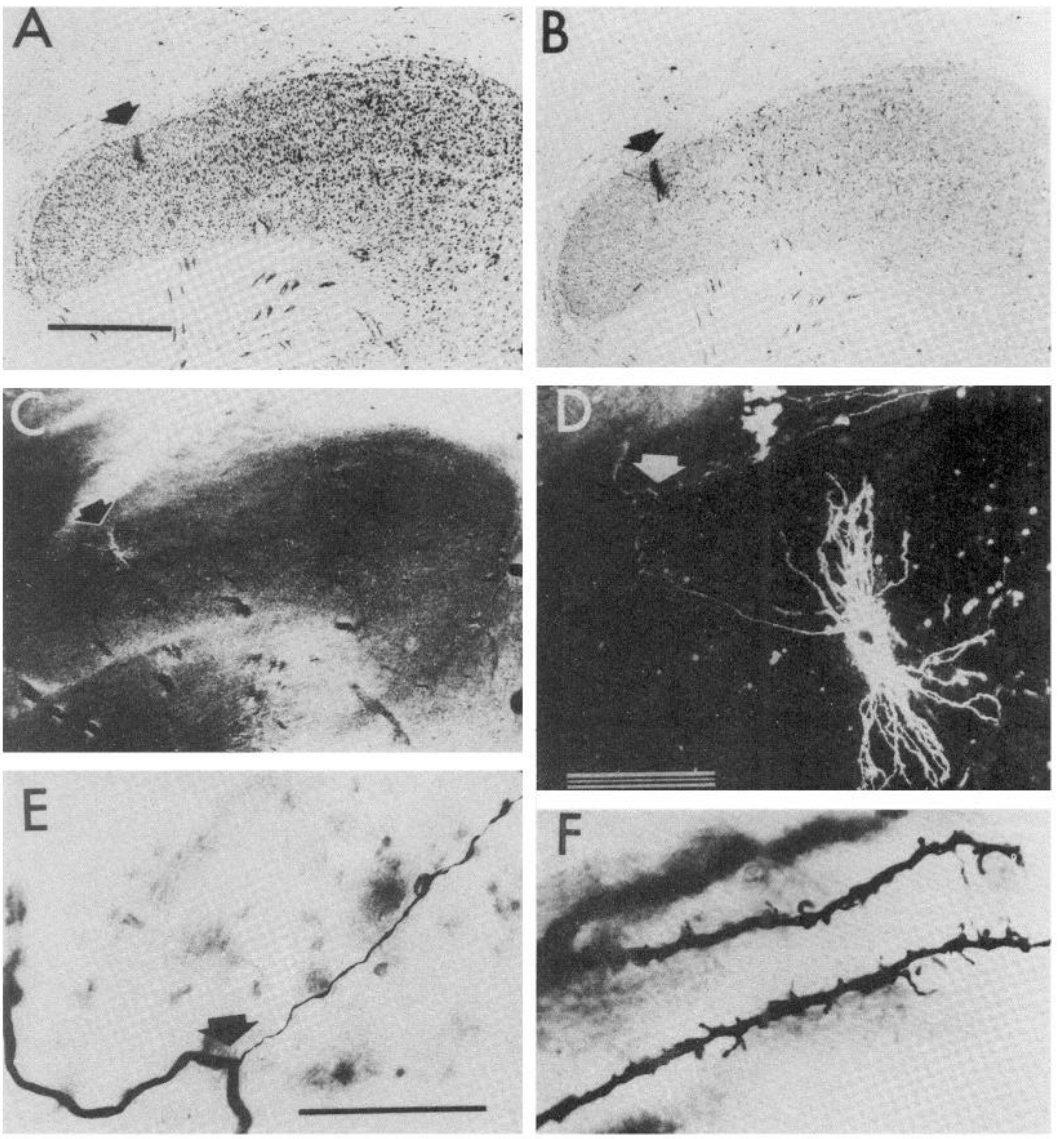

FIG. 15. Photomicrographs of the neuron drawn in Fig. 14. *A*, *B*, *C*: low-power views showing location of the neuron (arrow) in the lateral region of lamina A. The section is counterstained with cresyl fast violet. *A* is a brightfield view photographed with no filter, whereas *B* shows the same view photographed through a deep blue (Kodak Wratten 49B) filter. Note how the filter diminishes the effect of the Nissl stain while it enhances contrast between the HRP-filled neuron and the background. *C* shows the same field of view in darkfield. The scale in *A* is 1 mm and applies as well to *B*, *C*. *D*: medium-power, darkfield montage showing axon course and perigeniculate collaterals. The arrow indicates the point at which these collaterals emerge from the parent axon, a region shown again in *E*. Scale: 200 μm. *E*: high-power, brightfield view of axonal collateral branching (arrow) in the perigeniculate nucleus. Note the thin collateral branch. Scale: 50 μm and applies as well to *F*. *F*: high-power, brightfield view of typical dendritic region. Note the filamentous appendages.

lustrated in Fig. 25 are obtained from material sectioned in the coronal plane. The geniculate projection lines are tilted such that they are more anterior dorsally (63). Therefore, a dendritic tree truly oriented along projection lines would seem less oriented if viewed obliquely to the projection lines in the coronal plane. We might have

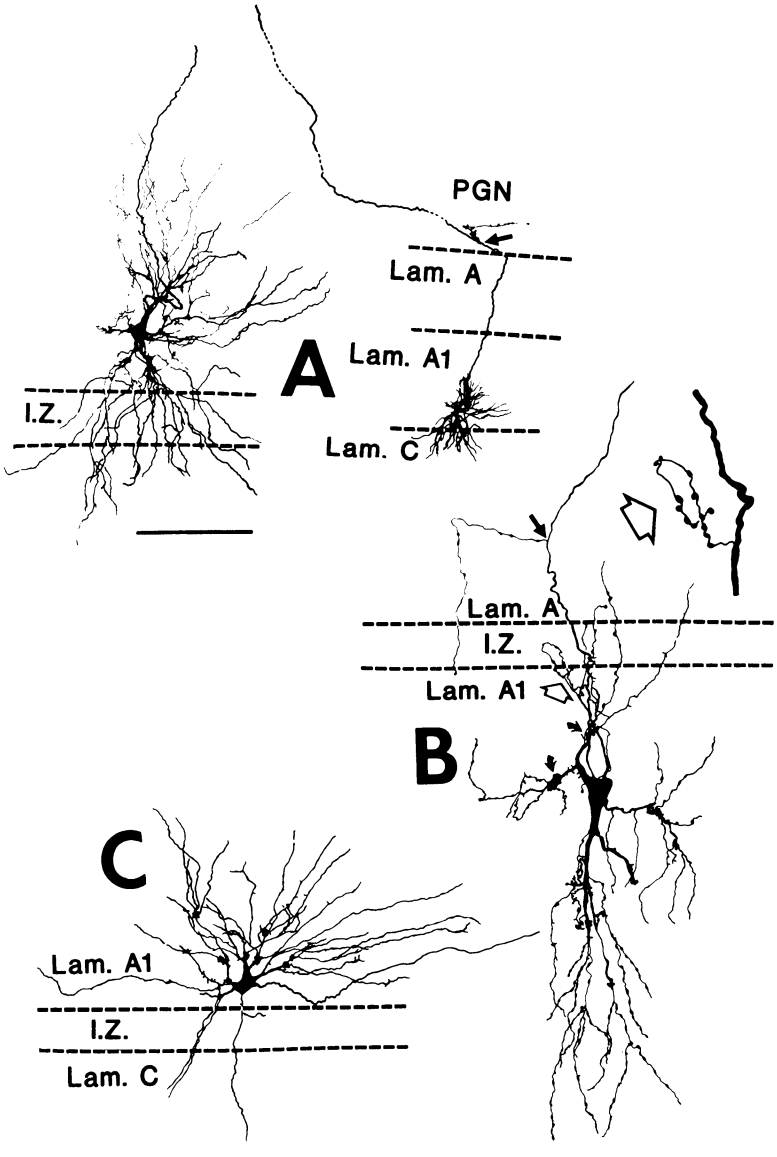

FIG. 16. Drawings of three relay Y-cells with class 2 morphological features. All have grapelike clusters appended at numerous dendritic branch points. Despite some translaminar dendrites for each cell, these appended clusters are all located in the same lamina as the soma. *A*: lamina A1 neuron drawn in higher (left) and lower (right) powers. The cell is further illustrated in Fig. 17. Note the ventral dendrites that course through the interlaminar zone (I.Z). into lamina C. The axon (right drawing) courses vertically through lamina A and the perigeniculate nucleus (PGN), at which point a fine collateral arborization can be seen (arrow; see also Fig. 17*B*). *B*: lamina A1 neuron with the most vertically oriented dendrites of any Y-cell. The cell is further illustrated in Fig. 18. Large grapelike clusters are seen at many dendritic branch points (curved, filled arrows show two examples; see also Fig. 18*A*, *B*). The axon issues two intrageniculate collateral branches near the interlaminar zone. The dorsal one (straight, filled arrow) is also shown in Fig. 18*C*. The ventral one (small, open arrow) is redrawn at higher power in the inset (large, open arrow). Swellings along this latter collateral are probably presynaptic terminals. Finally, note the beaded appearance of the dendrites peripheral to the first branch point (see also Fig. 18*D*). *C*: lamina A1 neuron with several dendrites coursing down into lamina C. Scales are as follows: left drawing of *A*, 100 μm; right, 250 μm; main drawing of *B*, 100 μm; inset 50 μm; *C*, 100 μm.

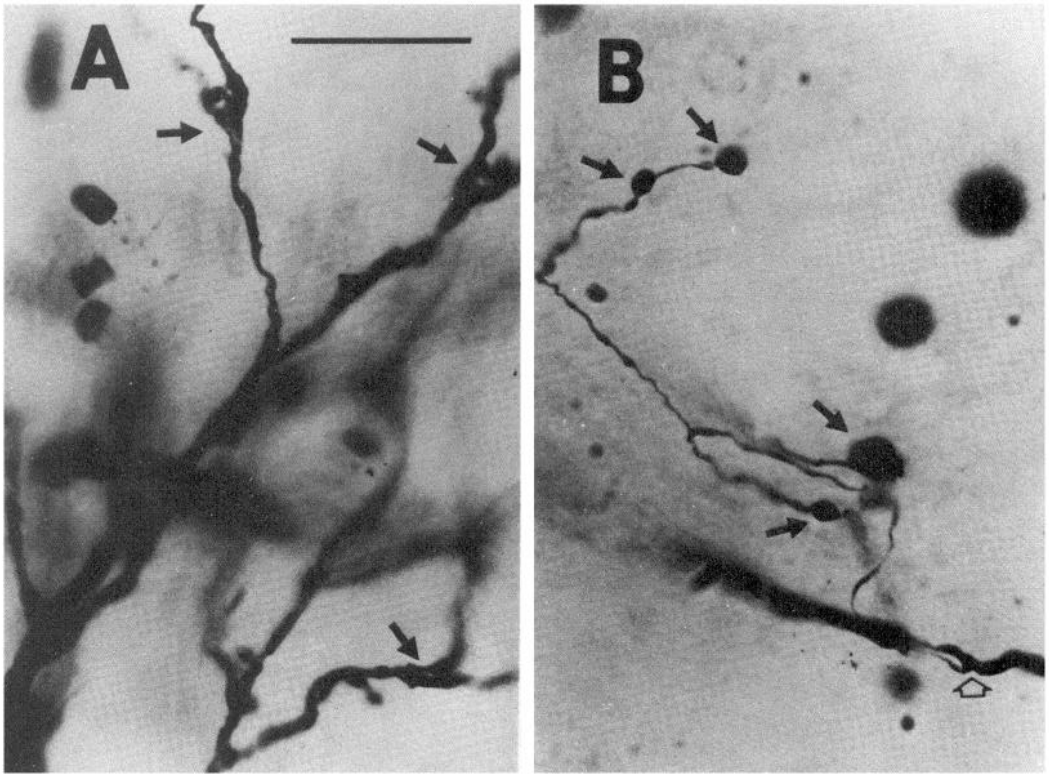

FIG. 17. Photomicrographs of class 2 Y-cell drawn in Fig. 16*A*. *A*: region of dendrites showing several, small grapelike clusters at dendritic branch points (arrows). Part of the soma can be seen in the lower left corner. *B*: axon collaterals in perigeniculate nucleus from region indicated by arrow in Fig. 16*A*. The open arrow here points to a fine branch emerging from the thicker parent axon. Numerous swellings (filled arrows) can be seen along and at the end of collateral branches. These swellings are probably presynaptic terminals. Scale: 10 μm in *A* and applies as well to *B*.

underestimated this feature for X-cells. However, all but one of our X-cells were located in the middle third of the nucleus where the discrepancy between projection lines and the coronal plane is minimal (roughly 10°) and the degree of underestimation is probably small.

Relationships among dendritic geometry, cell size, and receptive-field size

As mentioned above, the total number of intersections between the dendrites and concentric rings can be considered a rough measure of dendritic extent. Figure 26*A* shows that this measure correlates with soma size for all cells ($r = +0.58$, $P < 0.001$). However, the correlation is better for the subpopulations of both X-cells ($r = +0.82$, $P < 0.001$) and Y-cells ($r = +0.83$, $P < 0.001$). The functions relating these variables are essentially parallel for X- and Y-cells, but they are shifted toward larger somata for Y-cells. The ratio of these variables is statistically different for the X- and Y-cell populations ($P < 0.001$ on a Mann-Whitney U test). In other words, given that Y-cells have larger somata than do X-cells and that both cell types have equally extensive dendritic trees, soma size and dendritic extent are otherwise correlated highly and equally for X-cells and for Y-cells.

Figure 26*B* illustrates the relationship between receptive-field center size and dendritic extent. These values are reasonably well correlated for X-cells ($r = +0.78$, $P < 0.001$) but not at all for Y-cells ($r = +0.06$, $P < 0.2$), and the X-cell population differs significantly from the Y-cell population in this relationship ($P < 0.001$ on a comparison of z scores).

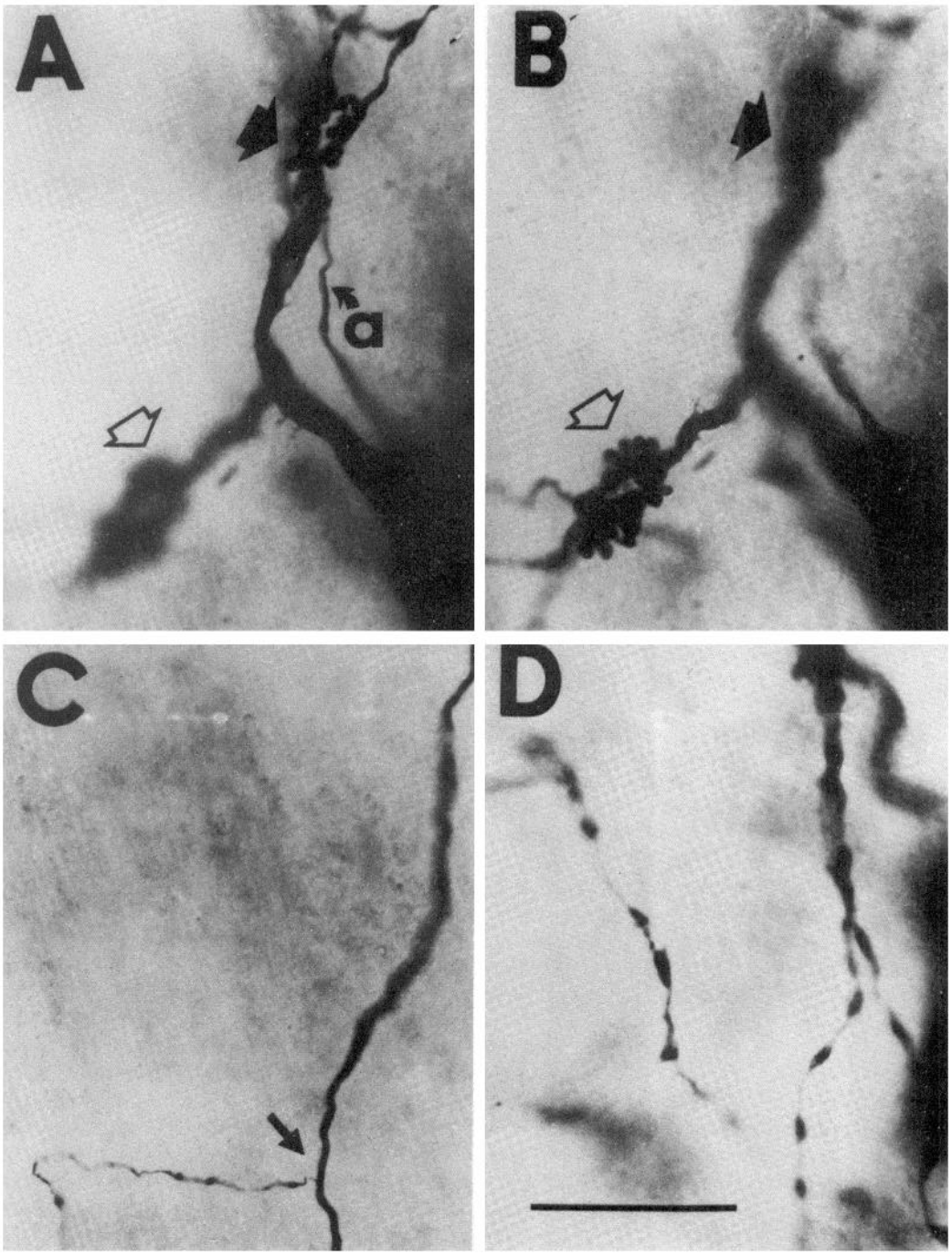

FIG. 18. Photomicrographs of class 2 Y-cell drawn in Fig. 16*B*. *A*, *B*: large, grapelike clusters (larger arrows) at dendritic branch points seen in the same field of view at two different focal planes. These clusters are indicated by the curved, filled arrows in Fig. 16*B*. The axon (a) can also be seen coursing from the soma. *C*: intrageniculate axon collateral. The arrow points to the same branch point as is indicated by the straight, filled arrow in Fig. 16*B*. Note that along the fine collateral branch are swellings that might represent presynaptic terminals. *D*: examples of beaded dendrites found peripheral to the initial dendritic branch point. This field of view is from the most ventral position of the dendritic tree. Scale: 25 μm in *D* applies as well to *A*–*C*.

TABLE 2. *Physiological properties of illustrated neurons*

Cell Type	Center Type	Center Size, deg	Eccentricity, deg	OX Latency, ms	Dominant Eye	Lamina of Soma	Figure
X	On	0.35	4.5	2.4	Contra	A	3*A*; 4*A*, *B*
X	On	0.35	2.0	1.9	Ipsi	A1	3*B*; 4*C*, *D*
X	On	0.45	26.0	2.4	Contra	A	5*A*; 6
X	Off	0.30	10.5	1.8	Contra	A	5*B*
X	Off	0.80	14.0	1.5	Ipsi	A1	7*A*, *B*; 8*A*
X	Off	0.50	9.0	1.7	Ipsi	A1	7*C*; 8*B*, *C*
X	On	0.40	2.5	1.8	Ipsi	A1	7*D*
X	Off	0.35	10.0	1.9	Contra	A	9*A*, *B*; 10
X	Off	0.40	7.0	2.0	Ipsi	A1	9*C*
X	Off	0.40	6.5	2.1	Ipsi	A1	9*D*; 11
Y	On	1.50	29.0	1.2	Contra	C*	12*A*; 13*A*, *B*
Y	On	1.50	4.0	1.1	Ipsi	A1	12*B*; 13*C*
Y	Off	1.20	31.0	1.4	Ipsi	A	14; 15
Y	On	1.00	2.5	1.3	Ipsi	A1	16*A*; 17
Y	On	1.05	15.0	1.2	Ipsi	A1	16*B*; 18
Y	On	0.75	7.5	1.3	Ipsi	A1	16*C*
W	On	0.25	6.0	4.0	Contra	C*	21; 22

* Denotes C-laminae.

It follows from Fig. 26*A*, *B* that soma size should relate to receptive-field center size for X-cells, but not Y-cells. The correlations are illustrated in Fig. 26*C* and show a less clear difference between X- and Y-cells than might be expected. X-cells display only a fair correlation for these parameters ($r = 0.64$, $P < 0.001$), and the Y-cell correlation is only marginally worse ($r = 0.45$, $P < 0.05$).

The significance of the relationships illustrated in Fig. 26 and their differences among X- and Y-cells is largely unclear. Some of these data will be reconsidered in the DISCUSSION.

Axon diameters of X- and Y-cells

Axon diameters of the 20 X- and 17 Y-cells with HRP-filled axons (see above) were measured with the same optical equipment employed for the cell drawings. We used a drawing tube attachment on a microscope with a 100× oil objective (NA, 1.32) and a relatively narrow-band, deep blue filter (Kodak Wratten 48A or 49B). The blue filter serves two purposes: it enhances contrast between the diaminobenzidine-HRP reaction product and the background (cf. Fig. 15*A*, *B*); and the use of narrow-band, short-wavelength light optimizes resolution through the light microscope. Under ideal conditions (very thin sections, proper cover slips, monochromatic, short-wavelength light, etc.), the theoretical resolution of such an instrument is 0.2–0.3 μm. Our thick sections undoubtedly reduce this resolution, and we feel that we are capable of no better than 0.5-μm precision in our measurements of axon diameters. We consequently made these to the nearest 0.5 μm. They were taken at a distance of 100–200 μm from the soma and within this range, 20 loci were pseudorandomly selected and the measurements averaged. Averaging was done because many axons appear variable in diameter (Fig. 27) and we wished to obtain a representative measure of average axon diameter for each cell.

Figure 28*A* shows the frequency histograms of axon diameters for the X- and Y-cells in our sample. As expected, Y-cells possess larger axons than do X-cells on average ($P < 0.001$ on a Mann-Whitney U test), although overlap is present in our data. Figure 28*B* shows further that larger somata are associated with larger axons. This correlation holds not only for the entire neuronal population ($r = +0.80$; $P < 0.001$) but also for the separate X-cell ($r = +0.80$, $P < 0.001$) and Y-cell subgroups ($r = +0.58$, $P < 0.01$). Ferster and LeVay (19) noted a similar trend.

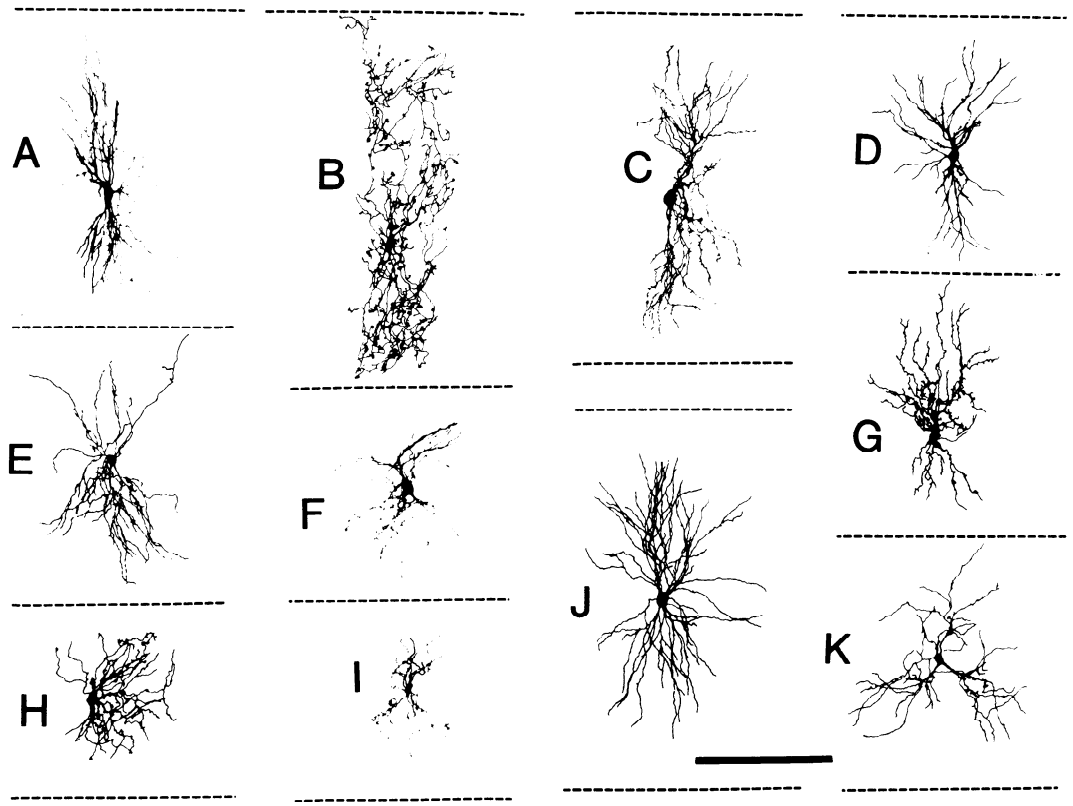

FIG. 19. Summary drawings of 11 representative X-cells. The laminar borders are indicated by the dashed lines. Note the small somata, the generally vertical orientation of dendrites, and the failure of any dendrites to cross laminar borders. Neurons among this group illustrated in other figures are as follows: *B* can be found in Figs. 3*B*, 4*C*, *D*; *C*, in Figs. 5*A*, 6; *D*, in Fig. 9*C*; *E*, in Figs. 9*D*, 11; *G*, in Figs. 3*A*, 4*A*, *B*; *I*, in Fig. 5*B*; *J*, in Figs. 9*A*, *B*, 10; and *K*, in Fig. 7*D*. Scale: 200 μm.

DISCUSSION

These data have led us to three general conclusions, one of which was expected and two of which are rather surprising. The expected conclusion is that geniculate X-cells differ morphologically from Y-cells, although considerable heterogeneity exists within each neuronal class. A rather unexpected conclusion derives from the observation of several geniculate relay cells with morphological class 3 features (25), a morphological type hitherto thought to be associated strictly with interneurons (16, 17, 48, 49, 79). We conclude from this that class 3 morphological properties may not relate generally to interneurons, and suggest that the basic concept of a distinct class of intrageniculate interneurons should be reconsidered. Finally, and also surprisingly, our data suggest both that electrode sampling based on soma size may play less of a role than assumed and also that the geniculate X- to Y-cell ratio is less than 2 to 1, whereas many prior estimates (e.g., Refs. 47, 68, 71) place the ratio at 5 or 10 to 1. Because for technical reasons our data base is small and because these conclusions regarding interneurons and the geniculate X- to Y-cell ratio are surprising, we wish to emphasize the qualified nature of these conclusions.

Potential artifacts

Before we discuss our interpretations of the data, we shall briefly discuss some potential artifacts of our methodology. These fall into physiological and morphological categories.

PHYSIOLOGICAL. Two sources of physiological artifact can be considered. First, the

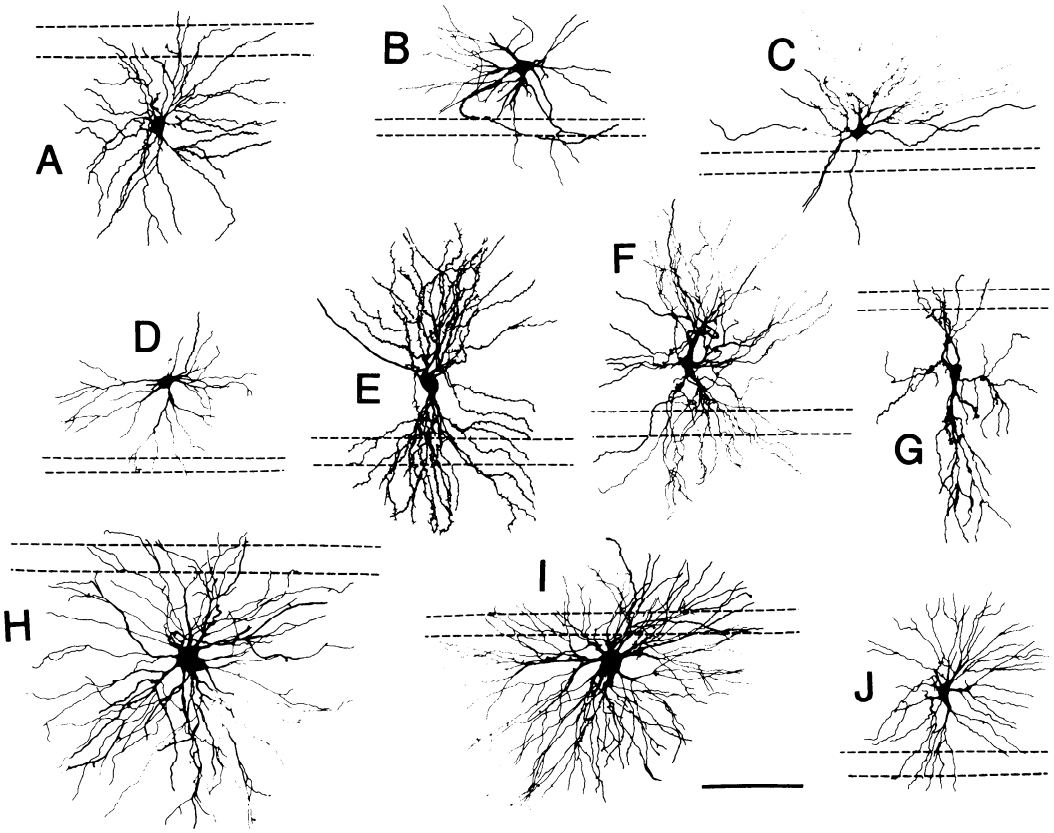

FIG. 20. Summary drawings of 10 representative Y-cells. Relevant laminar borders are indicated by parallel, dashed lines which demarcate the interlaminar zone. Note that somata are large, that the dendritic trees of these cells usually show no obvious orientation, and that every cell has some dendrites that cross laminar borders. Neurons among this group illustrated in other figures are as follows: *C* can be found in Fig. 16*C*; *E*, in Figs. 14, 15; *F*, in Figs. 16*A*, 17; *G*, in Figs. 16*B*, 18; *H*, in Figs. 12*B*, 13*C*; and *I*, in Figs. 12*A*, 13*A*, *B*. Scale: 200 μm.

HRP-stained neuron might be different from that which we studied electrophysiologically. For instance, after our physiological study, the electrode tip might have come out of one cell and immediately penetrated a second, and the latter neuron was stained. This seems an extremely unlikely possibility and, in any case, could not have been a general source of error because we always monitored a cell's activity intracellularly before, during, and after HRP iontophoresis (see MATERIALS AND METHODS). We never saw evidence of such a potential artifact.

Second, we cannot be certain how representative our neuronal sample is. While we have presented evidence of little or no bias based on soma size (see Fig. 24*B*; see also below), this analysis does not address other sources of sampling artifact. For instance, neurons that might not exhibit regenerative action potentials could be missing from our sample. However, the morphological data obtained in this study are quite similar to those obtained from purely morphological studies (e.g., Nissl stains and Golgi impregnations) despite the different potential biases that might affect these studies. That is, we accept whatever anatomical data we obtain, and the only plausible bias in selecting these data are based on electrode sampling. Golgi studies yield data that are dependent on the capriciousness of the unpredictable impregnation of neurons and the investigator's subjective decision as to what constitutes a sufficiently impregnated neuron to be included in the sample. Despite these different poten-

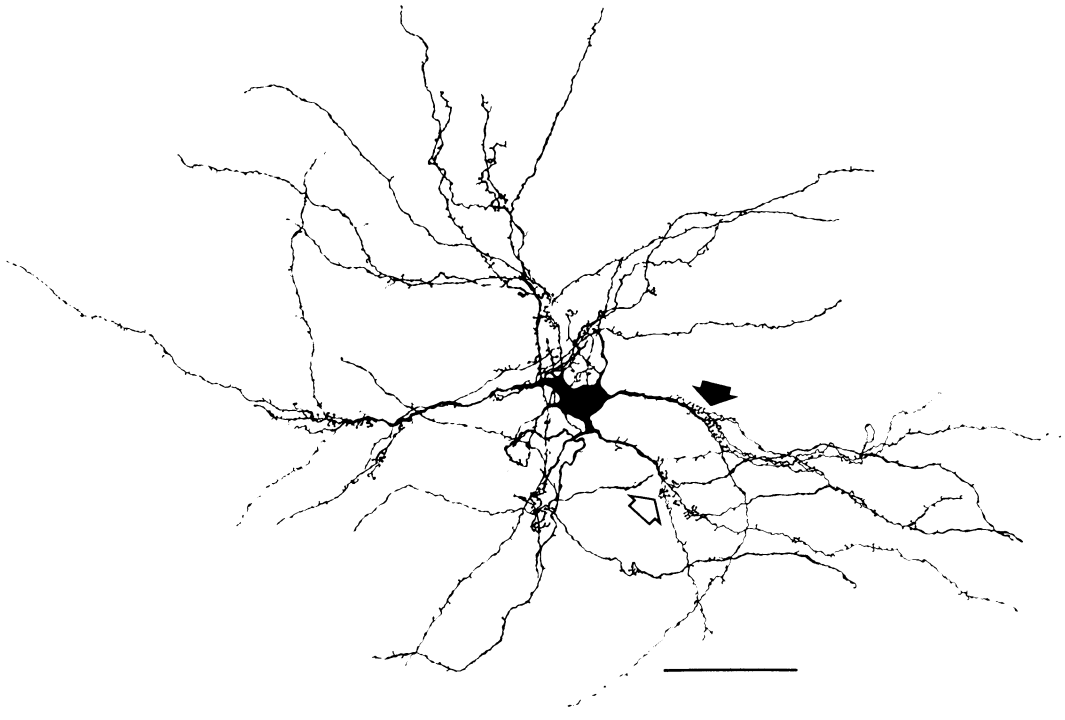

FIG. 21. Drawing of a W-cell located in the C-laminae. The scale is 50 μm and is oriented roughly parallel to the lamination. Thus dendrites are also oriented in this direction. This dendritic orientation plus the small soma and fine dendrites are consistent with class 4 morphology. However, several of the dendritic branch points have clustered appendages (e.g., arrows) which could be construed as a class 2 morphological characteristic. These appendages are further illustrated in Fig. 22.

tial sources of sampling artifact, the morphological data we obtained are remarkably similar to morphological data from other studies (e.g., Refs. 16, 25, 48, 80).

MORPHOLOGICAL. The possibility, however unlikely, exists that injecting HRP into a neuron distorts its shape. For instance, soma size could be affected. It could either increase, due to the extra volume of HRP injected and/or to osmotic imbalances caused by the injection that result in uptake of water by the cell, or decrease, due to osmotic imbalances that result in loss of water. However, the similarity of our soma size distribution with that obtained with a Nissl stain render such an artifact extremely unlikely. Furthermore, soma sizes of various soma-dendritic types in our sample are in the range described by Guillery (25) for similar types after Golgi impregnation.

It is also possible that HRP-filled cells do not reflect an accurate picture of dendritic or axonal morphology. The HRP might not routinely enter fine dendritic processes or appendages or fine axonal processes. This possibility also exists for Golgi impregnation and is a potential artifact that is difficult to discount. It is also possible that some of the dendritic beading, varicosities, or appendages we have described result from distortions or artifacts created either by degenerative changes in injured neurons or by increased intracellular pressure operating on the weaker areas of membrane. This latter possibility might be analogous to the creation of vascular aneurysms. However, such an artifact seems unlikely since the morphological features we have described in our sample of HRP-filled neurons all have been previously described in studies of Golgi impregnations (16, 25, 80). Our current ultrastructural studies of these HRP-filled neurons (82) may shed some light onto the question of whether or not any of these morphological details are indeed artifacts.

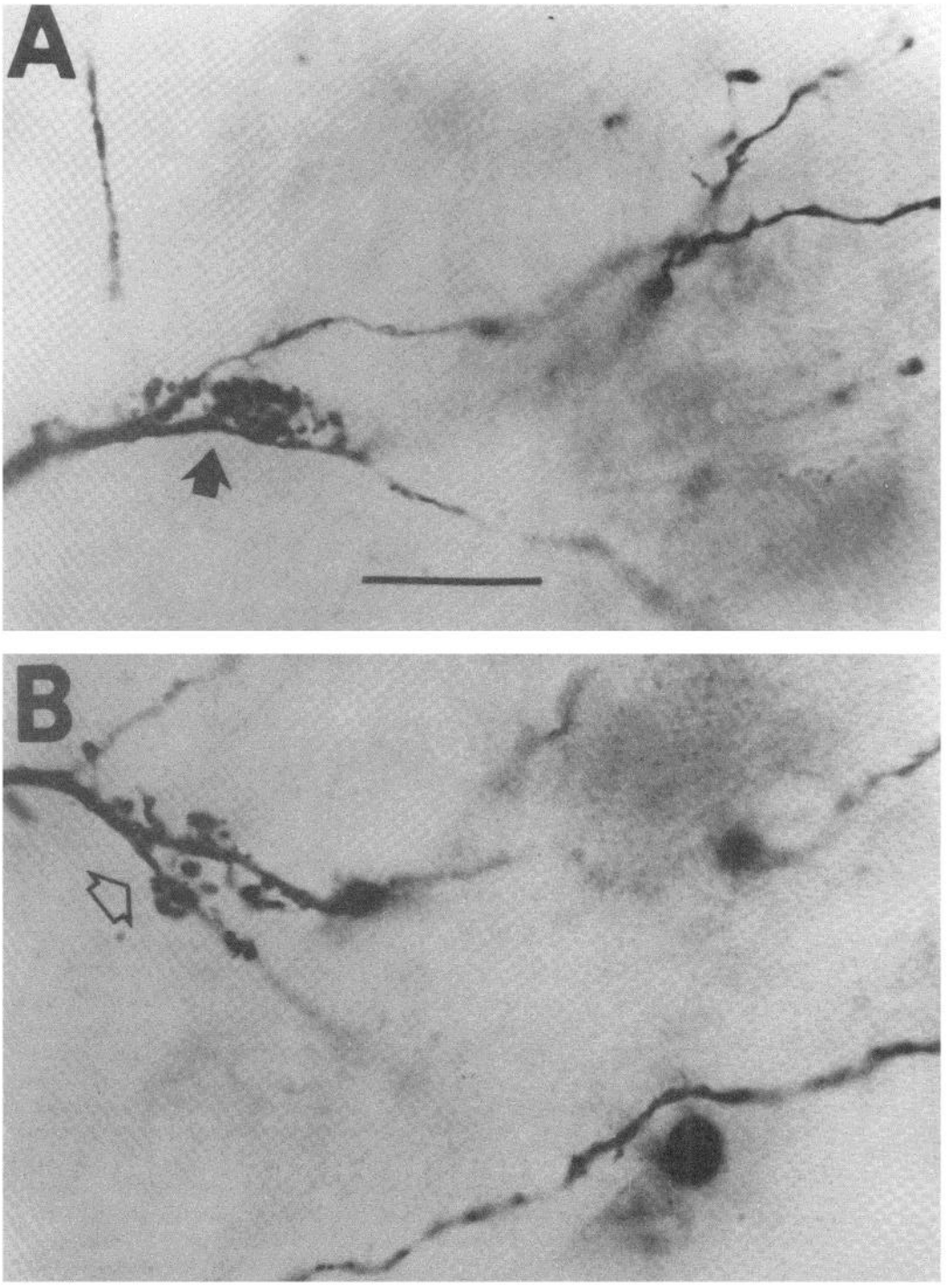

FIG. 22. Photomicrographs of dendritic regions from cell drawn in Fig. 21. *A*: grapelike clusters appended at dendritic branch point (arrow). This region is indicated by the filled arrow in Fig. 21. *B*: grapelike cluster appended at dendritic branch point (arrow). This region is indicated by the open arrow in Fig. 21. Scale: 20 μm in *A* and applies as well to *B*.

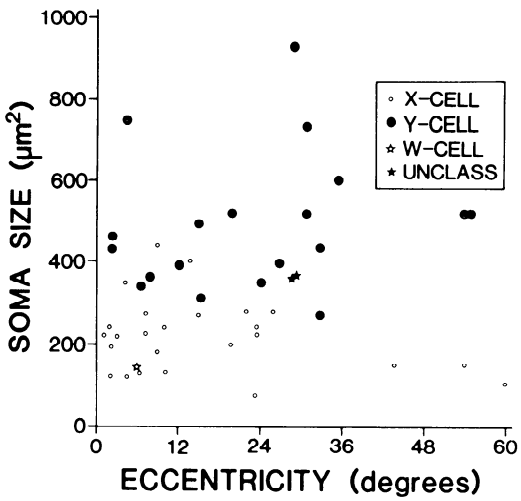

FIG. 23. Plot of soma size versus receptive-field eccentricity from the area centralis representation for each of the 47 geniculate neurons in our sample. No relationship between these variables is seen (see text).

Thus, while we cannot exclude the possibility of physiological or anatomical artifacts in our data, we feel that the likelihood of their occurrence is small and almost certainly has not led us to incorrect conclusions. A more likely source of interpretational error could be our limited sample size of neurons.

Differences between X- and Y-cell morphology

The major finding of this study is that, in the lateral geniculate nucleus, X-cells have different morphological features than do Y-cells. While expected, this result is not trivial, because it seemed equally logical, as suggested in INTRODUCTION, to imagine that all functional (and structural) differences between X- and Y-cells are limited to the retina. If at least some of the morphological differences described for geniculate X- and Y-cells represent the basis of functional differences in geniculate circuitry, then differences between the X- and Y-cell pathways are reinforced in the lateral geniculate nucleus. These differences between X- and Y-cell structure are discussed below, first, in terms of prior morphological classification schemes, and second, in terms of a scheme that permits reasonable identification of X- and Y-cells solely on morphological grounds.

OTHER MORPHOLOGICAL CLASSIFICATION SCHEMES. Since the scheme of Guillery (25) seems that most widely used to classify the morphology of geniculate neurons in the cat, we shall use this as a starting point with which to compare our morphological results. As outlined in INTRODUCTION, Guillery (25) described class 1, class 2, class 3, and class 4 morphological types among these cells and also emphasized that 40% of his sample had intermediate or unclassified morphology. Our sample (including the W-cell) also includes these morphological types and we, too, found morphologically intermediate or unclassified cells (see Table 1). The intermediate and unclassified cells raise questions about the completeness of Guillery's (25) classification scheme as well as its relationship to functional classification. Nonetheless, Table 1 clearly shows that the Guillery (25) classification scheme relates rather well to X- and Y-cells. Overlap exists only for the class 2 category although, as noted in RESULTS, class 2 Y-cells can be distinguished structurally from class 2 X-cells.

Although the Guillery (25) scheme is useful and has some functional relevance, it was not always completely clear (to us) into which class certain cells belong. Several of the differentiating criteria seem somewhat vague or qualitative. For instance, a cell was considered to be at least partially class 2 if several of the primary or secondary branch points had some grapelike or bulbous appendages. There is considerable variation among our class 2 cells in the size, number, and precise location (relative to the branch points) of these appendages. A similar range in density and appearance of the complex stalked appendages characteristic of our class 3 cells is also evident. The possibility exists that different investigators might apply different criteria to these characteristics and place the same cell population into somewhat different distributions of the Guillery (25) classification scheme, and this possibility seems particularly strong for classes 2 and 3. Partly for this reason we shall attempt below to outline differences between X- and Y-cell morphology in a manner independent of the Guillery (25) scheme, although many of the same structural features are considered.

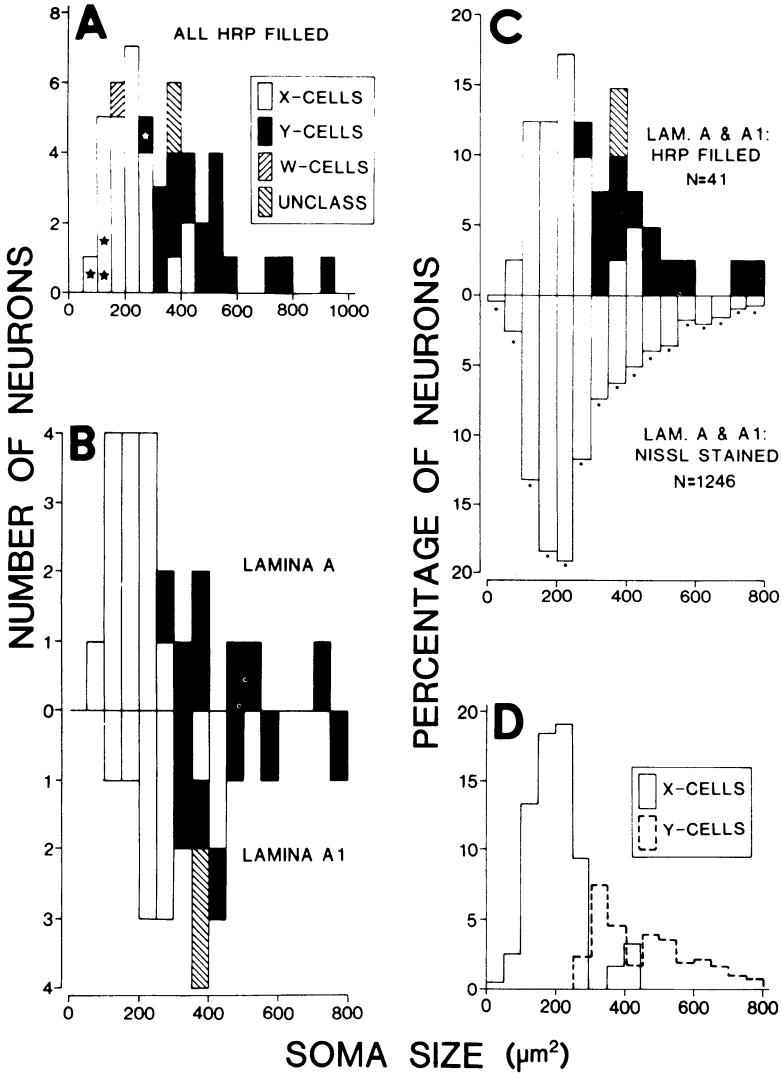

FIG. 24. Soma size distributions for geniculate neurons. *A*: distributions for the entire sample of 47 physiologically and morphologically studied cells. Stars represent the three X-cells and one Y-cell that were not identified as relay cells. Physiological classification of these cells is indicated by the box. Note that the unclassified cells have soma sizes in the zone of overlap between those of X- and Y-cells. *B*: separate distribution for each of the A-laminae. For both X- and Y-cells, lamina Al somata are larger than those in lamina A, but the difference is statistically significant only for X-cells (see text). *C*: distributions for somata limited to laminae A and A1. The upper histogram represents the subpopulation from *A* of 41 neurons limited to the A-laminae (i.e., the five Y-cells and one W-cell from the C-laminae are removed). The lower histogram represents the soma size distribution for a total of 1,246 neurons from adjacent, Nissl-stained sections in 11 of the cats (see text). A separate histogram was compiled for each cat. The present histogram was constructed by computing the mean value for each bin from the 11 separate histograms, and the standard error of these means is shown by dots above each bin. Note the similarity in distributions of the upper and lower histograms (see text). *D*: estimate of relative X- and Y-cell size distributions for the A-laminae computed from *C*. From *C*, upper, we concluded that all soma sizes below 250 μm^2 belong to X-cells; and all above 450 μm^2, to Y-cells. For bins representing intermediate soma sizes, we multiplied the percentages in *C*, lower, by the relative fraction of X- and Y-cells from *C*, upper. In this analysis, we did not include the two physiologically unclassified cells. These calculations lead to the X- and Y-cell distributions in *D*, and from this we conclude that roughly 35% of the neurons in the A-laminae are Y-cells (see text).

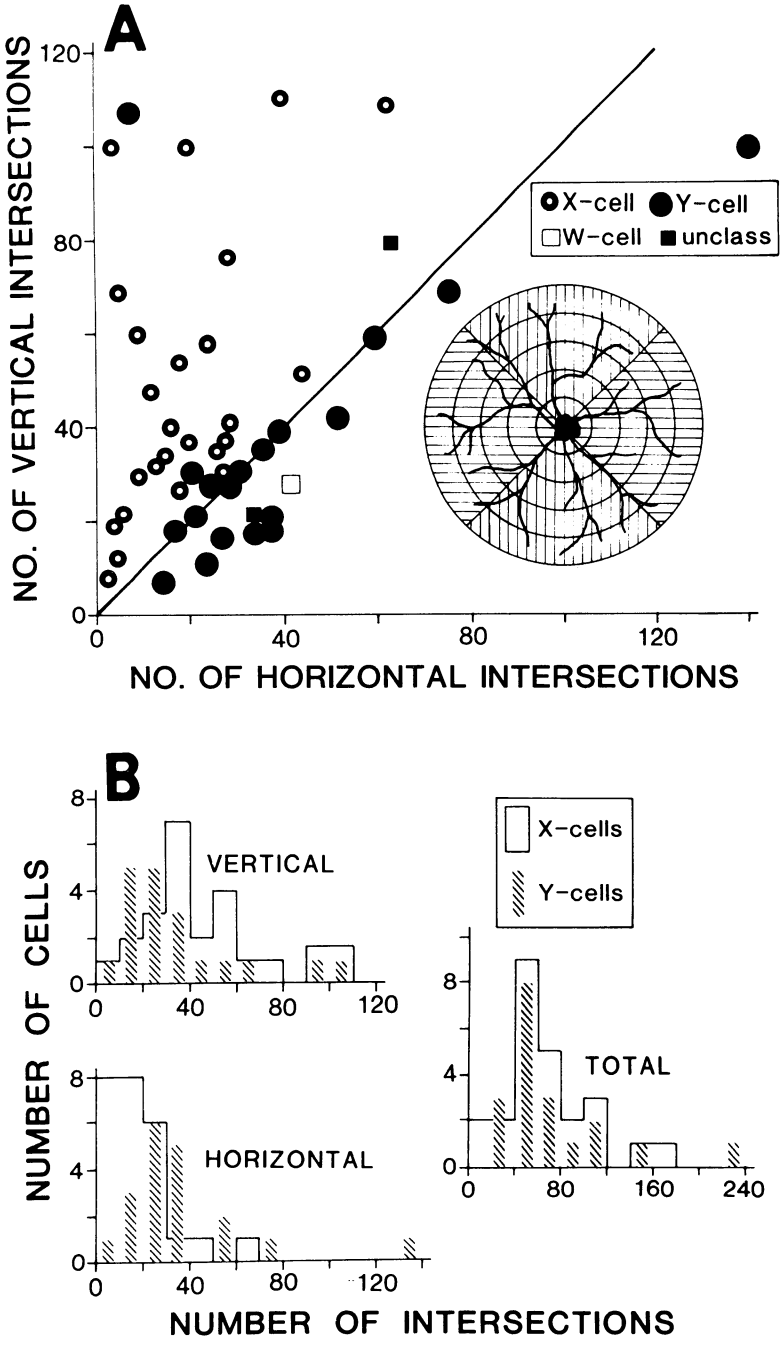

FIG. 25. Numbers of dendritic intersections with five concentric circles, spaced 50 μm apart and centered on the soma (see inset in *A*), for the 47 HRP-filled cells in our study. The inset in *A* also illustrates the manner by which the zones of these intersections were divided into vertical quadrants (vertical hatching) and horizontal quadrants (horizontal hatching) with respect to the lamination. *A*: scatter plot of number of horizontal and vertical intersections for each cell. The box shows the key, and the line of slope 1 is drawn to indicate the relationship expected for radially symmetric dendritic trees. Both X- and Y-cells demonstrate a positive correlation between their numbers of vertical and horizontal intersections, but the relationship for X-cells differs from that of Y-cells (see text). *B*: numbers of vertical, horizontal, and total intersections (total number equals vertical plus horizontal numbers) for X- and Y-cells. The box shows the key. X-cells have more vertical and fewer horizontal intersections than do Y-cells, and no difference is seen in the numbers of total intersections (see text).

A related morphological classification scheme that has received considerable attention recently was described by LeVay and Ferster (48). These authors noted that a population of neurons in the A-laminae contain a curious cytoplasmic structure, the "cytoplasmic laminated body" (see Refs. 28, 58, 59, 72, 84 for a description of these cytoplasmic structures among other neuronal populations). In the A-laminae, cells with cytoplasmic laminated bodies have intermediate soma sizes (roughly 15–25 μm in diameter) plus a distribution and cortical projection pattern reminiscent of X-cells (i.e., projections to area 17 only; see Ref. 76). In the A-laminae, cells without the cytoplasmic structures can be divided into a larger group (roughly 20–40 μm in diameter) whose neurons have a distribution and cortical projection pattern reminiscent of Y-cells (i.e., projections to areas 17 and 18; see Ref. 76), and a smaller group (roughly 10–25 μm in diameter). LeVay and Ferster (48) then showed that each of nine Golgi-impregnated class 1 cells had a large soma without a cytoplasmic laminated body, eight of nine class 2 cells had the cytoplasmic structure, and each of six class 3 cells had a small soma without the structure. Cells not placed into one of these classes were not described although such cells represented 40% of Guillery's (25) population. LeVay and Ferster (48) consequently proposed that in the A-laminae, the class 1 cells are Y-cells, representing roughly one-third of the neurons, the class 2 cells are X-cells, representing roughly two-fifths of the neurons, and the class 3 cells are interneurons, representing roughly one-fourth of the neurons (see also Refs. 43, 66).

Our data contradict some aspects of the LeVay and Ferster (48) proposal and support others. Table 1 shows that X- and Y-cells are not isomorphic with class 2 or 1 morphology, respectively. Also, some of our sample of class 3 cells (and all of our sample of cells intermediate between classes 2 and 3) are identified relay X-cells and not interneurons. Thus, the majority of cells in our sample with at least some class 3 morphological features are clearly relay neurons.

On the other hand, the relative numbers and soma size distribution of X- and Y-cells in our data closely match these parameters, as suggested by the data of LeVay and Fers-

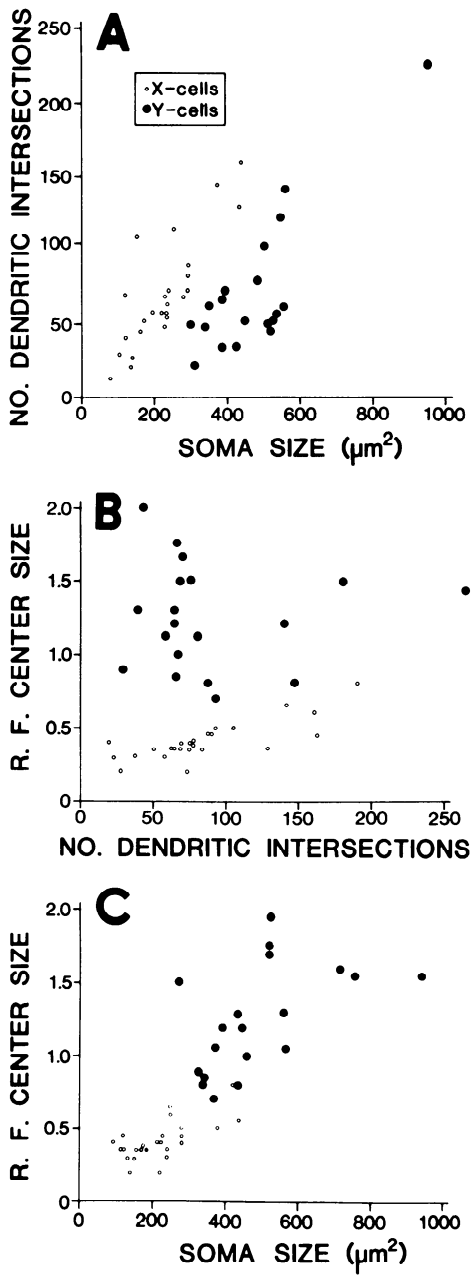

FIG. 26. Relationships among soma size, total number of dendritic intersections (see Fig. 25), and receptive-field center size for X- and Y-cells. The key is shown in *A*. *A*: scatter plot of soma size and number of dendritic intersections. A positive correlation of these variables exists for both X- and Y-cells. Relationships for X- and Y-cells seems similar, with that of Y-cells shifted toward larger somata than is that of X-cells (see text). *B*: scatter plot of number of dendritic intersections and receptive-field center size. A positive correlation for these variables is seen among X-cells but not Y-cells (see text). *C*: scatter plot of soma size and receptive-field center size. A slightly better correlation for these variables is seen for X-cells than for Y-cells (see text).

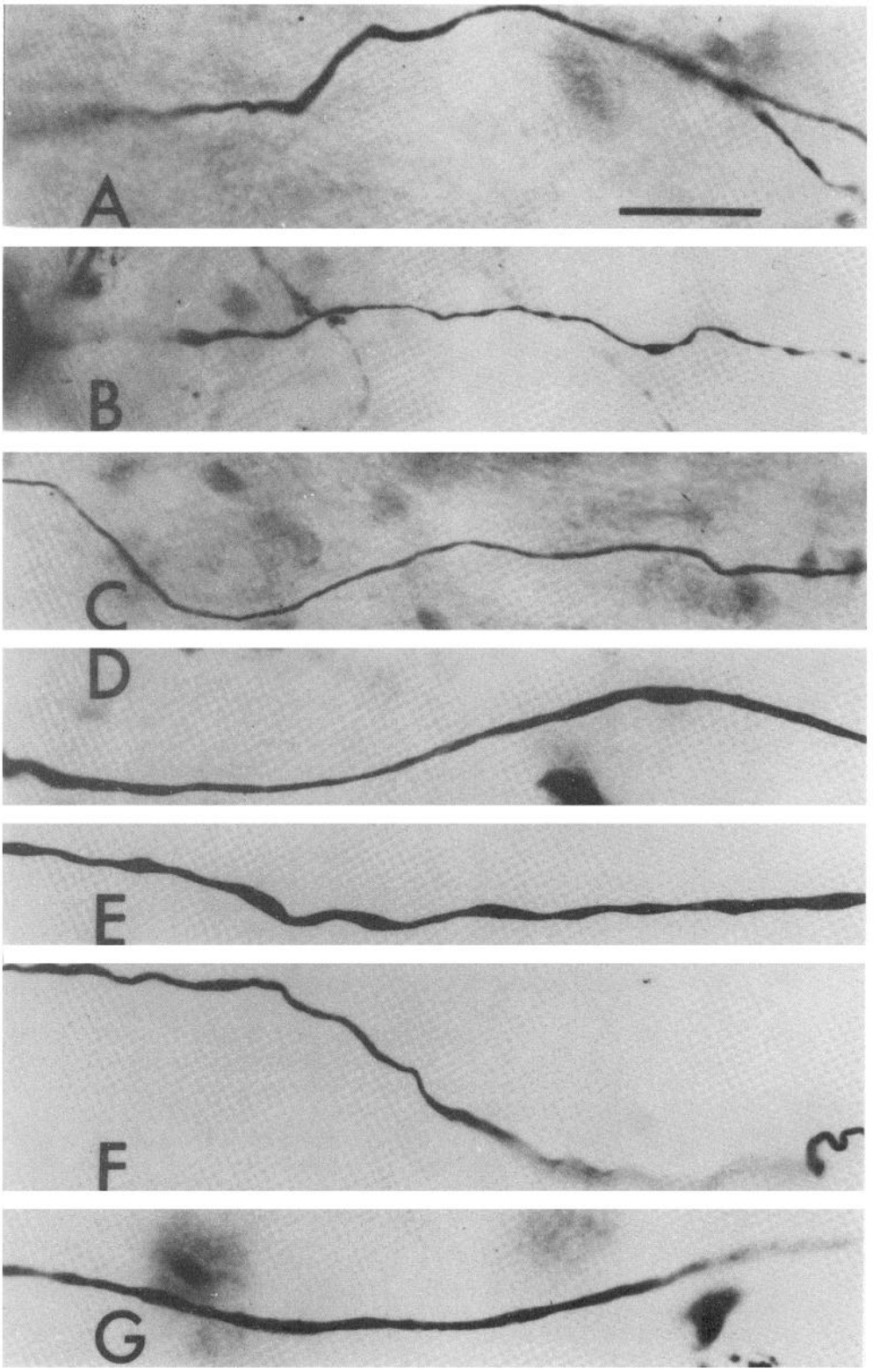
A
B
C
D
E
F
G

ter (48). Figure 29 shows a comparison of the distribution proposed by these authors for the middle of lamina A (redrawn from Fig. 7B of Ref. 48) with the distribution of X- and Y-cells from the A-laminae of our present study. The distribution of Y-cells versus other cell types is indistinguishable in the two sets of data ($P > 0.2$ on a χ^2 test). Thus we support the rather surprising LeVay and Ferster (48) suggestion that Y-cells comprise one-third or more of the cells in the A-laminae (see also below). However, our distribution of cells other than Y-cells are all X-cells which, with three exceptions, are identified relay cells, whereas LeVay and Ferster (48, 49) suggest that 25% of their entire sample are interneurons. As a result, we suggest that Y-cells comprise roughly 35% of relay neurons in the A-laminae (see also below), while LeVay and Ferster (48) place the fraction close to 50%. Perhaps these authors have overestimated the number of interneurons and perhaps relay X-cells include many smaller cells without cytoplasmic laminated bodies. This seems likely, since we found relay X-cells with class 3 morphology and small somata. Other current estimates of interneurons generally derive from the distribution of unlabeled geniculate neurons after large HRP injections into cortex. However, such experiments offer discrepent estimates for interneurons (cf. Refs. 23, 49, 53), and there may be artifactual reasons why some relay neurons would not be labeled (see also below). Such estimates, then, should be considered maximum for interneuron numbers. In any case, our data can be taken as indirect support for the LeVay and Ferster (48) proposal that neurons with cytoplasmic laminated bodies are X-cells (but that not all X-cells have this cytoplasmic structure). We are currently attempting to test this directly by searching for these cytoplasmic structures with appropriate histological procedures in physiologically identified and injected cells.

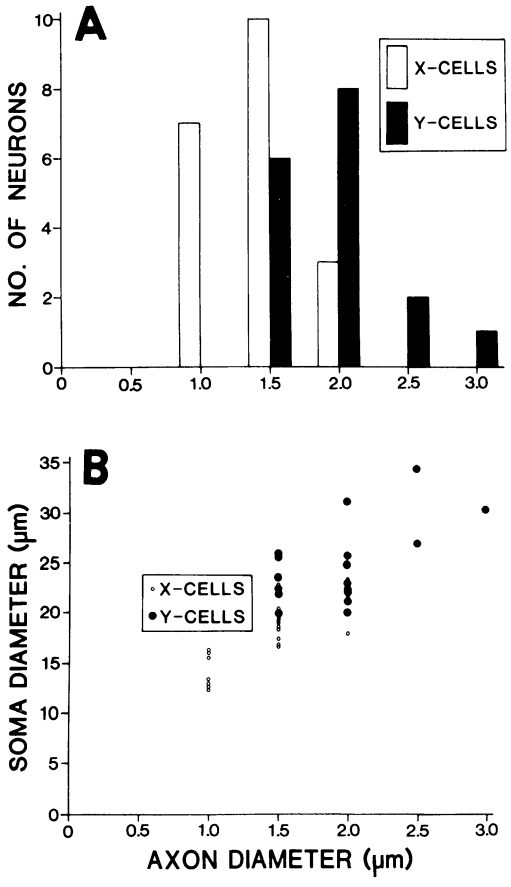

FIG. 28. Axon diameters and their relationship to soma diameter for X- and Y-cells. Keys are shown in boxes. *A*: frequency histogram of axon diameters. Y-cells tend to have larger axons than do X-cells, although some overlap exists (see text). *B*: scatter plot of axon diameter and soma diameter for X- and Y-cells. These variables are positively correlated for both cell types (see text).

MORPHOLOGICAL FEATURES OF X- AND Y-CELLS. From our data, we can list a series of five distinguishing morphological characteristics for geniculate X- and Y-cells: *1*) Y-cells have some dendrites that cross laminar boundaries (the one Y-cell exception was faintly stained and not a confirmed relay cell), whereas X-cells do not; *2*) Y-cells tend

FIG. 27. Photomicrographs of representative axons from X- and Y-cells. These views include regions from which diameter measurements were taken. Note the variability in apparent diameter along some axons. *A–C*: axons of X-cells. *D–G*: axons of Y-cells. Scale in *A*: 20 μm and applies as well to *B–G*. Note that Y-cell axons are thicker than are those of X-cells.

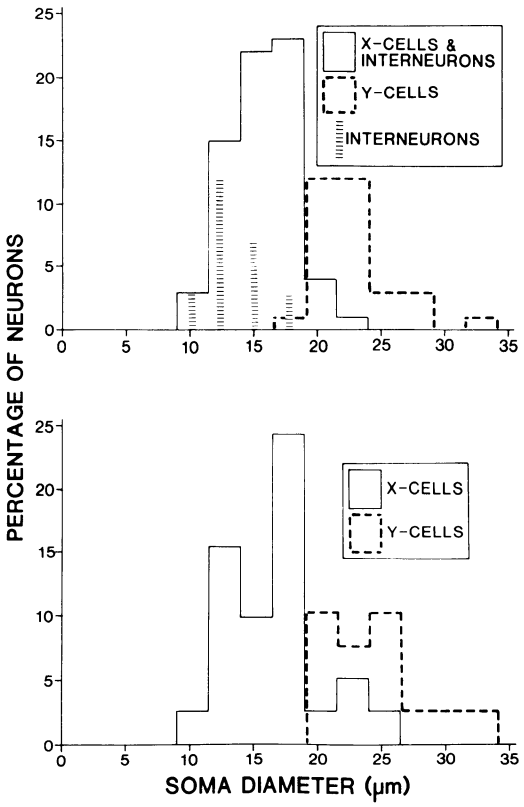

FIG. 29. Comparison of soma size distributions between data of LeVay and Ferster (48) (upper) and data from the present paper (lower). Data of LeVay and Ferster are redrawn from Fig. 7B of Ref. 48 and represent somata from the anteroposterior and mediolateral middle of lamina A in a normal cat. Our data represent both laminae A and A1. Note the similarity in distributions between our data and those of LeVay and Ferster both for Y-cells and also for other neurons (i.e., X-cells plus interneurons). Cells thought to be interneurons by LeVay and Ferster (48) are shown separately in the upper histogram; most of the neurons from our distribution are confirmed relay cells (see text for further details).

to have larger somata with thicker primary dendrites than do X-cells *3*) Y-cells tend to have thicker axons than do X-cells; *4*) Y-cells tend to have radially symmetric dendritic trees, while those of X-cells tend to be elongated along projection lines; and *5*) Y-cells tend to have simple, spinelike dendritic appendages, except for the grapelike appendages of the class 2 Y-cells, whereas X-cells usually have complex, stalked processes that may occur anywhere along the dendrites. In addition, fine axonal collaterals in the perigeniculate nucleus occur much more frequently for Y-cells than for X-cells, but this could be an artifact due to more difficulty in filling such fine processes from the thinner X-cell axons.

We suggest that the above list of morphological differences can be used with reasonable confidence to distinguish X-cells from Y-cells based on anatomical data alone. These differences can be considered as analogous to the "battery of tests" approach advocated by Rowe and Stone (62) to identify X- and Y-cells from physiological data. We are therefore proposing a morphological classification scheme with a functional basis, a scheme that is somewhat different from that proposed by Guillery (25). The two schemes can be compared, and it should be clear from our results that a class 1 neuron would be a Y-cell, a neuron with any class 3 features would be an X-cell, and a class 2 neuron could be identified either as an X- or Y-cell on the basis of soma, dendrite, and axon size, the shape of the dendritic tree, and whether or not any dendrites cross laminar borders. Figure 30 schematically summarizes many of these morphological features for X- and Y-cells.

CORRELATIONS AMONG MORPHOLOGICAL AND PHYSIOLOGICAL PARAMETERS. In RESULTS, we point out significant correlations for these neurons among several parameters. While these correlations may be statistically significant, their biological significance is not usually clear. We feel, however, that several merit further comment and speculation.

One concerns the strong relationship between soma size and dendritic extent (Fig. 26*A*). Dendritic extent has been defined in terms of dendritic intersections with five concentric rings, 50 μm apart, centered on the soma (see RESULTS). It is not entirely clear what features determine soma size, but a number of authors have suggested that larger geniculate somata are associated with more extensive axonal and/or terminal arborizations in cortex (e.g., Refs. 26, 50). However, Fig. 26*A* suggests that dendritic extent may also play a major role in determining geniculate soma size. It is interesting that X- and Y-cells seem to demonstrate quite similar relationships between these two variables, but that the functions are shifted so that equal dendritic extent is matched to

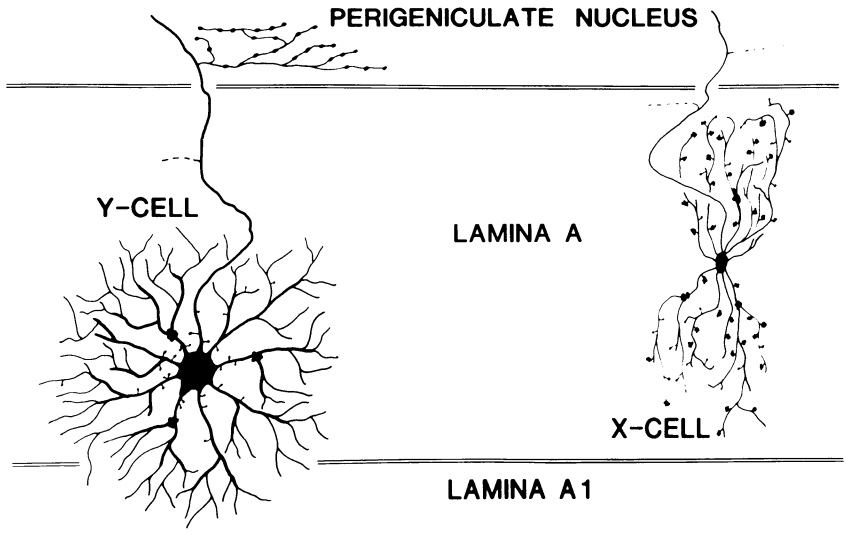

FIG. 30. Schematic drawing summarizing typical morphological features for an X-cell and a Y-cell. Typical differences indicated include the following: *1*) the Y-cell has translaminar dendrites and the X-cell does not; *2*) the Y-cell has a larger soma and thicker dendrites than does the X-cell; *3*) the Y-cell has a thicker axon than does the X-cell; *4*) the Y-cell has a radially symmetric dendritic tree, whereas the X- cell dendrites are oriented perpendicular to the lamination; *5*) the Y-cell has fewer and simpler dendritic appendages than does the X-cell, except for some complex, grapelike appendages occasionally found near dendritic branch points of both cells; and *6*) the Y-cell is more likely than is the X-cell to have axon collaterals in the perigeniculate nucleus (*PGN*) while both cells occasionally have intrageniculate axon collaterals.

a soma larger for a Y-cell than for an X-cell. This observation is consistent with the notion that a variable other than dendritic extent (i.e., axonal and/or terminal arborizations in cortex) also constributes to soma size. That is, if Y-cells have larger axonal distributions and far more synapses in cortex, this would mean that they would have larger somata than would X-cells despite equal dendritic extents. Y-cells do seem to have larger axonal arborizations than do X-cells, both because individual Y-cells typically project to areas 17 and 18 while X-cells project only to area 17 (23, 76) and also because within area 17 the Y-cell axons distribute more widely than do X-cell axons (19, 24). It has been repeatedly suggested that the abnormally small geniculate somata seen in animals raised with visual deprivation may be due to a reduced extent of terminal arborization in cortex (26, 50), but our data suggest the possibility that this could also be related to a reduced dendritic extent for deprived neurons. Experiments are currently underway on visually deprived cats to test this possibility.

A second correlation of interest concerns that between soma size and axon diameter (Fig. 28*B*), and this has already been noted by Ferster and LeVay (19) for geniculate neurons in the cat. Such a relationship has also been assumed for retinal ganglion cells, but it has not yet been directly demonstrated to our knowledge. The significance of this relationship between axon and soma size for geniculate neurons is not at all clear, and it may be that the two parameters are related because they have a common cause. That is, perhaps a more extensive axonal arborization requires both a larger soma to provide the metabolic machinery for synaptic maintenance as well as a larger axon to permit freer axoplasmic transport. If so, then differences in conduction velocity, which are usually correlated with differences in axon diameter, might be an epiphenomenon of axonal arborization and have no further significance for processing of visual information. We emphasize that this is pure speculation and that we do not conclude that conduction velocity is insignificant for visual processing, only that it may be.

Finally, the relationship between receptive-field center size and dendritic extent is of interest because it is strong for X-cells but absent for Y-cells. That there should be any correlation at all for these parameters is puzzling since geniculate neurons typically received excitatory receptive-field input from one or very few optic tract axons (8). This does suggest that receptive-field dimensions may be transmitted differently by geniculate X- and Y-cells.

DIFFERENCES BETWEEN LAMINAE A AND A1. Soma sizes in the cat's lateral geniculate nucleus are slightly larger on average for lamina A1 than for lamina A (27, 29, 42). A common explanation for this has been that lamina A1 contains a higher Y-cell percentage than does lamina A and that geniculate Y-cells are larger than are X-cells (35, 57, 83). Our data suggest an additional or alternative explanation. That is, both X- and Y-cells in lamina A1 are larger than their counterparts in lamina A, but this difference is statistically significant only for the X-cells.

MORPHOLOGICAL VARIABILITY AMONG X- AND Y-CELLS. Although X-cells possess morphological features distinct from those of Y-cells, the drawings and photomicrographs shown in RESULTS also serve to underline the morphological variability within each of these functional classes. The electrophysiological data we obtained for these neurons offer no obvious functional correlation for most of this variability. Whether this reflects an inadequacy of our available electrophysiological data or indicates certain morphological features with little functional relevance is not at all clear. Much more data are needed to address this issue.

Class 3 relay cells

Perhaps our most surprising result is the observation of relay neurons with class 3 morphological features. Such morphology has generally and confidently been associated with interneurons.[4] There are at least two possible explanations that may require a reevaluation of the interneuron concept for the lateral geniculate nucleus.

SUBGROUPS OF CLASS 3 MORPHOLOGY? First, it is clear that class 3 morphology should no longer be considered completely isomorphic with interneuronal function. Perhaps two subgroups of class 3 neurons exist, one of which represents relay neurons and the other, interneurons. As Figs. 3 and 4 show, our sample of class 3 neurons is not morphologically homogeneous. Tombol (79) has, in fact, described two such general groups morphologically: one has an axon that ramifies largely within the dendritic tree and the other has an axon that projects at least to other laminae. Examples of the former were not seen in our sample, and these may be the true interneurons. We may have missed them because our sample size of class 3 cells is small. Also, if these cells do not generate action potentials (with short axons, they might have no need for regenerative action potentials) or if they have very low levels of spontaneous activity, they would not be readily detected with our standard recording procedures. Incidentally, all of the class 3 cells in our sample did generate typical action potentials.

EXISTENCE OF INTERNEURONS? The second possibility is that interneurons simply do not exist in appreciable numbers as a unique cell class within the A-laminae. We feel that no means of positively identifying a geniculate interneuron currently exists. Their presence has been inferred from negative evidence that is not easy to interpret. Anatomically, such evidence usually consists of either failure to demonstrate a projection axon after Golgi impregnation or failure to label the neuron retrogradely following HRP injections into cortex. The physiological analog is a failure to activate the neuron antidromically after electrical stimulation of cortex.

There are, however, many reasons why a relay neuron might fail to have its axon stained after Golgi impregnation (e.g., myelinated axons are difficult to impregnate), to transport HRP retrogradely (e.g., factors controlling such HRP labeling are poorly understood and various studies report widely variant percentages of labeled geniculate neurons after HRP injections of cortex; cf. Refs. 23, 49, 53), or to propagate an antidromic spike (e.g., such propagation failure could occur at axonal branch points). As an example of this last reason, Dubin and Cleland (14) proposed a positive means of elec-

[4] Guillery, however, left open the possibility that class 3 cells are relay cells. He wrote, "in view of the incomplete staining of the axons it remains possible that some of these [class 3] cells have axons that leave the lateral geniculate nucleus" (Ref. 25, p. 36).

trophysiologically identifying interneurons. These authors suggested that only such cells could be activated from cortex transynaptically. However, Figs. 7*A* and *B* and 8*A* illustrate one of several examples we have seen of relay cells that display transynaptic activation from cortex.

Although class 3 cells in Golgi preparations have been described with only locally ramifying axons (79), it is possible that the cells possess unimpregnated projection axons. In other words, it is conceivable that the same cell can project an axon to cortex (and thus act as a "relay" cell) and still contribute an axonal network for local processing (and thus act as an "interneuron"). A comparison of the histograms in Fig. 24*A* and *B* suggest that, if interneurons indeed exist as a unique class, they must represent a rather small percentage of the geniculate neuronal population (53).

Another reason to reconsider the evidence for the existence of geniculate interneurons is that other circuits not requiring such cells seem available to carry out any proposed interneuronal function. For instance, perigeniculate neurons project axons down among the geniculate laminae (1, 2, 40), and these neurons receive input from collaterals of relay cell axons (see RESULTS and Refs. 3, 14). Perigeniculate neurons are thus excellent candidates for the basis of any proposed geniculate interneuronal circuitry. Additional intrageniculate circuitry is provided both by intrageniculate collaterals of relay cell axons (see RESULTS) and also by dendrodendritic synapses (16, 17). Although Famiglietti (16) argues that some of these synapses derive from relay cell dendrites, Famiglietti and Peters (17) seem to suggest that these presynaptic dendrites issue from interneurons because they have class 3 morphology. However, our data raise the possibility that interneurons might not exist as a unique class of geniculate cells (see above). This consequently raises the possibility that many or all of the class 3 cells with presynaptic dendrites described by Famiglietti and Peters (17) might be relay cells. If, indeed, class 3 relay cells possess presynaptic dendrites, this would be most interesting since axon terminals of relay cells in cortex possess round vesicles and make asymmetric contacts with postsynaptic elements (22), whereas the dendrodendritic synapses have flattened or pleomorphic vesicles and make symmetric contacts (17). We are currently applying ultrastructural methods to investigate this interesting possibility (82).

We emphasize that it is not our contention that intrageniculate interneurons do not exist. Rather, we suggest that the assumptions concerning their existence should be qualified and reconsidered since it has not yet been possible to obtain direct positive evidence for the presence of such cells. Our data clearly discredit the common assumption that all class 3 cells are interneurons.

Relative numbers of X- and Y-cells

Another general assumption not fully supported by our data is that electrodes selectively favor large somata for recording (e.g., Refs. 21, 36, 47, 68). This assumption predicts that an electrophysiological sample of single units would include an overestimate of cells with large somata. So and Shapley (68, 71) have argued that this sampling bias coupled with the larger presumed size of Y-cell somata has led to electrophysiologically obtained X- to Y-cell ratios of 1 to 1 or less when the true ratio is closer to the retinal estimates of 5 or 10 to 1. These authors report that when they record extracellularly with cruder metal electrodes, they find a larger geniculate Y-cell percentage (roughly 50%), but with "finer" micropipettes, they record many fewer Y-cells (10–20%) because these micropipettes have small tips, which make them less biased for larger somata (68, 71).[5]

One might expect intracellular recording to be even more difficult than extracellular

[5] So and Shapley (68, 71) suggest that they have largely overcome electrode sampling problems by using fine micropipettes. The conclusion that these micropipettes are indeed fine derives from their impedance range, which was reported to be 5–15 MΩ. However, So and Shapley (68, 71) filled their electrodes with physiological saline which, compared to the more conventional 4 M NaCl solution, is a rather nonconductive electrolyte. In our informal comparisons, we found that micropipettes that had an impedance of 5–15 MΩ when filled with physiological saline became low-impedance electrodes (<1 MΩ) when filled with 4 M NaCl. Since Hoffmann, Stone, and Sherman (34) used micropipettes with an impedance range of 5–15 MΩ with 4 M NaCl, these electrodes probably had finer tips than those used by So and Shapley (68, 71). Therefore, it seems most unlikely that So and Shapley (68, 71) obtained fewer geniculate Y-cells because of finer electrode tips than were used previously.

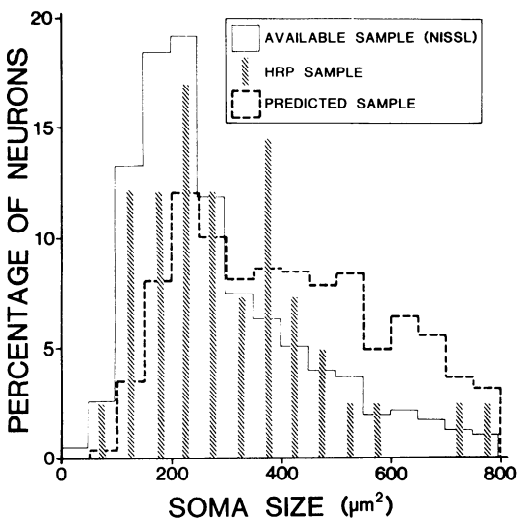

FIG. 31. Soma size distributions of neurons from laminae A and A1. The box shows the key. The available sample, based on Nissl-stained material, and our sample of HRP-filled neurons are taken from Fig. 24*C*. To construct the predicted sample, we applied an algorithm whereby each neuron was assigned a sampling probability proportional to its soma volume (cf. Ref. 36). The predicted sample thus represents the expected result from electrode biases acting on the available sample of neurons, and note that the predicted sample includes more large and fewer small neurons than does the available sample. Of particular interest is the observation that our actual sample of HRP-filled neurons differs from the predicted but not from the available sample. Our data consequently do not support the notion of electrode sampling biases based on soma size (see text for details).

recording among small somata, and thereby predict that our sample of cells should be highly biased in favor of large somata. For the A-laminae, Fig. 31 shows the soma size distribution of the predicted electrophysiological sample (dashed outline) that was derived from the available sample based on Nissl-stained material (solid outline). The derivation for the distribution of the predicted sample is based on an algorithm whereby the probability of recording a neuron is directly proportional to that neuron's soma volume. This algorithm is common to considerations of electrode sampling biases (36; see also Refs. 21, 68, 71). Thus, the predicted sample has more large somata and fewer smaller ones than does the available sample. However, our actual soma distribution of HRP-filled neurons (cross-hatched bars) is not statistically different from that of the available sample ($P > 0.2$ on a χ^2 test) but differs significantly from that of the predicted sample ($P < 0.001$ on a χ^2 test). Figure 31 thus suggests little or no electrode sampling bias based on soma size (see also Fig. 24*C*), at least for intracellular recording of these geniculate neurons.

Furthermore, as mentioned above, we have concluded from these soma size distributions that Y-cells represent roughly 35% of the neurons in the A-laminae. This value is very close to that suggested by LeVay and Ferster (48) on purely anatomical grounds. Thus, the X- to Y-cell ratio would be roughly 2 to 1 if few or no interneurons exist (53), and roughly 1 to 1 if as many as 25% interneurons exist (e.g., Refs. 23, 48, 49). This, in turn, suggests that X- to Y-cell ratios based on extracellular recording may not be as dramatically biased in favor of large somata as is generally assumed.[6] The fact is that, despite a widespread willingness to accept the conventional notion that large somata are selectively recorded by electrodes, there is little direct evidence for this, and we understand precious little about the factors that do control electrode sampling. For instance, perhaps dendritic geometry and the possibility of regenerative potentials along some dendrites (54, 85) contributes more to electrode sampling biases than does soma size. Figure 25*B* shows that, on the average, X- and Y-cells have equal dendritic extents.

We must nonetheless emphasize that, while our data do not generally support the notion of electrode sampling based on soma volume (36), neither do they strongly oppose this notion. Although other authors (21, 68, 71) have suggested that electrode sampling biases can increase the recorded Y-cell fraction by a factor of 5 or more, our data suggest a more modest consequence of such biases. A consideration of Figs. 24*D* and 31 predicts that the recorded Y-cell percentage based on sampling due to soma volume should be 60%. This represents a relatively modest sampling bias of less than a factor of 2 due to the relatively large size of Y-cells. In other words, given the soma size

[6] One of us (S. M. Sherman) has analyzed all data accumulated during the past 8 years from our laboratory. This analysis indicates that, with micropipettes of 5–15 MΩ impedance at 100–200 Hz used for extracellular recording, our sample of A-laminae cells with receptive fields of 5–20° eccentric from the area centralis includes an X- to Y-cell ratio that is between 1 and 1.5 to 1.

distributions in Fig. 24*D*, soma size alone should have a relatively modest effect on recorded Y-cell numbers. We cannot rule out the possibility from our data that this predicted, modest effect of electrode sampling does not contribute to Y-cell numbers recorded extracellularly. In other words, we conclude that electrode sampling biases based on soma size have relatively little effect on recorded geniculate X- and Y-cell ratios.

Comparison with retinal studies

As noted above, we now estimate that the X- to Y-cell ratio in the A-laminae is between 1 and 2 to 1. This ratio is probably smaller when all geniculate regions are considered because of the predominance of Y-cells and rarity of X-cells in the medial interlaminar nucleus (13, 45, 55). Yet, as mentioned above, retinal estimates place this ratio at between 5 and 10 to 1 (12, 21, 52, 75, 81). Since practically all retinal X- and Y-cells project to the lateral geniculate nucleus (21; see also Refs. 47, 61, 77), any shift in cell ratios between retina and lateral geniculate nucleus due to differential projections seems unlikely.

Two other explanations, singly or in combination, seem more likely. First, the geniculate X- to Y-cell ratio may in fact be little different from the retinal ratio due to errors in estimating the retinal or geniculate value. On the one hand, due to our small sample size, our estimates of the geniculate ratio may be incorrect. On the other hand, due to the indirect method of assigning soma size classes to X- and Y-cell groups, Y-cell numbers may have been underestimated for the retina. That is, no one has yet reported on a direct structure/function correlation for retinal X- and Y-cells, as has been performed in the present study for geniculate neurons. Second, and perhaps more interesting, is the possibility that both retinal and geniculate estimates of relative X- and Y-cell numbers are approximately correct. If so, the X- and Y-cell pathways must have different divergence and/or convergence properties as they pass from retina through the lateral geniculate nucleus to visual cortex. Strictly for the purpose of simplifying our speculation, we shall assume that relatively little convergence occurs in the retinogeniculate pathways for either X- or Y-

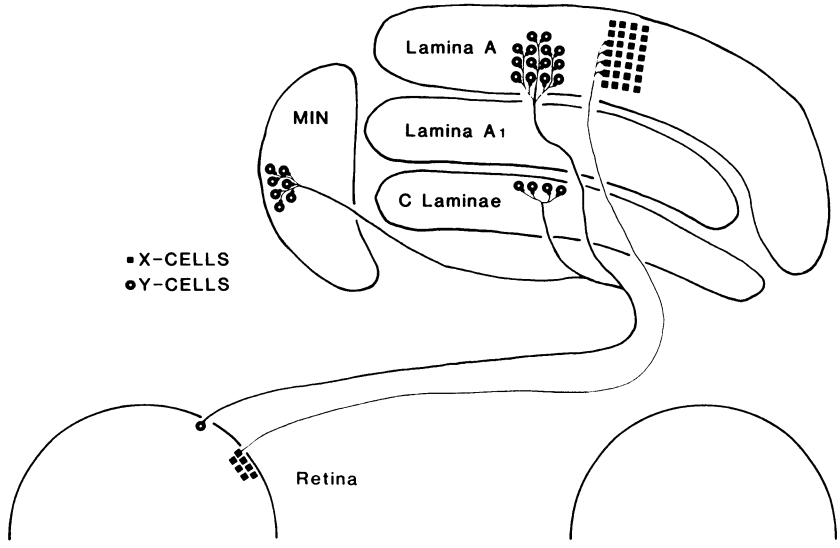

FIG. 32. Schematic drawing to illustrate different retinogeniculate divergence patterns for X- and Y-cell pathways. Only two retinal axons, one X-cell and one Y-cell, are shown and only from the contralateral eye. There should presumably be 5–10 X-cell axons for each Y-cell axon. For added simplicity, no convergence among retinogeniculate synapses is drawn; significant convergence in either pathway could be incorporated by altering the drawing to include proportionately more divergence for that pathway. As represented, each retinal X-cell innervates roughly 4 geniculate X-cells, and the number for the Y-cell pathway is roughly 20–30. The much larger divergence in the Y-cell pathway, with consequently more collateral axon branches, is needed to explain the lower X- to Y-cell ratios suggested for the lateral geniculate nucleus than suggested for the retina (see text).

cells (8). In very rough terms, we suggest that, throughout the lateral geniculate nucleus (including the medial interlaminar nucleus), X- and Y-cells occur in approximately equal numbers. The suggested ratio between the number of geniculate neurons and retinal ganglion cells is roughly 4 to 1 (64). Since estimates suggest that relatively few geniculate neurons are W-cells, but that they reflect about half of the retinal ganglion cell population (21, 83), the geniculate-to-retinal neuron ratio is probably between 5 and 10 to 1 if just X- and Y-cells are considered. Given this, a retinal X- to Y-cell ratio of between 5 and 10 to 1, and a geniculate X- to Y-cell ratio of roughly 1 to 1, it follows that each retinal X-cell axon commonly terminates onto roughly 4 geniculate X-cells, whereas each retinal Y-cell axon branches to provide inputs for 20–30 geniculate Y-cells. Figure 32 illustrates this schematically. If X- and/or Y-cell axons display significant convergence in their retinogeniculate connections, this scheme could be altered to include proportionately more divergence than illustrated. Thus, in functional terms, the X-cell retinogeniculate pathway includes 4 times as much divergence as convergence, whereas the value is 20–30 times as much divergence as convergence for the Y-cell pathway. The need to support such an extensive axonal arborization could account for the presumed large somata and axons of retinal Y-cells (4, 12, 21, 52, 75, 81).

This line of reasoning suggests that one function of the lateral geniculate nucleus in the cat may be to increase the relative contribution of the Y-cell pathway from retina to cortex. Given the aformentioned large terminal axon arborizations of Y-cells compared to X-cells in cortex, this relative expansion of the Y-cell pathway may continue central to the lateral geniculate nucleus. Such a suggestion is compatible with the recent hypothesis that Y-cells play a key role in the basic processing of visual stimuli (46, 69).

Conclusions

It is clear from our data that geniculate X-cells do have morphological features that are quite distinct from those of Y-cells. This, in turn, suggests that differences in the X- and Y-cell pathways are not limited to retina and simply relayed by more central structures, but rather suggests that further differences between X- and Y-cells occur in the lateral geniculate nucleus. Perhaps related to this is our suggestion above that geniculate circuitry seems to amplify the Y-cell pathway by increasing the Y- to X-cell ratio from its retinal value. At a more general level, differences in dendritic morphology between geniculate X- and Y-cells may relate to their different nonretinal inputs (i.e., cortical, perigeniculate nucleus, brain stem, etc.) that also contribute to the information processing among geniculate relay cells.

ACKNOWLEDGMENTS

We thank Sally Gibson for her excellent technical assistance.

This research was supported by Public Health Service Grant EY03038.

S. M. Sherman was the recipient of Research Career Development Award EY00020.

Present address of M. J. Friedlander: Dept. of Physiology and Biophysics, University of Alabama in Birmingham, Birmingham, AL 35294.

Present address of C.-S. Lin: Dept. of Anatomy, Duke University, Durham, NC 27706.

Received 24 October 1980; accepted in final form 26 January 1981.

REFERENCES

1. AHLSEN, G. AND LINDSTROM, S. Axonal branching of functionally identified neurones in the lateral geniculate body of the cat (Abstract). *Neurosci. Lett.* Suppl. 1: S156, 1978.
2. AHLSEN, G. AND LINDSTROM, S. Projection of perigeniculate neurones to the lateral geniculate body in the cat (Abstract). *Neurosci. Lett.* Suppl. 1: S367, 1978.
3. AHLSEN, G., LINDSTROM, S., AND SYBIRSKA, E. Subcortical axon collaterals of principal cells in the lateral geniculate body of the cat. *Brain Res.* 156: 106–109, 1978.
4. BOYCOTT, B. B. AND WASSLE, H. The morphological types of ganglion cells of the domestic cat's retina. *J. Physiol. London* 240: 397–419, 1974.
5. BULLIER, J. AND HENRY, G. H. Ordinal position of neurons in the cat striate cortex. *J. Neurophysiol.* 42: 1251–1263, 1979.
6. BULLIER, J. AND HENRY, G. H. Neural path taken by afferent streams in striate cortex of the cat. *J. Neurophysiol.* 42: 1264–1270, 1979.
7. BULLIER, J. AND HENRY, G. H. Laminar distribution of first-order neurons and afferent terminals in cat striate cortex. *J. Neurophysiol.* 42: 1271–1281, 1979.
8. CLELAND, B. G., DUBIN, M. W., AND LEVICK,

W. R. Sustained and transient neurones in the cat's retina and lateral geniculate nucleus. *J. Physiol. London* 217: 473–496, 1971.

9. CLELAND, B. G. AND LEVICK, W. R. Brisk and sluggish concentrically organized ganglion cells in the cat's retina. *J. Physiol. London* 240, 421–456, 1974.
10. CLELAND, B. G. AND LEVICK, W. R. Properties of rarely encountered types of ganglion cells in the cat's retina and an overall classification. *J. Physiol. London* 240: 457–492, 1974.
11. CLELAND, B. G., LEVICK, W. R., MORSTYN, R., AND WAGNER, H. G. Lateral geniculate relay of slowly conducting retinal afferents to cat visual cortex. *J. Physiol. London* 255: 299–320, 1976.
12. CLELAND, B. G., LEVICK, W. R., AND WASSLE, H. Physiological identification of a morphological class of ganglion cell. *J. Physiol. London* 248: 151–171, 1975.
13. DREHER, B. AND SEFTON, A. J. Properties of neurones in cat's dorsal lateral geniculate nucleus: a comparison between medial interlaminar and laminated parts of the nucleus. *J. Comp. Neurol.* 183: 47–64, 1979.
14. DUBIN, M. W. AND CLELAND, B. G. Organization of visual inputs to interneurons of lateral geniculate nucleus of the cat. *J. Neurophysiol.* 40: 410–427, 1977.
15. ENROTH-CUGELL, C. AND ROBSON, J. G. The contrast sensitivity of retinal ganglion cells of the cat. *J. Physiol. London* 187: 516–552, 1966.
16. FAMIGLIETTI, E. V. Dendro-dendritic synapses in the lateral geniculate nucleus of the cat. *Brain Res.* 20: 181–191, 1970.
17. FAMIGLIETTI, E. V. AND PETERS, A. The synaptic glomerulus and the intrinsic neurons in the dorsal lateral geniculate nucleus of the cat. *J. Comp. Neurol.* 144: 285–334, 1972.
18. FERNALD, R. AND CHASE, R. An improved method for plotting retinal landmarks and focusing the eyes. *Vison Res.* 11: 95–96, 1971.
19. FERSTER, D. AND LEVAY, S. The axonal arborizations of lateral geniculate neurons in the striate cortex of the cat. *J. Comp. Neurol.* 182: 923–944, 1978.
20. FRIEDLANDER, M. J., LIN, C.-S., AND SHERMAN, S. M. Structure of physiologically identified X- and Y-cells in the cat's lateral geniculate nucleus. *Science* 204: 1114–1117, 1979.
21. FUKUDA, Y. AND STONE, J. Retinal distribution and central projections of Y-, X-, and W-cells of the cat's retina. *J. Neurophysiol.* 37: 748–772, 1974.
22. GAREY, L. J., AND POWELL, T. P. S. An experimental study of the termination of the lateral geniculo-cortical pathway in the cat and monkey. *Proc. R. Soc. London Ser. B* 179: 41–63, 1971.
23. GEISERT, E. E. Cortical projections of the lateral geniculate nucleus in the cat. *J. Comp. Neurol.* 190: 793–812, 1980.
24. GILBERT, C. D. AND WIESEL, T. N. Morphology and intracortical projections of functionally characterized neurones in the cat visual cortex. *Nature London* 280: 120–125, 1979.
25. GUILLERY, R. W. A study of Golgi preparations from the dorsal lateral geniculate nucleus of the adult cat. *J. Comp. Neurol.* 238: 21–50, 1966.
26. GUILLERY, R. W. Binocular competition in the control of geniculate cell growth. *J. Comp. Neurol.* 144: 117–130, 1972.
27. GUILLERY, R. W. AND STELZNER, D. J. The differential effects of unilateral lid closure upon the monocular and binocular segments of the dorsal lateral geniculate nucleus in the cat. *J. Comp. Neurol.* 139: 413–422, 1970.
28. HERMAN, M. M. AND RALSTON, H. J., III. Laminated cytoplasmic bodies and annulate lamellae in the cat ventrobasal and posterior thalamus. *Anat. Rec.* 167: 183–196, 1970.
29. HICKEY, T. L. Development of the dorsal lateral geniculate nucleus in normal and visually deprived cats. *J. Comp. Neurol.* 189: 467–481, 1980.
30. HICKEY, T. L. AND GUILLERY, R. W. An autoradiographic study of retinogeniculate pathways in the cat and the fox. *J. Comp. Neurol.* 156: 239–254, 1974.
31. HOCHSTEIN, S. AND SHAPLEY, R. M. Quantitative analysis of retinal ganglion cell classifications. *J. Physiol. London* 262: 237–264, 1976.
32. HOCHSTEIN, S. AND SHAPLEY, R. M. Linear and nonlinear subunits in Y cat retinal ganglion cells. *J. Physiol London* 262: 265–284, 1976.
33. HOFFMANN, K.-P. AND STONE, J. Conduction velocity of afferents of cat visual cortex: a correlation with cortical receptive field properties. *Brain Res.* 32: 460–466, 1971.
34. HOFFMANN, K.-P., STONE, J., AND SHERMAN, S. M. Relay of receptive-field properties in dorsal lateral geniculate nucleus of the cat. *J. Neurophysiol.* 35: 518–531, 1972.
35. HOLLANDER, H. AND VANEGAS, H. The projection from the lateral geniculate nucleus onto the visual cortex in the cat. A quantitative study with horseradish peroxidase. *J. Comp. Neurol.* 173: 519–536, 1977.
36. HUMPHREY, D. R. AND CORRIE, W. S. Properties of pyramidal tract neuron system within a functionally defined subregion of primate motor cortex. *J. Neurophysiol.* 41: 216–243, 1978.
37. IKEDA, H. AND WRIGHT, M. J. Receptive field organisation of "sustained" and "transient" retinal ganglion cells which subserve different functional roles. *J. Physiol. London* 227: 769–800, 1972.
38. IKEDA, H. AND WRIGHT, M. J. Spatial and temporal properties of "sustained" and transient" neurones in area 17 of the cat's visual cortex. *Exp. Brain Res.* 22: 363–383, 1975.
39. JANKOWSKA, E., RASTAD, J., AND WESTMAN, J. Intracellular application of horseradish peroxidase and its light and electron microscopial appearance in spinocervical tract cells. *Brain Res.* 105: 557–562, 1976.
40. JONES, E. G. Some aspects of the organization of the thalamic reticular complex. *J. Comp. Neurol.* 162: 285–308, 1975.
41. JOSHUA, D. E. AND BISHOP, P. O. Binocular single vision and depth discrimination. Receptive field disparities for central and peripheral vision and binocular interaction on peripheral single units in cat striate cortex. *Exp. Brain Res.* 10: 389–416, 1970.
42. KALIL, R. A quantitative study of the effects of monocular enucleation and deprivation on cell growth in the dorsal lateral geniculate nucleus of the cat. *J. Comp. Neurol.* 189: 483–524, 1980.
43. KALIL, R. AND WORDEN, I. Cytoplasmic laminated bodies in the lateral geniculate nucleus of normal

and dark reared cats. *J. Comp. Neurol.* 178: 469–486, 1978.

44. KITAI, S. T., KOCSIS, J. D., PRESTON, R. J., AND SUGIMORI, M. Monosynaptic inputs to caudate neurons identified by intracellular injection of horseradish peroxidase. *Brain Res.* 109: 601–606, 1976.
45. KRATZ, K. E., WEBB, S. V., AND SHERMAN, S. M. Studies of the cat's medial interlaminar nucleus: a subdivision of the dorsal lateral geniculate nucleus. *J. Comp. Neurol.* 181: 601–614, 1978.
46. LEHMKUHLE, S., KRATZ, K. E., MANGEL, S. C., AND SHERMAN, S. M. Spatial and temporal sensitivity of X- and Y-cells in the dorsal lateral geniculate nucleus of the cat. *J. Neurophysiol.* 43: 520–541, 1980.
47. LENNIE, P. Parallel visual pathways: a review. *Vision Res.* 20: 561–594, 1980.
48. LEVAY, S. AND FERSTER, D. Relay cell classes in the lateral geniculate nucleus of the cat and the effects of visual deprivation. *J. Comp. Neurol.* 172: 563–584, 1977.
49. LEVAY, S. AND FERSTER, D. Proportions of interneurons in the cat's lateral geniculate nucleus. *Brain Res.* 164: 304–308, 1979.
50. LEVAY, S., WIESEL, T. N., AND HUBEL, D. H. The development of ocular dominance columns in normal and visually deprived monkeys. *J. Comp. Neurol.* 191: 1–51, 1980.
51. LEVENTHAL, A. G. AND HIRSCH, H. V. B. Receptive-field properties of different classes of neurons in visual cortex of normal and dark-reared cats. *J. Neurophysiol.* 43: 1111–1132, 1980.
52. LEVICK, W. R. Form and function of cat retinal ganglion cells. *Nature London* 254: 659–662, 1975.
53. LIN, C.-S., KRATZ, K. E., AND SHERMAN, S. M. Percentage of relay cells in the cat's lateral geniculate nucleus. *Brain Res.* 131: 167–173, 1977.
54. LLINÁS, R. AND SUGIMORI, M. Calcium conductances in Purkinje cell dendrites: their role in development and integration. *Prog. Brain Res.* 51: 323–334, 1979.
55. MASON, R. Cell properties in the medial interlaminar nucleus of the cat's lateral geniculate complex in relation to the transient/sustained classification. *Exp. Brain Res.* 22: 327–329, 1975.
56. MCILWAIN, J. T. AND CREUTZFELDT, O. D. Microelectrode study of synaptic excitation and inhibition in the lateral geniculate nucleus of the cat. *J. Neurophysiol.* 30: 1–21, 1967.
57. MITZDORF, U. AND SINGER, W. Laminar segregation of afferents to lateral geniculate nucleus of the cat: an analysis of current source density. *J. Neurophysiol.* 40, 1227–1244, 1977.
58. MORALES, R. AND DUNCAN, D. Multilaminated bodies and other unusual configurations of endoplasmic reticulum in the cerebellum of the cat. An electron microscope study. *J. Ultrastruct. Res.* 15: 480–489, 1966.
59. MUGNAINI, E. The histology and cytology of the cerebellar cortex. In: *The Comparative Anatomy and Histology of the Cerebellum. The Human Cerebellum, Cerebellar Connections, and Cerebellar Cortex*, edited by O. Larsell and J. Jansen. Minneapolis: Univ. of Minnesota Press, 1972, p. 201–264.
60. O'LEARY, J. A structural analysis of the lateral geniculate nucleus of the cat. *J. Comp. Neurol.* 73: 405–430, 1940.
61. RODIECK, R. W. Visual pathways. *Ann. Rev. Neurosci.* 2: 193–225, 1979.
62. ROWE, M. H. AND STONE, J. Naming of neurones. *Brain Behav. Evol.* 14: 185–216, 1977.
63. SANDERSON, K. J. The projection of the visual field to the lateral geniculate and medial interlaminar nuclei in the cat. *J. Comp. Neurol.* 143: 101–118, 1971.
64. SANDERSON, K. J. Visual field projection columns and magnification factors in the lateral geniculate nucleus of the cat. *Exp. Brain Res.* 13: 159–177, 1971.
65. SANDERSON, K. J. AND SHERMAN, S. M. Nasotemporal overlap in visual field projected to lateral geniculate nucleus in the cat. *J. Neurophysiol.* 34: 453–466, 1971.
66. SCHMIDT, M. L. AND HIRSCH, H. V. B. A quantitative study of the occurrence and distribution of cytoplasmic laminated bodies in the lateral geniculate nucleus of the normal adult cat. *J. Comp. Neurol.* 189: 235–247, 1980.
67. SEKULER, R., PANTLE, A., AND LEVINSON, E. Physiological basis of motion perception. *Handbook of Sensory Physiology*. Vol. VIII. Perception, edited by R. Held, H. W. Leibowitz, and H.-L. Teuber. Berlin: Springer, 1978, p. 67–96.
68. SHAPLEY, R. AND SO, Y. T. Is there an effect of monocular deprivation on the proportions of X and Y cells in the cat lateral geniculate nucleus? *Exp. Brain Res.* 39: 41–48, 1980.
69. SHERMAN, S. M. The functional significance of X and Y cells in normal and visually deprived cats. *Trends Neurosci.* 2: 192–195, 1979.
70. SHOLL, D. A. The organisation of the visual cortex in the cat. *J. Anat.* 89: 33–46, 1955.
71. SO, Y. T. AND SHAPLEY, R. M. Spatial properties of X and Y cells in the lateral geniculate nucleus of the cat and conduction velocities of their inputs. *Exp. Brain Res.* 36: 533–550, 1979.
72. SOTELLO, C. AND ANGAUT, P. The fine structure of the cerebellar central nuclei in the cat. I. Neurons and neuroglial cells. *Exp. Brain Res.* 16: 410–430, 1973.
73. STANFORD, L. R., FRIEDLANDER, M. J., AND SHERMAN, S. M. Morphology of physiologically identified neurons in the C laminae of the cat's lateral geniculate nucleus. *Soc. Neurosci. Abstr.* 6: 583, 1980.
74. STEVENS, J. K. AND GERSTEIN, G. L. Spatiotemporal organization of cat lateral geniculate receptive fields. *J. Neurophysiol.* 39: 213–238, 1976.
75. STONE, J. The number and distribution of ganglion cells in the cat's retina. *J. Comp. Neurol.* 180: 753–772, 1978.
76. STONE, J. AND DREHER, B. Projection of X- and Y-cells of the cat's lateral geniculate nucleus to areas 17 and 18 of visual cortex. *J. Neurophysiol.* 36: 551–567, 1973.
77. STONE, J., DREHER, B., AND LEVENTHAL, A. G.

Heirarchical and parallel mechanisms in the organization of visual cortex. *Brain Res. Rev.* 1: 345–394, 1979.

78. STONE, J. AND FUKUDA, Y. Properties of cat retinal ganglion cells: a comparison of W-cells with X- and Y-cells. *J. Neurophysiol.* 37: 722–748, 1974.
79. TOMBOL, T. Two types of short axon (Golgi 2nd) interneurons in the specific thalamic nuclei. *Acta Morphol. Acad. Sci. Hung.* 17: 285–297, 1969.
80. UPDYKE, B. V. A Golgi study of the class V cell in the visual thalamus of the cat. *J. Comp. Neurol.* 186: 603–620, 1979.
81. WASSLE, H., LEVICK, W. R., AND CLELAND, B. G. The distribution of the alpha type of ganglion cells in the cat's retina. *J. Comp. Neurol.* 159: 419–438, 1975.
82. WILSON, J. R., FRIEDLANDER, M. J., AND SHERMAN, S. M. Synaptic morphology of X- and Y-cells in the cat's dorsal lateral geniculate nucleus. *Soc. Neurosci. Abstr.* 6: 583, 1980.
83. WILSON, P. D., ROWE, M. H., AND STONE, J. Properties of relay cells in the cat's lateral geniculate nucleus: a comparison of W-cells with X- and Y-cells. *J. Neurophysiol.* 39: 1193–1209, 1976.
84. WINFIELD, D. A. Cytoplasmic laminated bodies in the visual cortex of the cat. *Brain Res.* 161: 544–548, 1979.
85. WONG, R. K. S., PRINCE, D. A., AND BASBAUM, A. I. Intradendritic recordings from hippocampal neurons. *Proc. Natl. Acad. Sci. USA* 76: 986–990, 1979.